Hydrothermal Liquefaction of Biopulp

Waste Management and Sustainable Bioblendstock Production

Sadetmahaleh, Komeil Kohansal

DOI (link to publication from Publisher):
10.54337/aau528220765

Publication date:
2023

Document Version
Publisher's PDF, also known as Version of record

HYDROTHERMAL LIQUEFACTION OF BIOPULP: WASTE MANAGEMENT AND SUSTAINABLE BIOBLENDSTOCK PRODUCTION

BY
KOMEIL KOHANSAL SADETMAHALEH

DISSERTATION SUBMITTED 2023

AALBORG UNIVERSITY
DENMARK

HYDROTHERMAL LIQUEFACTION OF BIOPULP: WASTE MANAGEMENT AND SUSTAINABLE BIO-BLENDSTOCK PRODUCTION

Ph.D. Dissertation

Komeil Kohansal Sadetmahaleh

AALBORG UNIVERSITY
DENMARK

AAU Energy, Aalborg University

Dissertation submitted: February 2023

PhD supervisor: Associate Prof. Thomas Helmer Pedersen,
Aalborg University

Assistant PhD supervisor: Prof. Lasse Aistrup Rosendahl,
Aalborg University

PhD committee: Associate Professor Jakob Zinck Thellufsen
Aalborg University, Denmark

Associate Professor Patrick Biller
Aarhus University, Denmark

Professor Chunbao Xu
Western University, Canada

PhD Series: Faculty of Engineering and Science, Aalborg University

Department: AAU Energy

ISSN (online): 2446-1636
ISBN (online): 978-87-7573-757-4

Published by:
Aalborg University Press
Kroghstræde 3
DK – 9220 Aalborg Ø
Phone: +45 99407140
aauf@forlag.aau.dk
forlag.aau.dk

Printed in Denmark by Stibo Complete, 2023

Abstract

In the past decades, increasing attention has been drawn to reducing the transportation sector's carbon footprint by substituting conventional fossil fuels with renewable liquid fuels. Moreover, the challenges associated with the environmental-friendly disposal of municipal solid waste have urged the scientific communities and policymakers to explore alternative technologies. As a prospective technology, hydrothermal liquefaction (HTL) stands out as a competent technology for urban waste disposal along with a promising method of producing liquid fuel precursors. The flexibility of HTL in treating highly moist feedstocks enables it to be a great candidate in valorizing the embedded calorific value of the organic fraction of municipal solid waste (MSW) into an energy-dense intermediate product so-called biocrude. Despite the significant benefits, HTL and the resultant product-of-interest still encounter serious challenges that if remain untacked, can potentially dominate the technology readiness level, and risk its commercialization. The present work is built upon addressing various challenges in the development of continuous HTL, valorization of the aqueous phase affluent, and utilization of the upgraded biocrude as an alternative diesel blendstock.

In response to the heavily contaminated MSW (by non-biodegradable substances), the development of a seamless waste-to-biocrude scheme through the integration of a biomass pretreatment technique into the HTL process is closely studied in terms of biomass properties. The Ecogi® process yielding a moist feedstock (biopulp) was targeted as the primary mechanical pretreatment. The various aspects of the biopulp were thoroughly inspected. The biomass containing 15 to 25 wt. % of moisture, less than 1 wt. % of plastic contamination (db), and over 90 wt. % of convertible organics (db) was verified as an ideal slurry to be used in HTL as such. The chemical conversion of the biomass macromolecules to the intermediate product was investigated in different HTL operating conditions seeking the optimal temperature and homogeneous catalyst in lab-scale setups. Furthermore, the obtained results were utilized to establish a continuous bench-scale campaign. The results have shown that K_2CO_3-assisted subcritical (350 °C) yielded the highest biocrude yield (over 35 wt. %) with a superior saturation (H/C: 1.64). It has also been found that the biocrude was majorly composed of fatty acids and fatty amides originating from the high crude lipid content of the biopulp. The results of the continuous campaign showed that the presence of K_2CO_3 as a homogeneous catalyst can ensure a steadier operation by preventing intermediates repolymerization in the unit's preheaters. Moreover, the involvement of the alkali catalysts secured transferring the inorganic elements to the solid residue phase, facilitating feasible NPK recoveries.

To cope with the energy-intensive HTL wastewater treatment requirement and simultaneously aim to increase the energy distribution to biocrude, recirculation of the concentrated aqueous phase was performed in this study. Removal of the surplus water allows the value-chain to maintain uninterrupted operation without the need for biomass pre-drying. The primary results have shown that the evaporation of the aqueous phase could eliminate up to 30 wt. % of total nitrogen and 60 wt. % of ammonia while maintaining over 80 wt. % of the carbon into the cycle. The mass

distribution results revealed a significant increase in biocrude mass (over 8 wt. %), carbon (over 4 %), and energy recovery after consecutive recirculation. The chemical composition results on the other hand indicated a greater presence of N-containing compounds mainly in the form of fatty amides and N-heterocyclics in the subsequent cycles that if end up in the final fuel, might inversely affect the performance of the engine and the exhaust gases. Therefore, a hydrotreating step operating at two operating conditions was carried out. The results projected a higher N distribution in the consecutive hydrotreated biocrude possibly due to the refractory N-heterocyclics originating from the cyclization and Maillard reactions. Achieving a high nitrogen removal requires a severe hydrotreating condition (high temperature, H_2 partial pressure, and WHSV) that can in return negatively influence the process economy and trigger catalyst deactivation.

The resultant biocrude from the continuous campaign was subjected to another study to assess the capability of HTL fuel in being viewed as an on-specification diesel blendstock. The impact of a mild pre-stabilization step along with vacuum distillation was investigated in terms of distillate recovery and the chemical and physicochemical properties. Later, a multi-objective optimization method was developed to optimize the selection of the biocrude distillates (biodistillates mixture) and blend the mixture to the reference diesel. The produced blend fuels were then combusted in an internal combustion engine to monitor the fuel emission profiles. The results have shown that the raw and hydrotreated biocrudes substantially deviated from the specifications announced by EN590 for road diesel. Moreover, the challenges with blending and fuel storage stability were also detected resulting in disregarding them as the potential bioblendstocks. On the other hand, vacuum distillation considerably augmented the physicochemical properties of the fuel, allowing it to produce on-spec blendstocks. The mild hydrotreating (pre-stabilization) step significantly contributed to a higher distillate recovery from 22.6 to 55.6 wt. % through the removal of oxygenated compounds and prevention of repolymerization reactions during distillation operation. The results also indicate that the HTL value-chain could be optimized based on the most limiting blend walls to maximize the Bioblend share in the final fuel. The emission results heralded promising results for the hydrotreated biodistillate mixtures with comparable SO_2, THC, CO, and CO_2 to the reference diesel.

The outcome of the present Ph.D. thesis highlights the flexibility of the HTL process in valorizing highly moist urban waste. It also contributes to providing a beneficial pathway for the recirculation of the aqueous phase residual carbon to the process while treating wet biomass. The thesis addresses the challenges that correspond to the continuous HTL operation of the biopulp and provides a mathematical method to obtain on-spec blend road diesel. All in all, the results of the activities carried out in the framework of this thesis support the upscaling and development of future HTL value-chain schemes.

Resumé

I de seneste årtier har opmærksomheden på at reducere transportsektorens CO2-aftryk ved at erstatte de konventionelle fossile brændstoffer med bæredygtige flydende brændstoffer været stadigt stigende. Derudover er der kommet øget fokus blandt politikere og forskere på at finde nye teknologier til miljøvenlig afskaffelse af kommunalt affald. I den forbindelse er Hydrothermal liquefaction (HTL) en lovende teknologi til håndtering af organisk affald, der samtidig fungerer som en metode til at producere de kemikalier, der udgør forstadiet til flydende brændstoffer. Fleksibiliteten ved, at HTL kan behandle meget fugtige råmaterialer, gør processen velegnet til at nyttiggøre brændværdien af den organiske del af affaldet ved at skabe et produkt med høj energidensitet, kaldet en bio-råolie. På trods af de betydelige fordele er der stadig nogle udfordringer ved både teknologien og produktet, som skal håndteres for at opnå kommercialisering. Dette arbejde baserer sig på at adressere forskellige udfordringer i udviklingen af kontinuert HTL, nyttiggørelse af den producerede vandfase samt udnyttelse af den opgraderede bio-råolie som et alternativ til diesel.

Som reaktion på det stærkt forurenede organiske affald (af ikke-biologisk nedbrydelige stoffer) er udviklingen af en affald-til-bio-råolie-proces gennem integration af en biomasse-forbehandlingsteknik til HTL-processen nøje undersøgt med hensyn til biomassens egenskaber. Ecogi® processen, som resulterer i en meget fugtig blanding kaldet biopulp, er blevet undersøgt som den primære mekaniske metode til forbehandling af affaldet. De mange aspekter af biopulpen er blevet grundigt inspiceret. Biomassen indeholder 15 til 25 wt. % fugt, mindre end 1 wt. % plastikforurening på tør basis og mere end 90 wt. % konverterbare organiske stoffer på tør basis. Dette gør biomassen ideel til brug i HTL-processen. Den kemiske konvertering af biomassens makromolekyler er blevet undersøgt under forskellige operationsbetingelser i HTL-processen i laboratorieskala for at bestemme den optimale operationstemperatur samt den bedste homogene katalysator. Resultaterne viser, at brugen af K2CO3 under subkritiske betingelser (350 °C) giver det højeste udbytte af bio-råolie (mere end 35 wt. %) med den største brintmætning pr. kulstof (H/C: 1.64). Derudover kan det konstateres, at bio-råolien primært består af fedtsyrer og fedtamider, som kommer fra det høje lipidindhold i biopulpen. På baggrund af disse resultater er der ligeledes udført en kontinuert kampagne i lille skala. Resultatet af den kontinuerte kampagne viser, at tilstedeværelsen af K2CO3 som homogen katalysator kan sikre en mere stabil drift ved at forhindre repolymerisering i anlæggets forvarmere. Desuden sikrer tilstedeværelsen af alkalikatalysatorer, at de uorganiske stoffer overføres til det solide restprodukt, hvilket faciliterer genindvinding af NPK.

For at håndtere den energikrævende behandling af HTL-vandfasen og i et forsøg på at øge den energi, der overføres til bio-råolien, er der i dette studie blevet recirkuleret en opkoncentreret del af vandfasen som en del af fødeblandingen. Ved at fjerne det overskydende vand bibeholdes processens værdikæde uden et behov for ekstra forbehandling inkl. tørring af biomassen. De primære resultater viser, at inddampningen af vandfasen kan eliminere op til 30 wt. % af det totale nitrogenindhold i vandfasen samt 60 wt. % af ammoniakken, alt imens mere end 80 wt. % af kulstoffet forbliver i cyklussen. Produktfordelingen afslører en signifikant stigning i både massen af den producerede bio-råolie på mere end 8 wt. % og i

kulstofindholdet i bio-råolien på mere end 4 % samt energigenindvinding efter gentagne recirkuleringscyklusser. På den anden side indikerer den kemiske komposition en stigning i N-holdige stoffer, primært i form af fedtamider og N-hetrocykler, i de efterfølgende cyklusser som, hvis de ender i det endelige brændstof, kan have en negativ effekt på motorens ydeevne og udstødningsgassen. Derfor er et efterfølgende trin med hydrogenering ved to forskellige operationelle betingelser blevet udført. Resultaterne viser en højere N-fordeling i den efterfølgende opgraderede bio-råolie. Dette kan muligvis hænge sammen med de svært nedbrydelige N-hetrocykler, som stammer fra cykliserings- og Maillard reaktionerne. Det kræver voldsomme hydrogeneringsbetingelser (høj temperatur, højt partialtryk af brint samt WHSV), hvilket kan have en negativ effekt på procesøkonomien og derudover lede til deaktivering af katalysatoren.

Den resulterende bio-råolie fra den kontinuerte kampagne er blevet benyttet i et andet studie, for at vurdere om HTL-brændstoffet er egnet til at iblandes diesel efter de gældende specifikationer. Indflydelsen af et mildt stabiliseringstrin sammen med vakuumdestillering er blevet undersøgt med hensyn til destillatgenindvinding samt kemiske og fysisk-kemiske egenskaber. Efterfølgende er en multiobjektiv optimeringsmetode blevet udviklet for at optimere selektiviteten af bio-råolie destillater, så de blandede fraktioner kan blandes med referencedieslen. De producerede brændstoffer er blevet testet i en intern forbrændingsmotor for at overvåge brændstofemissionsprofilerne. Resultaterne viser, at den rå og den hydrogenerede bio-råolie afviger markant fra specifikationerne annonceret af EN590 for vejdiesel. Derudover er der også registreret udfordringer med iblandingen af bio-råolien samt stabiliteten af brændstoffet ved lagring, hvilket tilsammen afskriver disse bio-råolier som mulige dieselblandinger. På den anden side har de vakuumdestillerede bio-råolier vist sig markant at forbedre de fysisk-kemiske egenskaber af brændstoffet, hvormed det opfylder specifikationerne for iblanding i diesel. Det milde hydrogeneringstrin (forhåndsstabilisering) har bidraget signifikant til at øge destillatet fra 22.6 til 55.6 wt. % ved at fjerne oxygenerede stoffer og forebygge repolymeriseringsreaktioner under destilleringen. Desuden indikerer resultaterne, at HTL værdikæden kan optimeres baseret på de mest begrænsende fysisk-kemiske egenskaber for at maksimere bio-oliens andel i det endelige brændstof. Emissionsresultaterne er lovende for de hydrogenerede biodestillatblandinger med sammenligneligt indhold af SO_2, THC, CO og CO_2 som for referencedieslen.

Udbyttet af denne ph.d.-afhandling belyser fleksibiliteten ved HTL-processen til at nyttiggøre fugtigt organisk affald. Derudover bidrager afhandlingen med en fordelagtig metode til recirkulation af vandfasen som indeholder overskydende kulstof, imens den våde biomasse behandles. Afhandlingen adresserer udfordringer ved kontinuert operation af den biopulp-baserede HTL-proces, og den tilvejebringer en matematisk metode til at opnå et biobrændstof, som matcher iblandingskravene for diesel til vejtransport. Alt i alt støtter aktiviteterne belyst i denne afhandling opskaleringen og udviklingen af fremtidens HTL værdikæd.

Contents

Thesis Details

Thesis Title: Hydrothermal liquefaction of biopulp: Waste management and sustainable bio-blendstock production
Ph.D. Student: Komeil Kohansal Sadetmahaleh
Supervisor: Associate prof. Thomas Helmer Pedersen, Aalborg University
Co-Supervisor: Prof. Lasse Aistrup Rosendahl, Aalborg University

The main body of the thesis is based on the following scientific papers:

A. Komeil Kohansal, Saqib Toor, Kamaldeep Sharma, Rupa Chand, Lasse Rosendahl, and Thomas Helmer Pedersen. *Hydrothermal liquefaction of pretreated municipal solid waste (biopulp) with recirculation of concentrated aqueous phase.* (Biomass and Bioenergy, Elsevier). https://doi.org/10.1016/j.biombioe.2021.106032

B. Komeil Kohansal, Kamaldeep Sharma, Muhammad Salman Haider, Saqib Sohail Toor, Daniele Castello, Lasse Aistrup Rosendahl, Joscha Zimmermann, and Thomas Helmer Pedersen. *Hydrotreating of bio-crude obtained from hydrothermal liquefaction of biopulp: effects of aqueous phase recirculation on the hydrotreated oil.* (Sustainable Energy and Fuels, RCS). http://dx.doi.org/10.1039/D2SE00399F

C. Komeil Kohansal, Kamaldeep Sharma, Saqib Sohail Toor, Eliana Lozano Sanchez, Joscha Zimmermann, Lasse Aistrup Rosendahl, and Thomas Helmer Pedersen. *Bio-Crude Production Improvement during Hydrothermal Liquefaction of Biopulp by Simultaneous Application of Alkali Catalysts and Aqueous Phase Recirculation.* (Energies, MDPI). https://doi.org/10.3390/en14154492

D. Komeil Kohansal, Eliana Lozano Sanchez, Shivang Khare, Karl Oskar Pires Bjørgen, Muhammad Salman Haider, Lasse Aistrup Rosendahl, and Thomas Helmer Pedersen. *The actual potential of hydrothermal liquefaction-driven fuel in being used as an automotive diesel bio-blendstock.* (Submitted to Fuels, Elsevier)

Moreover, the following contributions and publications have been made during the Ph.D. period:

Publications

- Rupa Chand, Komeil Kohansal, Saqib Toor, Thomas Helmer Pedersen, Jes Vollertsen. *Microplastics degradation through hydrothermal liquefaction of*

wastewater treatment sludge. (Journal of cleaner production, Elsevier). https://doi.org/10.1016/j.jclepro.2022.130383

- Ayaz Ali Shah, Saqib Sohail Toor, Tahir Hussain Seehar, Komeil Kohansal Sadetmahaleh, Thomas Helmer Pedersen, Asbjørn Haaning Nielsen, and Lasse Aistrup Rosendahl. Bio-crude production through co-hydrothermal processing of swine manure with sewage sludge to enhance pumpability. (Fuel, Elsevier). https://doi.org/10.1016/j.fuel.2020.119407

- Kamaldeep Sharma, Komeil Kohansal, Antonio Jaime Azuara, Lasse Aistrup Rosendahl, Donghong Yu, and Thomas Helmer Pedersen. *Green and facile recycling of bauxite residue to the biochar-supported composite material for hydrothermal liquefaction of municipal solid waste.* (Submitted to Waste management, Elsevier)

Conference contributions:

- Komeil Kohansal, Kamaldeep Sharma, Saqib Toor, Thomas H Pedersen, Lasse Rosendahl. *Effect of different alkali catalysts on hydrothermal liquefaction of biopulp with the recirculation of the concentrated aqueous phase.* (Oral presentation at AIChe annual meeting, 2020)

- Komeil Kohansal, Lasse Rosendahl, Saqib Toor, and Thomas Helmer Pedersen. *Water and nitrogen management in hydrothermal liquefaction of urban waste.* (Oral presentation at the 28th e-European Biomass Conference and Exhibition (EUBC & E), 2020).

- Komeil Kohansal, Thomas H Pedersen, Saqib Toor, Kamaldeep Sharma, and Lasse Rosendahl. *Hydrothermal liquefaction of processed municipal solid waste; an overview of the challenges and opportunities.* (Oral presentation at TCS 2020 conference, 2020).

- Rupa Chand, Komeil Kohansal Sadetmahaleh, Thomas Helmer Pedersen, Saqib Toor, Jes Vollertsen. *The fate of microplastics when making sludge into crude oil–the impact of a hydrothermal liquefaction process on microplastics in wastewater treatment plant sludge.* (Oral presentation at Micro2020: Fate and Impacts of Microplastics: Knowledge and Responsibilities, 2020).

- Komeil Kohansal, Kamaldeep Sharma, Daniele Haider, Muhammad Salman, Saqib Sohail Toor, Daniele Castello, Lasse Aistrup Rosendahl, Joscha Zimmermann, and Thomas Helmer Pedersen. *Catalytic hydrotreating of bio-crude obtained from hydrothermal liquefaction of biopulp.* (Oral presentation at the 30th e-European Biomass Conference and Exhibition (EUBC & E), 2022).

- Kamaldeep Sharma, Komeil Kohansal, Antonio Jaime Azuara, and Thomas Helmer Pedersen. *Green Reduction of Bauxite Residue to Iron Zero-Based Catalyst for Hydrothermal Liquefaction of Municipal Solid Waste. (Oral presentation at the 28th e-European Biomass Conference and Exhibition (EUBC & E), 2022)*

This thesis has been submitted for assessment, partially fulfilling the Ph.D. degree. The thesis is mainly based on the above-listed submitted and published scientific papers. Parts of the papers are directly or indirectly used in the extended summary of the thesis. The co-author statements are provided to the assessment committee and are also available to the faculty. The thesis is not acceptable for open publication in the present form but only limited and closed circulation as copyright may not be ensured.

Preface

به نام زن زندگی آزادی[1]

"What would you do if you weren't afraid?[2]*"* I whispered to myself while going down the airplane stairs on 1st September 2019 at Aalborg airport. There was quite a journey ahead, but I knew *searching a maze was always better than remaining in a cheeseless station*[2]. And I was right. It was a long, challenging, and adventurous journey full of ups and downs, lightsome and gloomy moments, but I enjoyed every corner of it.

I would like to express my gratitude to my supervisor, Associate prof. Thomas Helmer Pedersen for supporting and encouraging me to learn, grow, and prosper. I am also grateful to my co-supervisor, Prof. Lasse Aistrup Rosendahl, for giving me the opportunity to work on the project I was in love with. I also like to thank my colleague and friends in the team 'Advanced Biofuels', Mohammad, Antonio, Swanand, Fatma, and others. I extend my gratitude to my supervisor at NTNU, Norway, Prof. Terese Løvås, and my colleagues Karl, Shivang, and others in the team 'Comkin' who hosted and munificently helped me during my stay abroad studies.

I must appreciate my family in Aalborg, Soha, my dearly loved wife, and best friend, who walked alongside me through all the Ph.D. and life's ups and downs. I would also like to thank my beloved family in Iran, my parents and siblings, Mohammad and Maryam, who loved, supported, and encouraged me in every step I have taken. Last but not least, a big thanks to Mina, Majid, Mastideh, Hamed, Samaneh, Alireza, Bahare, Amir, and Sayeh, whom I rely on the most during tough times.

This thesis is submitted to the faculty of Engineering and Science, Aalborg University, Denmark, as a requirement for fulfilling the degree of Doctor of Philosophy. The Ph.D. program was initiated on September 2019 within the Advanced biofuel research group at the Department of Energy technology (now known as AAU Energy). The project was funded and supported by European Union's Horizon 2020 Research and Innovation Programme under grant agreement no. 818413 (NextGenRoadFuels project).

[1] *In the name of 'Woman, Life, Freedom'*

[2] *Spencer Johnson, Who Moved My Cheese?*

To all the Iranian women. To Mom, Soha, and Maryam.

Nomenclature

HTL	Hydrothermal Liquefaction	NaOH	Sodium hydroxide
IEA	International Energy Agency	Na_2CO_3	Sodium carbonate
GHG	Green House Gas	K_2CO_3	Potassium carbonate
MSW	Municipal Solid Waste	HCOOH	Formic acid
BP	Biopulp	TAN	Total Acid Number
EROI	Energy Return On Investment	TOC	Total Organic Carbon
HT	Hydrotreating	TN	Total Nitrogen
APR	Aqueous Phase Recirculation	NH_4^+-N	Total Ammonia
TRL	Technology Readiness Level	STA	Simultaneous Thermogravimetric Analyzer
NPK	Nitrogen, Phosphorus, and potassium	TGA	Thermogravimetric analysis
AD	Anaerobic Digestion	SimDis	Simulated Distillation
MECs	Microbioal Electrolysis Cells	ICP-AES	Inductively Coupled Plasma Atomic Emission Spectroscopy
MFCs	Microbioal Fuel Cells	FTIR	Fourier Transform Infrared spectroscopy
HTG	Hydrothermal Gasification	GC–MS	Gas Chromatography-Mass Spectrometry
H_2	Hydrogen gas	ER	Energy Recovery
CO	Carbon monoxide	HHV	Higher Heating Value
CO_2	Carbon dioxide	DCM	Dichloromethane
SO_2	Sulfur dioxide	AC	Acetic Acid
NOx	Nitrogen oxides	CA	Citric acid
THC	Total Hydrocarbon	MEK	Methyl ethyl ketone
TPM	Total Particulate Mass	WHSV	Weight Hourly Space Velocity
TPN	Total Particulate Number	AET	Atmospheric Equivalent Temperature
RWGS	Reverse Water Gas Shift	TBP	True Boiling Point
BC	Biocrude	IBP	Initial Boiling Point
BCD	Biocrude Distillate cut	S	Sulfur content
HTBC	Hydrotreated Biocrude	N	Nitrogen content
HTD	Hydrotreated biocrude Distillate cut	ρ	Density
BCDM	Distillate Mixture of Biocrude	v	Kinematic viscosity
HTDM	Distillate Mixture of Hydrotreated Biocrude	η	Dynamic viscosity
Ref	Reference Diesel	MC	Microcarbon residue

C_0	HTL Control Run	WC	Water content
$C_{(1-n)}$	Cycle 1-n	CP	Cloud Point
KOH	Potassium hydroxide	CI	Cetane Index
FAME	Fatty Acid Methyl Ester	dp	Differential Pressures
DAF	Dry Ash Free	MFC	Mass Flow Controller
db	Dry basis	WGS	Water Gas Shift
OACIC	Optically Accessible Compression Ignited Chamber		
MFSP	Minimum Fuel Selling Price		

Part I: Extended Summary

Chapter 1: Introduction

On November 13, 2021, after almost two weeks of intense negotiations, COP26 revealed the concluded agreement on accelerating the immediate climate action and completing the Paris rulebook. As short-term diplomacy, the so-called Glasgow Climate Pact was decided to focus on driving the actions across four global achievements, including Mitigation, Adaption, Finance, and Collaboration. In the mitigation section, the countries agreed on strengthening commitments on stretching goals of the Paris rulebook, where 195 countries established ambitious targets to limit the temperature increase (ΔT) below 2 °C to that of the pre-industrial average.

1.1. Climate Change or Climate Action: that is the question!

According to the National Aeronautics and Space Administration (NASA), the global surface temperature of the earth has increased by 0.84 °C compared to the average temperature from 1951 to 1980. The monitored data declares a skyrocketing trend with an exponential pace after 1980. The last decade (2011-2020) and 2020 were respectively recognized as the warmest decade and year on record (1). Scientists have considered an average increase of 2 °C as the verge of catastrophic and dangerous climate events, such as changing 'water cycle' speed and precipitation, rising sea levels, acidic ocean water, changes to ocean currents, the risk to life on lands and marine life, etc. Data also reveal that with the current pace of human activities, industrialization, and Greenhouse gas (GHG) emissions, the average earth temperature will rise to around 4 °C by 2100, that likely risks life on earth (2).

GHG emissions, including but not limited to carbon dioxide, methane, sulfur dioxide, and nitrous oxides having a heating-trap effect, are known as the chief drivers of global warming. Carbon dioxide is known as the earth's most crucial GHG emission since it absorbs and radiates the heat toward the earth maintaining a hospitable temperature. However, the accumulation of CO_2 in the atmosphere due to human thirst for energy imbalances its concentration and leads to higher radiations toward the blue planet. A great deal of the emitted CO_2 originates from burning fossil fuels to meet the energy demands of the industrialized world. The underground energy-dense liquid/solid/gas fuel precursors contain the carbon in the fossilized organic material formed over millions of years. However, human activities in the past centuries are exhuming the buried carbon into the carbon cycle in a relatively short period of time. With the concurrent deforestation, the generated carbon-containing gases (e.g., CO_2, CO, and CH_4) accumulate in the atmosphere and ultimately result in global warming. Atmospheric CO_2 data reported by the Global carbon project revealed that from 1750 to 1840, the net CO_2 concentration was well-kept below 300 ppm; however, after the industrial revolution, the ascending trend was initiated and leveled up to 420 ppm in 2021 (3).

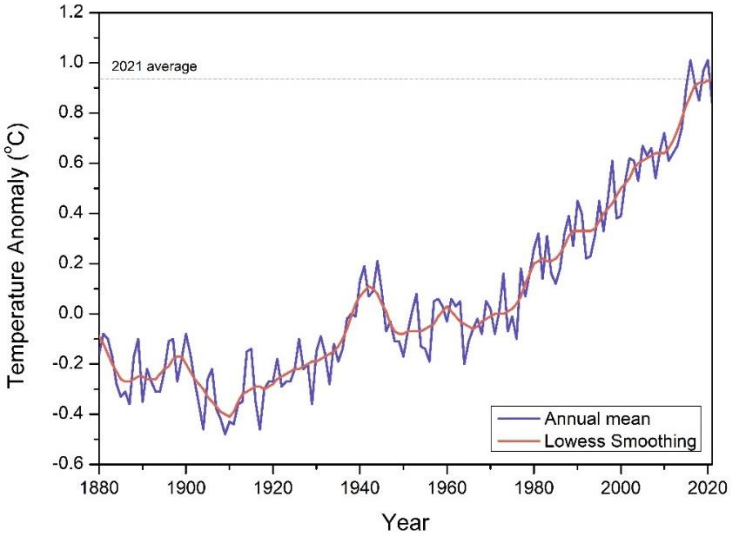

Figure 1. Global temperature index (Credit: NASA/GISS) (1).

In response to the catastrophic footprints of human-being on natural resources and ecosystem services, the United Nations World Commission on Environment and Development released a report outlining the first institutionalized definition of sustainable development as '*Sustainable development is a development that meets the needs of the present without compromising the ability of future generations to meet their own needs*' in 1987 (4). In 2015, the integration and indivisibility of Sustainable Development Goals to address global challenges such as climate change, environmental degradation, inequality, poverty, etc. were declared in United Nations General Assembly. In the same year, the Paris agreement reflected the urgent threat of climate change by announcing a temperature goal set, by which the increase in the global mean temperature should principally be held below 2 °C above the pre-industrial levels and be further limited to 1.5 °C. The convention also asserted that in order to reduce the impacts and risks of climate change, the parties should aim to reach the global peaking of GHG as soon as possible. International Energy Agency's '2 °C scenario' (2DS) outlined a 70 % CO_2 emission reduction goal by 2060, by which the chance of limiting the average global temperature to 2 °C by 2100 will increase by at least 50 %. The United States Environmental Protection Agency (EPA) has named the most practical strategies to mitigate GHG emissions, focusing on energy efficiency, using renewable energies, supply chain, waste reduction, and diversion strategies, reducing methane emissions, and increasing fuel efficiency in transportation and logistics of which **using renewables** and **changing the waste management strategies** are of high priority (5).

1.1.1. Role of Renewables in the Transportation Sector

As shown in **Figure 2**, the world is still highly reliant on the fossil fuels such as oil, natural gas, and coal. To cope with the emerging climate change, global warming and

to comply with the Paris agreement, scientists and policymakers have requested an instantaneous shift to renewable energies. Substitution of conventional fossil-based fuels with renewables can greatly omit adding more GHG to the ecosystem.

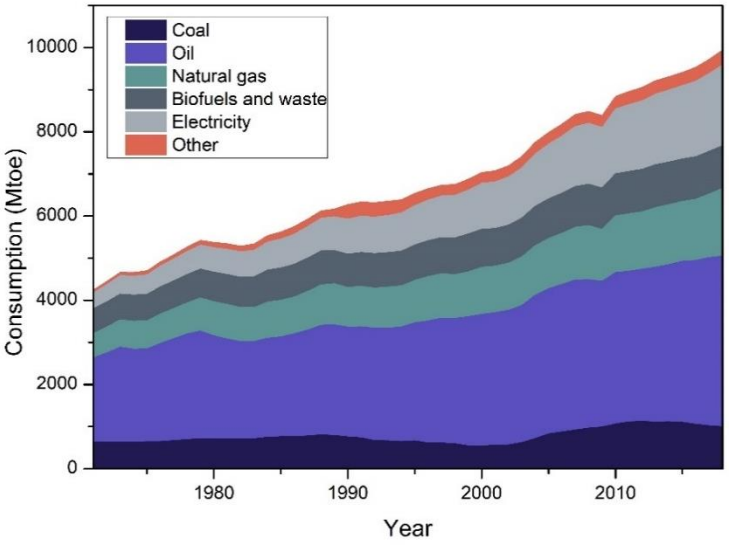

Figure 2. Worldwide energy consumption as a function of energy source (6).

As shown in **Figure 2**, by early 2020, over 40 % of the world's annual energy demand was fulfilled by fossil-based oil (6). Road transport, non-energy use, and aviation are the three primary consumers of petrocrude fuels, with 49.2, 16.7, and 8.6 % of the contribution, respectively. Additionally, the statistics have shown that in 2020, the share of final energy consumption of the EU's transportation sector has reached a considerable number of 30 %. The statistics also disclosed that the transportation sector is responsible for 23 % of global CO_2 emissions (7). Therefore, the world seemingly needs urgent incorporation of renewables into the transportation sector. Despite the electrification strategies taken by many countries, developing electric vehicles and implementing the relevant infrastructure seem to be far-fetching goals. Therefore, the immediate substitution of conventional fuels with renewables that are compatible with the existing infrastructure can be viewed as a short and medium-term solution. Meanwhile, the data indicate that current liquid fuels such as gasoline and diesel are the leading energy carriers in the EU's transport sector (9). Therefore, a compatible alternative liquid biofuel that originates from in-cycle carbon material is highly demanded.

In 2005, IEA published the first World Energy Outlook reflecting the inflating oil demand and Hubbert's peak oil theory. The theory, in short, states that with the current use, approximately 50 years' worth of petroleum crude is left in the earth's natural oil reservoirs (10). They also concluded that with the disruption of oil supply, many critical industries, such as agriculture, transportation, pharmaceutical, etc., would experience unprecedented price shocks, which in turn cause unstable economies

worldwide. Furthermore, greenhouse gas emissions were highlighted to cause catastrophic climate changes if left unfettered (11). Therefore, many nations initiated widespread policies toward introducing renewable carbon-neural fuels to their annual energy expenditures.

Initially, the EU held first-generation biofuels such as bioethanol and biodiesel as pathways to mitigate climate change; however, further research has emphasized that crop-based fuels will soon lead to increased stress on land resources that ultimately end up in major deforestation. Moreover, first-generation biofuels can potentially inflate food prices and threaten food security. Apart from the socioeconomic impacts, first-generation biofuel production has indicated numerous environmental challenges, such as water consumption/pollution, biodiversity loss, atmospheric pollution, etc. (12). As a result, the sustainability of biofuels has become a vital policy topic. EU-Renewable Energy Directive (REDII-Annex IX) has set a series of strict regulations of sustainability criteria such as food security, biodiversity loss, and GHG emissions that must be applied before the commercialization of biofuel production from a particular feedstock in a specific region within the EU (13). Despite the existence of these policies supported by voluntary standards, the vulnerability of the feedstock supply chain to environmental and political unexpected events is still an unaddressed challenge. The following paragraphs take biodiesel as an instance to declare the considerable impact of a political event on the *'biofuel versus food'* debate.

Biodiesel is defined as the liquid fuel obtained from renewable raw materials such as vegetable and animal oils through the transesterification process. The process converts the structural crude lipid to ester molecules (biodiesel) and glycerol as a coproduct in the presence of an alcohol and process catalyst (14). Currently, biodiesel from virgin vegetable oils is beingly heavily introduced to the EU's transport sector due to its benefits of improving energy balance and security, reducing emissions, enhancing air quality, and optimizing engine operations. ASTM D6751 has regulated the blending scenarios of biodiesel with petroleum diesel/distillate. For instance, the biodiesel produced in the US is being consumed in blends with different ratios from 2% (B2), 5% (B5), 20 % (B20), to 100% (B100) (15). Moreover, to prolong the lifetime of compression-ignition vehicles, it is advised to use 1% biodiesel in the fuel due to its lubrication properties. Despite all the advantages given by first-generation biodiesel, biodiesel production significantly depends on food crops. Rapeseed, sunflower seed, soya, etc., are the main feedstock used in the EU’s biodiesel plants (16). The dependency on food crops could potentially risk food supply security and affordability in many cases.

Taking the Ukraine war as an instance, millions of people happened to be at risk of hunger because of food shortages and unstable economies. Ukraine and Russia supply a significant share of food crops that have a mutual application for biodiesel and food production(17). With the increasing food price resulting from the war and raising the pressure on biofuel producer companies, the 'food against biofuel' has again become a hot debate. The studies showed that the missing export of Ukrainian corn and other food crops could be addressed with a 50 % reduction of the grains utilized for biofuels. On the other hand, limiting biofuel production could potentially result in various diverse economic and environmental impacts like losing energy independency, farm income security, and directly and indirectly related jobs (18). Furthermore, it will

likely lead to increasing fossil fuel imports and carbon emissions contrary to the Paris agreement's target points. Seeking a solution that on one hand does not harm the food supplies and, on the other hand, can be altered with the renewable share of the road diesel, many scientists have suggested using the second generation renewable diesel originating from thermochemical processes such as pyrolysis and hydrothermal liquefaction (HTL).

1.1.2. Moving Toward Better Waste Management Strategies

As mentioned above, changing the waste management strategies is among the most immediate actions that need to be applied to diminish the environmental GHG emission footprint. According to Eurostat, the waste sector was the fourth-largest source of emissions, generating 3 % of total GHG emissions in 2017 (19). The ever-increasing human population and urbanization trend have led to an unprecedented peak in the generation of post-consumer wastes such as municipal solid waste (MSW). Presently, 55 % of the world's population resides in urban areas, which is 25 % higher compared to 1950, and estimations show that the number will further increase to 68 % by 2050. As stated by Eurostat, the average European MSW generation has reached the alarming level of 500 kg/y capita and, if it remains untacked, will continue to increase to 700 kg/y capita in the following decades (20).

EPA encircled the waste sector into industrial waste landfills and wastewater treatment systems, municipal solid waste (MSW) landfills, and facilities that operate combustors or incinerators to dispose solid waste. MSW landfills accounting for 82 % of total GHG emissions are among the main contributors to climate change derived from the waste sector (21). The EU's legislation has compelled waste treatment organizations to substitute landfills with recycling technologies. As a result, despite the sharp increment in waste generation, landfill application dropped by 60 %. However, it should be noted that the capacity of recyclable MSW is optimistically limited to 12 % plastic, 5 % glass, and 4 % metal constituents. MSW, on average, contains approximately 44 % of food and green waste that used to be landfilled, combusted, or composted (22). Due to the wet nature of the organic matter of MSW, combusting is typically associated with high energy demand and low energy efficiency. On the other hand, the composting operation raises concerns about producing bioaerosol, dust, and leachate that can adversely affect the surrounding air and subsurface areas (23). Moreover, direct combustion and composting are known as the second and third-largest waste sector GHG emitters.

When household waste is disposed, the organics get heavily polluted with other inorganic streams. However, emerging new segregation technologies, like mechanical, biological, and/or mechanical-biological treatment processes, have opened up the possibilities of taking advantage of the embodied energy in the organic waste stream. Among various biological treatments, the anaerobic digestion of biodegradable wastes into biogas has gained paramount interest due to its cost-effectiveness, high energy recovery, and process simplicity (24). Despite the remarkable benefits of anaerobic digestion in converting waste management challenges to energy production solutions, economic viability is still the main bottleneck that requires multidisciplinary research communities to support its

business-scale adoption and implementation (25). Moreover, the end product of the process is in the gaseous phase, which has minimal applications in some of the highly energy-consumer sectors such as transportation.

Therefore, adopting a process that not only can minimize organic waste disposal issues but also highly contributes to the production of a storable liquid fuel has attracted many interests. Pyrolysis and hydrothermal liquefaction (HTL) are specifically named as the most applicable thermochemical processes that can efficiently generate advanced biofuels by consuming the organic stream of MSW.

1.2. Hydrothermal Liquefaction: A Multi-Beneficiary Process

Hydrothermal liquefaction, abbreviated as HTL, is a thermochemical process that employs water to serve multiple functions, such as reaction medium and catalyst, to disintegrate the biomass's macromolecules. The bond breakage of the biomass's building blocks requires high activation energy. Therefore, HTL mainly carries out at high pressures (5-35 MPa) and mild temperatures (280-400 °C) (26). The inherent aqueous medium of the HTL process makes it a superior option to pyrolysis while valorizing wet biomass since it can phase out the energy-intensive pre-drying step from the feedstock value chain. Two sub-categories of HTL based on the operating temperature (and pressure) are sub/near critical and supercritical liquefactions named after the critical point of water (374.1 °C, 22.1 MPa). Subcritical and supercritical water behaves differently than water under ambient conditions due to the drastic variations in its physical-chemical properties.

Below its critical point, water presents a two-phase liquid-vapor equilibrium with a continuous gradual decrease of density before the vaporization point. On the contrary, a homogeneous fluid phase gets formed above the critical point. The density of the water, as shown in **Figure 3,** falls discontinuously when the process conditions approach the critical point of water, which has immense impacts on the diffusion properties and solvent power. Therefore, the choice of reaction temperature and pressure may greatly reflect the kinetics of the HTL process (catalytic effect) (27).

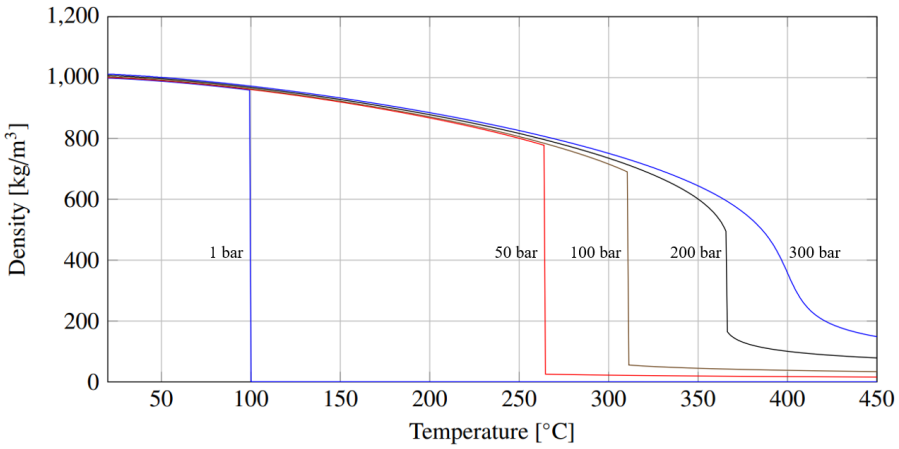

Figure 3. Density variations upon changing temperature and pressure (28).

The relative permittivity, also known as the dielectric constant, indicates the liquid polarity by measuring the absolute permittivity of the liquid divided by that of the vacuum. As a polar solvent, water merely dissolves highly polar molecules under ambient conditions and shows poor miscibility with hydrocarbons. However, at higher HTL processing conditions, the dielectric constant of water declines, resulting from reduced Columbus forces (hydrogen bonds) between the molecules. As a result, the water becomes a competent solvent for hydrophobic organic molecules (28). As shown in **Figure 4**, the static dielectric constant of water continuously decreases with increasing process temperature at constant pressure. Medium to low dielectric constants (subcritical water condition) promotes the degradation of macrochemicals, an excellent medium for ionic reactions. On the other hand, at very low dielectric constants in the supercritical region, water becomes a nonpolar solvent governing free radical reactions (29). Thus, the operational condition can significantly impact the HTL chemistry.

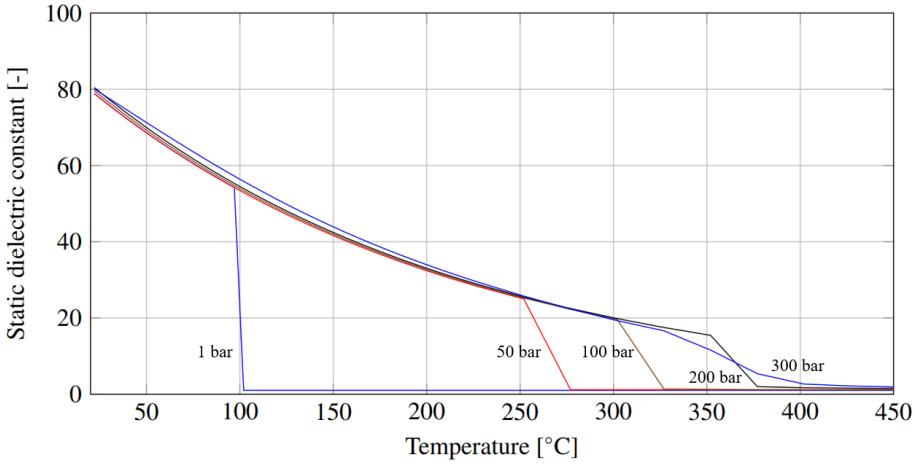

Figure 4. Dielectric constant variations upon changing temperature and pressure (28).

1.3. Challenges and Opportunities

1.3.1. Continuous HTL Operation of MSW

HTL is known as a biomass-agnostic technology that can take advantage of the embedded calorific value of different kinds of waste streams. Moreover, the organic fraction of MSW stands as a challenging issue for waste treatment organizations, as legislations strictly limit direct landfill. In recent years, studies have delved into exploiting different types of MSW in the HTL process aiming to optimize the process parameters and explore the governing chemical pathways (30). For instance, PNNLs 2021 SOT targeted the source-segregated pure food waste collected from different sites and assessed various scenarios of their valorization via HTL as the core technology (31). Bayat et al. investigated the HTL process parameters on food waste collected from a restaurant's dining hall (32). In Another study, Wang et al. utilized canteen food residue as a representative of the organics in MSW and studied the biocrude production and its upgrading (33). Despite having valuable information, the studies concerning HTL of organic fraction of MSW lack utilizing real biomass originating from municipalities and therefore have not been scaled up to commercial or even bench-scale. The reason is likely the incorporation of non-biodegradable substances with the organic fraction in the household-sorted MSW that potentially emerges several operational and technical challenges, such as pumping and slurry clogging issues in continuous units. As reported, achieving an uninterrupted and continuous HTL operation requires a pumpable, homogeneous, and stable slurry with an average particle size being less than 100 µm (34)(35). Therefore, the role of a biomass pre-treatment technology capable of removing the non-biodegradables and generating a homogeneous slurry is vital.

Regardless of the region, MSW generally contains food waste, garden waste, metals, non-metals, paper, glass, plastic, soil, etc. To avoid system clogging caused by depositions, the HTL feed has to contain minimal inorganic content, ideally below 10

% (db). Furthermore, the solid concentration, the so-called dry matter content of the slurry, is advised to be kept below 30 %, as otherwise, the process gets prone to a variety of operational challenges, such as issues associated with slurry clogging in the feeding system. Lower dry matter content could principally favor the smooth operation of a continuous HTL unit; however, it conversely sacrifices energy efficiency. Studies have concluded that 15-25 % dry matter is the optimal value (36). The required pre-treatment system should initially be able to remove the sizeable non-biodegradable material such as plastics, metals, and glass particles. The recovered stream can be separately transferred to recycling plants. The remnant consisting of a significant portion of biodegradable organics has to be mixed with water and pass through different grinding steps to achieve the appropriate particle size. Afterward, the ground slurry should expose to de-watering steps to tune the desired dry matter content (37).

Integration of the HTL process into an already existing MSW pre-treatment technology offers significant opportunities by ensuring the sustainability of the feedstock. There is minimal information regarding the valorization of real-life municipality-sourced MSW in the literature. Moreover, the impact of HTL operational conditions on the non-biodegradable free organic portion of MSW has not been addressed before.

1.3.2. Residual Aqueous Phase Treatment

During the HTL process, a complicated network of simultaneous reactions such as hydrolysis, decarboxylation, decarbonylation, and dehydration takes place, defragmenting the macrostructure of the biomass to HTL intermediates. The intermediates undergo various reactions, including cyclization, deamidation, amination, esterification, etc., to generate biocrude range molecules. Moreover, repolymerization reactions such as condensation can take part in producing heavy biocrude or solid residue components. Depending on the biomass' biochemical structure, various polar heteroatom-containing compounds like light acids and alcohols might end up in the aqueous phase, which is considered a cumbersome HTL by-product. Previous studies have shown that approximately 40-60 % of the input carbon might be distributed to the aqueous phase, leading to a considerable energy loss and complicating the technical scalability and economic viability of the process if it remains unaddressed (38,39).

Moreover, the aqueous phase is normally rich in primary nutrients such as nitrogen, phosphorus, and potassium (NPK). Techno-economic analysis results indicated that traditional treating of the HTL aqueous phase through existing wastewater treatment plants might contribute to 90 % of the HTL total waste disposal cost (40). On the other hand, the life cycle assessment carried out by Orifield et al. revealed that by recovering the energy from the aqueous phase, the energy return on investment (EROI) of the whole process could increase by 20 % (41). The gap between the scenarios with and without an efficient aqueous phase valorization is more prominent when using additives in the biomass slurry, such as alkali catalysts (considerable divergence in MFSP). Thereby, the aqueous phase valorization techniques should be significantly

improved to enhance the feasibility and technology readiness level (TRL) of the main process.

Various studies have exploited the nutrient-rich HTL aqueous phase to enhance microalgal growth (42,43). The results showed that, in many cases, algae cultivation in the aqueous phase could increase the biomass concentration compared to conventional synthetic media (44). Despite the advantages, some studies have witnessed the presence of growth inhibitors and toxic compounds in the HTL aqueous phase that could adversely affect strain growth (45). Dilution of the aqueous phase and incorporation of zeolite and activated carbon have been suggested for remediation of HTL-driven media; however, involving fresh water and expensive adsorbents can practically result in a lower economic viability of the HTL process (46,47). Anaerobic digestion (AD) of HTL aqueous phase to produce biogas has attracted extensive attention owing to its relatively greater resilience toward toxic substances (48). However, depending on the biomass and the HTL processing condition, the inhibitor compounds, such as phenols and heterocyclics, end up in the growth medium, negatively affecting the treatment process performance. To tackle the issue, the addition of activated carbon and/or integration of ozonation to AD have been proposed (49,50). The results revealed a significant enhancement in the biodegradability of refractory compounds, while the cost-effectiveness of the process was negatively impacted (50). Microbial electrolysis cells (MECs) and Microbial fuel cells (MFCs) are relatively new bioelectrochemical systems that involve waste organics in the production of electrons (51,52). Albeit Microbial cells have indicated a considerable performance in valorizing heavily concentrated wastewater streams, their scaling up and commercialization potential are yet to be explored (53).

Electrochemical and wet oxidation processes are other well-practiced technologies that can significantly decrease the chemical impurities of the water on one hand and valorize the organic carbon into C-containing gases (54). The produced CO_2 can potentially further convert to CO (RWGS), which, combined with H_2 gas, delivers the needed syngas for Fischer-Trpsch synthesis. Despite the benefits, valorization of the aqueous phase by this means introduces a significant capital cost to the biocrude value chain. Furthermore, the system is highly reliant on expensive H_2 gas. Although in the advanced designs, the HTL off-gas is deemed as a primary source of H_2, the system still requires an external intake of hydrogen. Hansen et al. analyzed the techno-economic properties of an HTL plant conjugated to an eFUEL system, including partial oxidation. The analyses have shown that the final fuel price is highly sensitive to the H_2 price (55).

Hydrothermal gasification (HTG) is among the thermochemical methods used for valorizing of HTL aqueous phase to essential chemical compounds, namely hydrogen, carbon dioxide, carbon monoxide, and methane at high temperatures (>400 °C) with or without the presence of catalysts (52). The obtained hydrogen gas has been suggested to be cycled into the hydrotreating process. HTG is also of particular interest as it offers a nearly complete degradation of all the retained organics, including toxic pollutants, but the required high temperature is an obstacle diminishing the economic viability of the process (56). Incorporating catalysts into HTG is reported to significantly increase H_2 production primarily through enhancing

the kinetics of water-gas shift and steam reforming reactions with the expense of additional cost that dominates its valuable environmental benefits.

Recent investigations have disclosed the potential of the aqueous phase to be recycled back to the main process to substitute the need for fresh water. By doing so, not only will the economic feasibility of the process incredibly enhance by generating more products of interest (biocrude), but also the environmental safety of the process can be guaranteed by producing fewer volumes of disposal water (aqueous waste). Hu et al. evaluated the impact of aqueous phase recirculation in a consecutive series of *C. vulguris* microalgae HTL reactions utilizing two homogeneous catalysts (Na_2CO_3 and HCOOH). The recirculation considerably contributed to a higher biocrude yield as well as lower aqueous disposal waste (57). Biller et al. studied the recirculation of HTL process water obtained from HTL of dried distillers grains with and without the presence of K_2CO_3 as a homogeneous catalyst in two separate sets of experiments. Significant enhancement in biocrude yield was obtained in both sets, with an early plateau reached when using the catalyst (30). A study by Zhu et al. reported a similar trend, concluding a visible biocrude yield promotion after three consecutive cycles while treating barely straw at hydrothermal liquefaction conditions (59). The quality of the biocrude has also been shown to experience variations after aqueous phase recirculation. Many studies have reported a higher carbon content in the subsequent cycle than that of the control test (57). Monitoring the heteroatom content has been of high importance since it can remarkably influence the proceeding upgrading scenarios. Various studies have indicated that recirculating the aqueous phase might unwantedly increase the heteroatom content of the ultimate product. For instance, Biller et al. observed a 1.9 wt. % nitrogen content increased during nine consecutive cycles, while the oxygen did not follow any specific trend (58). In another study, Shah et al. reported a 2.3 wt. % of nitrogen content elevation after eight cycles (60).

Limiting the viewpoint on biocrude makes aqueous phase recirculation seemingly a simple tradeoff between quality and quantity. However, as the complex matrix of the biocrude calls for further upgrading techniques to produce a marketable fuel, viewing the impact of aqueous phase recirculation through the whole value chain is crucial. To the author's best knowledge, there is no available literature investigating the impact of aqueous phase recycling on the quantity and quality of an upgraded HTL fuel. Moreover, a plethora of literature highlights the flexibility of the HTL process in valorizing different biomass types, including highly moist biomass. However, no HTL study has focused on finding a solution to recirculate the organic constituents of the aqueous phase to the process when dealing with wet feedstock.

1.3.3. Advanced Blendstock Production

To meet the energy security and affordability targets, HTL-driven renewable fuels have been widely researched in recent decades. Despite the advantages, the primary product of HTL, as such, is a highly viscous black liquid containing a significant load of high molar weight and heteroatom-containing constituents that do not fall into the range of marketable fuels. Additionally, the produced biocrude typically contains a substantial quantity of inorganics, mainly in the form of inorganic salts and metal-organo molecules such as metal porphyrins. Compared to petroleum products, it

generally has a relatively lower calorific value, lower H/C ratio, and a high share of heavy compounds that negatively affect its physicochemical properties. Therefore, it does not meet the requirements of drop-in transportation fuels. Hence, upgrading the raw biocrude has attracted notable interest in the literature and research communities. Various upgrading technologies have been adopted to augment the chemical, thermal, and physical properties of biocrudes, among which vacuum distillation is one of the most efficient.

Fractional distillation as an affordable physical upgrading technique has been continuously developed since the initial refineries were constructed. Being capable of organizing different biocrude commodities, it can physically simplify the matrix of the recovered fuel and hence facilitate producing renewable drop-in fuels such as gasoline and diesel. Distillation was reported to significantly improve the physical properties, such as viscosity and density of the recovered fraction compared to their precursor. The augmented viscosity can improve fuel atomization and potentially prevent various operational issues while combusting the fuels in engines (61). Watson et al. have reported a considerable TAN reduction in the high-end fractions. The lower acidity of the fuel secures the pipeline and the storage tanks from severe corrosion. They also monitored higher cold flow properties in the recovered fractions that can aid fuel transportation, storage, and handling, especially in cold environments (62). Pedersen et al. studied the fractional distillation of a biocrude obtained from glycerol-assisted HTL of aspen wood. The main findings revealed the tendency of light-oxygenated organics to be distributed in the lighter distillate fractions; therefore, lower O/C was witnessed in jet and diesel-ranged cuts (63). Other studies reported many other improvements in the diesel distillates' physical, chemical, and thermal characteristics of recovered distillates (19).

Diesel fuel provides a great range of efficiency, performance, and safety features and hence is being widely consumed in the transportation sector. With a relatively higher energy density, it offers more energy per unit of volume than that in gasoline. FuelsEurope has asserted that by 2022, diesel (Gasoil) is still the most demanded petroleum product in EU-27, accounting for 41.2 wt. % of refineries output. In the road fuel section, a gradually decreasing trend in gasoline demand was observed. In contrast, road diesel fuel demand significantly increased from approximately 125,000 Mtonnes per year in 2000 to 175,000 Mtonnes per year in 2022 and thus is still one of the main contributors to the high annual GHG emissions (64). The limited existing literature revealed a promising potential of biocrude in producing diesel equivalent fuel (20 to 40 wt.%) (65,66). Thereby, biocrude has been considered a prospective precursor for drop-in liquid transportation or blendstock fuel. However, the stringent diesel fuel specifications and the complex matrix of biocrude challenge the readiness of the HTL-derived diesel to be used as a drop-in automotive fuel. EN590, indicated in **Table 1**, has been introduced by European Committee for Standardization to regulate the physical properties of all road diesel fuels.

Table 1. EN590 specification for automotive diesel fuel.

Test	Unit	Limit	
		Min	Max
Cetane number	-	51.0	-
Cetane index	-	46.0	-
Density at 15 °C	g/L	820.0	845.0
Cloud point	°C	-	-7
Flash point	°C	55.0	-
Sulfur content	ppm	-	10
Viscosity at 40 °C	mm^2/s	2.0	4.5
Water content	ppm	-	200.0
FAME content	% m/m	-	0.1
Polycyclic Aromatics Content	% m/m	-	8.0
Oxidation Stability (16h)	g/m^3	-	25
Ash Content	% m/m	-	0.010
Carbon Residue	% m/m	-	0.30
Total Contamination	ppm	-	24.0

The oxygenated (and unstable) nature of the biocrude can result in condensation and repolymerization reactions in the distillation medium and lower the recovery yield. Moreover, the sulfur content and other deficient properties in the diesel fractions might deviate from the mentioned fuel specification. Thus, a pre-stabilization step that is capable of drastic oxygen and sulfur removal is seemingly required prior to vacuum distillation of the biocrude. Hoffman et al. fractionated a lignocellulosic-sourced biocrude in a vacuum distillation unit. The results demonstrated a considerable potential of the middle distillates in being introduced to the refinery units as co-processing streams. Moreover, the authors concluded an urgent need for biocrude stabilization (oxygen removal) prior to any further processing (66).

Like the refinery processes, thermal and catalytic cracking have been suggested by some studies to improve the chemical properties of biocrude (67). Despite the advantages, catalytic cracking and the excess energy given during the reaction result in very light hydrocarbons that, in turn, produce lighter fuel cuts after distillation, such as gasoline and jet fuel. On the other hand, catalytic cracking typically uses zeolite-based catalysts that are prone to be instantly poisoned and deactivated by the high nitrogen content of the biocrude.

Esterification is another practiced upgrading technique that has proven to benefit the biocrude in some aspects. Zhang et al. studied the impact of esterification on the physical properties of bio-oil. The results revealed an enhanced fluidity and lower viscosity after the upgrading process (68). Despite the advantages, the esterification of biocrude suffers from serious drawbacks. Firstly, the process consumes a

significant amount of chemicals and normally incorporates acid catalyst that causes challenging recoveries. Secondly, the process merely involves acids and alcohols and barely affects other oxygenates and heteroatom-containing molecules. Last but not least, using the transesterification reaction (**Eq. 1**), the process adds water to the upgraded biocrude, which might adversely impact the distillation process (69). To cope with the challenges, Chen et al. treated the HTL biocrude distillates through esterification instead of the biocrude bulk. The physicochemical properties of the resultant fuel were comparable to the considered reference diesel (69). However, the designed value chain still suffers from the presence of oxygenates in the distillation medium, which might bear lower distillate recoveries and high vacuum residue production.

$$RCOOH + R' - OH \rightarrow RCOOR' + H_2O \quad (1)$$

Another widely-researched thermochemical upgrading process is hydrotreating. Even under mild operational conditions, hydrotreating has proven to significantly stabilize the biocrude due to the low bond enthalpy of C-O and C-S. Deoxygenation commonly occurs through decarboxylation/decarbonylation, hydrodeoxygenation, or a combination of these reactions. Hydrotreating under mild conditions prevents severe coking and subsequently spans the lifecycle of the catalyst resulting in significantly fewer operational costs. Haider et al. studied the pre-stabilization of *Spirulina* microalgae and sewage sludge biocrudes under mild operating conditions (310-350 °C). They concluded that after 330 °C, maximum deoxygenation occurred in both biocrudes. Comparing the hydrotreating of the raw and stabilized biocrudes revealed a greater coke propensity in the case of raw feedstock (70). Therefore, implementing a pre-stabilization step before the vacuum distillation is seemingly inevitable in future biorefinery schemes.

Despite the physical and thermochemical upgrading processes, the resultant diesel fraction properties might still deviate from the standard specifications. Hence, blending HTL-upgraded diesel with the existing petroleum blendstocks is another strategy that can reduce the carbon footprint of fossil fuels in the ecosystem. Although biomass-based liquid fuel alternates are allowed in any proportion of road diesel, the final blend must comply with the fuel specifications (EN590). There are limited investigations concerning the miscibility of distillate mixtures with reference diesel fuels. Despite providing valuable information regarding the physical blending walls, the correspondence of the resultant fuel with marketable diesel in terms of physicochemical properties has rarely been addressed by previous studies (65)(71). Moreover, the mixing ratios were intuitively chosen, and the rationale was unaddressed. Therefore, there is a lack of a systematic mixing method that could optimize the mixing ratios as a function of physicochemical characteristics.

The primary ambition of developing renewable green drop-in and/or blend fuels is the reduction of hazardous emissions along with reducing fossil fuels and ensuring energy security. Although introducing a bioblend increases the share of biogenic carbon sources in the finished diesel fuel, the harmful gaseous air pollutants might still challenge the incentives commissioned by legislation. The HTL bioblend is typically denser in heteroatoms such as sulfur and nitrogen and contains more unsaturated compounds. Therefore, it is of paramount importance to study the evolution of engine

exhaust emissions after mixing bioblend with diesel. **Table 2** summarizes the main hazards of the emitted noxious waste during combustion.

Table 2. Potential hazards of the main fuel exhaust species.

Emission	Impact	Ref
NOx	• Production of nitric acid; ultimately leads to acid rain. • Production of smog in reaction with ultraviolet light. • Causing respiratory disorders and cardiopulmonary infections.	(72)
SOx	• Production of sulfuric acid; ultimately leads to acid rain. • Damaging plants' foliage and growth	(73)
PM (soot, dust, etc.)	• Causing serious cardiopulmonary illnesses • Reducing the visibility and causing haze	(74)
THC	• Causing dizziness, headaches, and nausea	(75)
CO	• Reducing the oxygen level in the cardiovascular system, eventually causing cancer (high levels) • Causing dizziness, headaches, fatigue, and confusion (low levels)	(76)
CO_2	• Elevating blood pressure and ultimately causing coma, convulsions, and asphyxia (high levels) • Causing headache, needle feeling in toes and fingers, and dizziness (low levels)	(77)

Despite the importance of emission control when introducing a new energy source to the market, there are very few studies investigating the impact of HTL-driven fuels on combustion gases. The existing literature mainly focused on combusting surrogates resulting from the constraints of producing a large quantity of fuel. Hossain et al. evaluated the performance and emission of a microalgae surrogate fuel in an internal combustion engine. The surrogate fuel rendered a comparable engine performance, lower CO, and particulate matter compared to the reference diesel with the expense of higher NOx emission (78). Moreover, Obeid et al. investigated the impact of N and S-containing constituents in various surrogate mixtures concerning their performance and emission profile. They proposed bunker fuel applications for heteroatom-laden surrogates as they significantly increased not only NOx and SOx, but also other gaseous species, such as PM (79). Yang et al. studied the combustion and spray behavior of stand-alone HTL fuel and in a mixture with commercial diesel. The study indicated promising results with respect to the HTL fuel performance; however, the study lacks the emission profiles (80). In this regard, an in-depth investigation of the emissions generated by incorporating different HTL fuels into a commercial reference diesel is highly demanded.

1.4. Research Questions and Objectives

Based on the challenges mentioned earlier, the main research questions in the framework of this thesis can be outlined as follows:

- How does integrating an MSW pretreatment process into HTL benefit the waste valorization value chain?
- What are the impacts of the most influential HTL parameters on the liquefaction of biopulp?
- How to perform aqueous phase recirculation while liquefying highly moist biomass?
- How does aqueous phase recirculation benefit and challenge the HTL process and final marketable fuel?
- What are the impacts of biocrude pre-stabilization on mass recovery, chemical and physicochemical properties of the resultant distillates?
- What is the current maximum blending potential of biopulp biocrude distillates in being used as an on-spec diesel blendstock?
- How does incorporating HTL blendstock influence the emission profiles of a compression engine?

The mentioned research questions will be thoroughly addressed by the defined objectives as follow:

- The first objective was to study the compositional, chemical, and physical properties of bioplup (organic fraction of MSW produced by the Ecogi® process) to prove the feasibility of its use in the HTL process.
- Secondly, the influences of the most crucial HTL parameters, including temperature and the presence of homogeneous catalysts, were evaluated in a lab-scale series of experiments. Thereafter, the research was expanded to bench-scale studies to highlight the process's operability and technical challenges when using biopulp as the primary feedstock.
- The third objective was to overcome the challenge of aqueous phase recirculation while treating wet biomass. Thereafter, the evolution of HTL products in terms of organic and inorganic content was monitored to detect the possible challenges emerging by aqueous phase recirculation.
- Lastly, the production of a competent HTL-driven diesel blendstock that could fulfill the standard specifications was targeted. The competence of the obtained blends was also evaluated by screening various emissions after combusting the fuels in a compression engine.

The research objectives aid in addressing the sustainable development goals shown in **Figure 5**.

Figure 5. The relevance of the research objectives of the thesis to Sustainable Development Goals.

1.5.Thesis Outline

The Ph.D. work is in the framework of NextGenRoadFuels project funded by the European Union's Horizon 2020 Research and Innovation Programme under grant agreement no. 818413. The project's overall objective was to justify hydrothermal liquefaction technology as a flexible, viable, and sustainable pathway in producing drop-in/blendstock bio-based fuels for the road transportation sector using three different urban wastes, namely, sewage sludge, municipal solid waste, and woody biomass.

The chapters of the thesis are outlined as follows:

Chapter 2: This chapter gathers all the methodologies and characterization instruments, and pathways involved in the production and analysis of HTL raw biocrude, upgraded products, and combustion emission profiles.

Chapter 3: This chapter is initially built upon a comprehensive understanding of biomass by characterizing the various aspects, from physical properties to microplastic pollutants. Thereafter, the effects of process parameters on batch-scale HTL experiments are studied. The driven information is used to carry out a continuous pilot-scale campaign aiming to understand the challenges and produce sufficient biocrude quantity for further studies.

Chapter 4: This chapter addresses the difficulties associated with the valorization of the HTL aqueous phase through its recirculating to the main process while treating highly moist biomass. By this means, the capability of the HTL in evading the cost-prohibitive pre-drying process is emphasized. To establish a comprehensive overview, the challenges along with the devised process pathway are investigated through a complementary study, employing hydrotreating of the obtained biocrude samples.

Chapter 5: The fifth chapter utilizes the mass-produced biocrude in the continuous unit to elucidate more on the practical applications of HTL-driven fuel by producing different blendstocks via two main upgrading technologies. The challenges related to

the deficient physicochemical properties of the biocrude, leading to its potentially limited applications are spotlighted. The distillate fractions derived from raw and partially hydrotreated biocrude are subjected to a systematic multiobjective blending optimization complying with automotive diesel standards. Finally, the obtained blended fuels are combusted in a compression engine to investigate their emission profiles.

Chapter 6: This chapter includes the overall conclusions drawn by the Ph.D. work and suggests the needed potential complementary future research.

A summary of the Ph.D. project is visualized in **Figure 6**.

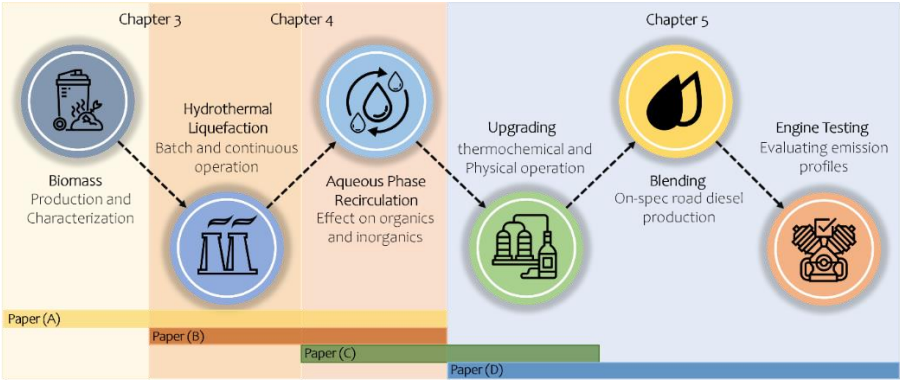

Figure 6. Outline of the Ph.D. project.

Chapter 2. Methodology

This chapter elucidates the methods used within the Ph.D. project. The relevancy of the chapter points toward the dependency of the obtained results and the drawn conclusions on the choice of processing and analyzing techniques. Moreover, this chapter touches upon the inadequate and challenging analyzing techniques and suggests relevant advanced methods that might be employed in future investigations.

2.1. Feedstock Production

So-called 'biopulp', a pretreated source-segregated organic fraction of municipal solid waste, was collected from Gemidan Ecogi A/S, Frederikshavn, DK. The biopulp is the primary product of the Ecogi® process developed by Gemidan A/S. In essence, the Ecogi® process mechanically separates household "green bags" by wet maceration followed by a 6 mm screening/filtration process into a biopulp containing a significant share of organic substances of the collected MSW. The reject fraction contains a vast majority of non-biodegradable materials such as glass, metals, plastics, etc. To reduce the biomass clogging risk in the bench-scale unit, it was downsized and homogenized using wet hammer milling installed with a 1 mm screen at Euromilling A/S, Tølløse, DK.

2.2. Feedstock Characterization

The characteristics of the biopulp can vary depending on the season and tuning of the Ecogi® process according to the targeted product. Despite the ability of HTL to process highly moist feedstocks, the first objective of analyzing the biomass was to assess the available degradable organics in the HTL medium. In this regard, to achieve an insight toward the potentially convertible portion of as-received feedstock, moisture content was determined using a Kern MLS-D infrared moisture analyzer by heating the samples from ambient temperature to 120 °C. A simultaneous thermogravimetric analyzer (STA) (PerkinElmer, USA) was utilized to evaluate the proximate properties of the biomass. The apparatus was programmed to heat up from 50 to 900 °C in 90 min with a ramp of 10 K/min under an N_2 atmosphere. The flow gas was then switched to O_2 to burn out the fixed carbon and determine the ash content of the biomass. The procedure reported by Conti et al. was utilized to compute the volatile matter and fixed carbon (81). When notified, the ash content of the feedstock was analyzed according to the ASTM D482 standard method (atmospheric condition) in an electric muffle furnace (Protherm Furnaces, Turkey), with the following program: 1) heating at 105 °C for 8 hr, 2) ramping up to 775 °C for 3 hr, 3) holding isothermally at 775 °C for 1 hr.

The crude fat content of the feedstock was determined by a soxhlet method, where the setup was loaded with petroleum ether as the extraction solvent. As Mariotti et al. suggested, the crude protein content of the biomass can be estimated by multiplying the nitrogen content by a coefficient of 6.25 (Jone’s factor) (82). However, a solid

determination can be achieved using techniques like Kjeldahl analysis (specifically for biopulp). Lastly, the lignocellulosic content of the feedstock was calculated by difference.

The elemental composition of the feedstock was evaluated through an elemental analyzer (Perkin Elmer, 2400 Series II CHNS/O) operated in CHN mode. The oxygen content of the biomass, on the other hand, was determined by difference. The CHNS was not employed in this study due to the low concentration of S in biomass and possible inaccuracy when operating by the given method. Instead, an inductively coupled plasma atomic emission spectroscopy (ICP-AES) was utilized to detect the Sulfur content along with other inorganic elements. The detailed procedure is elaborated elsewhere (83). The calorific value of the biomass was quantified using a bomb calorimeter (IKA 2000, Germany) following the ASTM D4809 standard.

The physical impurities of the biopulp, such as plastic, metal, and glass contaminants, were exclusively determined at AnalyTech Miljølaboratorium A/S. Moreover, the macro and microplastics of the feedstock were analyzed, aiming to assess the accuracy of the Ecogi® process in segregating different types of polymers. After a series of pre-extraction steps (Paper E), the particles (10-500 μm) were analyzed through a micro-Fourier Transform Infrared spectroscopy (μ-FTIR) coupled with an imaging technique. The apparatus from Agilent technologies was associated with an Agilent 670 IR spectroscope and a Cary 620 FTIR microscope. The macro plastic particles (>500 μm) underwent the same pre-extraction steps, but a filtration step using a 500 μm sieve was added between each process. The particles were lastly identified through an ATR-FTIR instrument from Agilent Technologies, equipped with a diamond ATR and a Cary 630 FTIR spectrometer. The particle number and mass were determined employing a software called 'siMPle'. The polymer types were distinguished using the library database of OMNIC software. More information on the analysis technique can be found elsewhere (84).

2.3. Hydrothermal Liquefaction in Lab-scale Batch Reactors

The micro-scale experiments were performed in two parallelly operating 12 ml stainless steel batch reactors. The custom-made reactors (AAU workshop, Aalborg, Denmark) were built using fittings and tubes provided by Swagelok. The use of microbatch reactors secures the flexibility of the process and practical screenings. Moreover, the performance of different HTL conditions could be tested, setting aside the operational challenges such as cloggings rooted in high inorganic content or pumping issues. The reaction setup was equipped with online thermocouples and pressure transducers, allowing continuous monitoring of the reaction state. A schematic view of the setup is visualized in **Figure 7**. The specific amount of biomass slurry (7-8 g, with or without catalyst) was firstly charged to the reactor tube. The reactors were then carefully purged and sealed using N_2 gas (99.9 % purity) at 2 MPa to prevent the oxidation of the HTL products in the presence of O_2. The loaded reactors were then submerged in a preheated fluidized sandbath (Techne SBL-2D, USA) and maintained at the operating temperature for a specific amount of time (residence time) when a mechanical agitator (with a frequency of 450 min^{-1}) was

utilized to properly mix the reactor constitutes. Thereafter, the reactors were quenched into an ambient temperature water bath and held for 15 min.

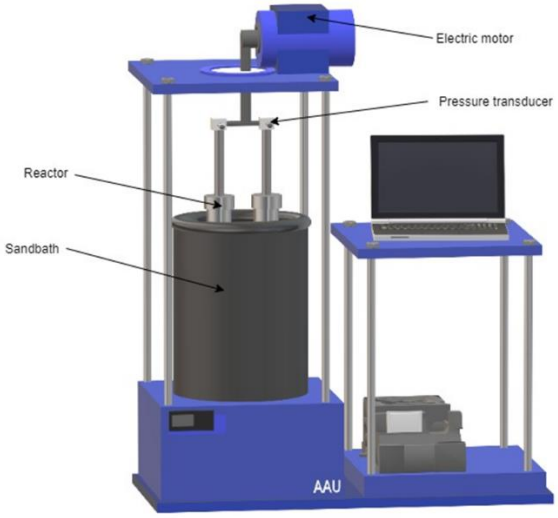

Figure 7. The microbatch setup used for HTL (and HT) experiments.

Additionally, a 400 ml autoclave reactor was used to carry out the HTL experiments when a greater quantity of HTL products was required. Moreover, higher quantities aided in decreasing the risk of losing products while separating could potentially result in mass and elemental balance errors. In each experiment, around 234 g of the biomass slurry was loaded into the stainless-steel reactor. The reactor was similarly purged with N_2 and pressurized up to 2 MPa. The desired operational temperature was maintained using a 1.75 kW electric ceramic furnace with a relatively slow heating rate (around 4 K/min). Note that, unlike the microbatch system, the loaded reactor had to endure the heating phase due to the configuration of the setup. The constituents of the reactor were mixed adequately with an internal mixer. The experiment was terminated by removing the heater and cooling down the reactor using a compressed air system (~5 K/min). The system is schematically shown in **Figure 8,** where electric cables and cooling pipes are removed for simplicity.

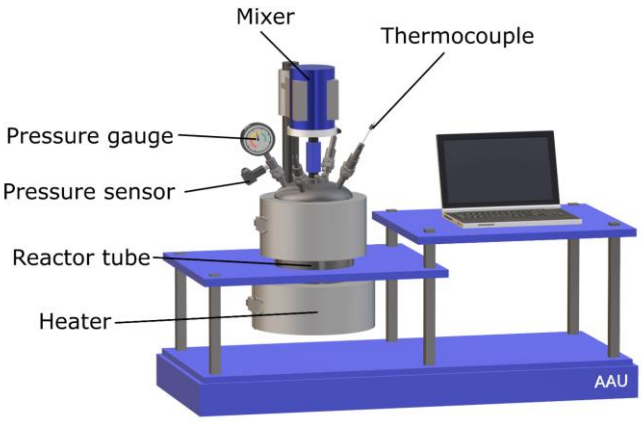

Figure 8. The autoclave setup used for HTL experiments.

Despite the advantages given by larger capacity that translates to a higher biocrude production, the lengthy heating and cooling rates may result in unexpected product ranges by exposing the HTL intermediates to different temperature zones. The following sections will elaborate more on the effect of different batch systems used in HTL studies.

2.3.1. Product Separation

After completing the process, the constituents of the reactor, including the pristine aqueous phase, were poured out into a sampling vial without the addition of any solvents. The reactor was then eluted with the least dichloromethane (DCM) possible to extract the adhered products to the inner walls of the reactor. DCM was chosen as the extraction solvent because it is associated with a relatively higher energy recovery (ER) and lower extraction energy required, irrespective of the utilized feedstock (85). The extracted material was subsequently filtered (5-13 µm) to remove the solid residue. The residual water in the filtrate was then gravimetrically separated using a separation funnel. The bottom phase in the funnel was transferred to a vacuum rotary evaporator (Büchi R210, USA) operating at 60 °C under 50 KPa. After 15 min of operation, the solvent was extracted, and the biocrude phase was stored for analysis.

2.3.2. Aqueous Phase Recirculation

The acquired aqueous phase from the microbatch or autoclave reactor was initially filtered using a 5-13 µm mesh size filter paper. Note that the recovered solids were also taken into account while calculating the mass and elemental balances. The filtrate was further concentrated through a Büchi R210 vacuum rotary evaporator at 65 °C when the vacuum was reduced from atmospheric condition to 8 KPa in a stepwise manner. A thick foam layer emerged in the evaporator flask as soon as the vacuum was applied to the rotary system. A Heidolph foam brake with a flask clamp was implemented in the system to address the issue and prevent the disruption of the usual

evaporation procedure. Additionally, two droplets of an anti-foaming agent (marine oil or n-Octanol) were added to the evaporation flask. Due to the highly moist nature of the biomass used in this study, recirculation of the aqueous phase with excess water could significantly vary the dry matter content of the slurry and reflect drastic changes in the HTL products' distribution **(Figure 9b)**.

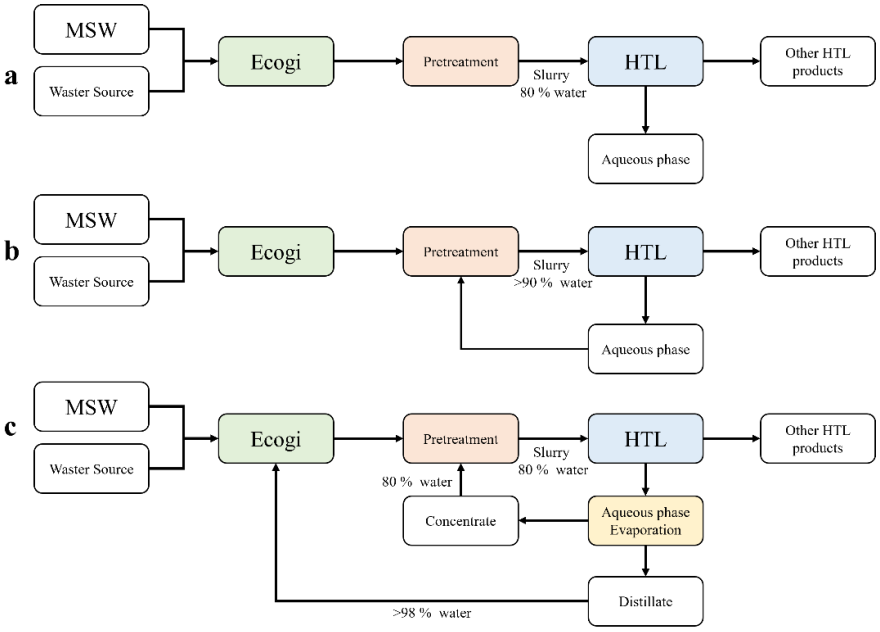

Figure 9. a) Typical HTL process without valorization of the aqueous phase, b) HTL process with direct aqueous phase recirculation, and c) HTL process with recirculation of concentrated aqueous phase.

Therefore, the evaporation proceeded until the concentrated aqueous phase's moisture equaled that of biomass. The evaporated surplus water was collected in the output of the evaporation system and denoted as the 'Distillate' phase, whereas the concentrated phase was labeled as 'Concentrate'. To fulfill the ambitious goals of the circular economy, the distillate was hypothesized to be a great candidate for being used as a water source in the Ecogi® process, where it can mitigate the need for freshwater applications (**Figure 9c**). In this regard, the distillate samples were collected and underwent various analyses. On the other hand, the concentrate was replaced with a certain quantity (10 wt. %) of biomass in a subsequent HTL cycle. For instance, in a typical microbatch run, 7 g of biomass slurry was processed, while in the succeeding cycle, 0.7 g of the slurry was replaced by the same amount of concentrated aqueous phase. In this way, the total constituents and dry matter content of the slurry remained constant during different cycles. The remaining steps were performed as mentioned in the previous section.

2.4. Hydrothermal Liquefaction in Bench-scale Continous Unit

The continuous HTL experimental setup used in this study was designed and commissioned by Steeper energy and AAU located at Aalborg Øst, Denmark. The system was designed to operate up to 450 °C and 35 MPa with a maximum flow rate of 30 kg/h slurry. The system was firstly heated up to the set-point temperature using circulating pressurized deionized water. After establishing the desired process condition, the feed was switched to the feedstock slurry. The slurry was initially pressurized through a pressure feed pump and then heated in two serially connected heaters prior to entering an approxímatally 10 L reactor. After being processed in the reactor, the effluents were cooled down and depressurized using a heat exchanger and capillary system, respectively. When possible, the products were transferred to a gravimetric separator to separate the aqueous phase and biocrude. However, in many cases, the products formed a homogeneous emulsion, resulting in an impractical gravimetric separation. In such cases, the cooled HTL effluent was collected in a single phase named 'Emulsion'. The process flow diagram of the system is illustrated in **Figure 10**.

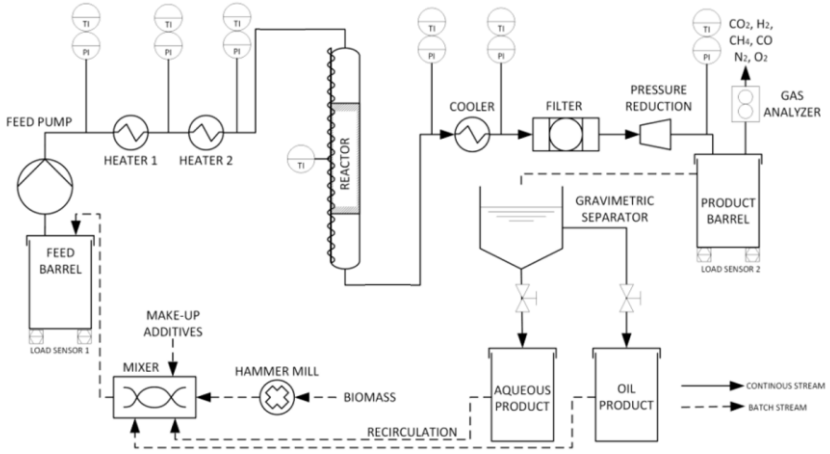

Figure 10. process flow diagram of the CBS1 pilot plant (46).

2.4.1. Product Separation

A gas flow meter was utilized to measure the volume flow of the HTL gaseous products. The gas composition was analyzed through a built-in online IR apparatus in the unit. The liquid products (either separated aqueous phase/biocrude or emulsion) were periodically sampled every 1 hr to acquire several mass balances per run. Receiving the liquid products in a stable emulsion could potentially complicate the separation of the biocrude. To break this emulsion, several steps were taken: 1) In the first stage of separation, acetic acid (AC) was added to the bulk emulsion. For each ton of emulsion, about 15 liters of AC (80 % purity) was added. This resulted in a

phase separation into a supernatant fraction termed "oilsand", consisting of the biocrude, solids, and some residual water. A bottom phase representing the majority of the HTL aqueous phase, 2) The oilsand top phase was first isolated by draining the HTL aqueous phase for the bottom of the experimenting tank, 3) The oilsand was then mixed with demineralized water, citric acid (CA), and Methyl ethyl ketone (MEK) in different ratios to figure out the best separation condition possible. This led to two different phases; a top MEK/biocrude phase and a bottom CA solution, 4) After mixing the oilsand with water, MEK, and CA, a grey precipitate was observed at the bottom of the tank. For this reason, the two-phase liquid products were drained from the top of the tank to another tank. 5) The oilsand with water, MEK, and CA mixture was then processed through a two-phase centrifuge at approx. 300 kg/hr. The centrifugation separated the liquids from solids, 6) MEK/biocrude and CA solution were gravimetrically separated, 7) MEK/biocrude solution was filtered through a 5 μm filter, and 8) MEK was removed from the biocrude by thermal evaporation. A summary of the separation procedure can be found in **Figure 11**.

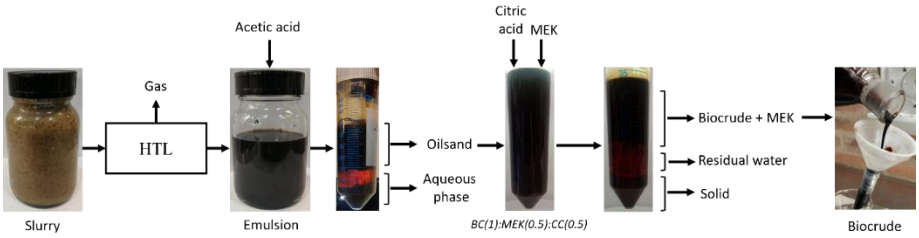

Figure 11. Flow diagram of the emulsion separation process.

2.5. HTL Process Conditions

Process conditions in HTL are the main parameters that need to be tuned prior to the initialization of a mass production run. Type of biomass, reaction temperature (interconnected to the operational pressure), presence/type of catalyst, and dry matter content of the feedstock slurry are named among the most critical factors that can significantly dominate the operation and product quality and quantity. This Ph.D. project establishes all the experiments on merely biopulp; therefore, the impact of biomass type was withdrawn. Moreover, the biomass used was utilized as received, and the dry matter content of the slurry was pre-determined, so it was also set aside as a governing parameter. Instead, the impacts of reaction temperature, type, and presence of the catalyst in the biomass slurry were investigated in the present study.

2.6. Hydrotreating in Lab-scale Batch Reactors

Batch hydrotreating experiments were carried out in the same setup elaborated previously. However, the reactors were loaded with 4 g of biocrude and 2 g of pre-activated Ni-Mo/Al_2O_3 catalyst provided by Shell A/S, Fredericia, Denmark. The feedstock and catalyst loading were not optimized in this study, and the author used the results of previous studies (86)(87). Four stainless steel spheres were added to the

reaction medium to enhance the mixing of the reactor constituents. The reactors were purged using N_2 to ensure air depletion. Afterwards, the reactors were pressurized to 8 MPa using H_2 gas. The following steps were performed as mentioned before, while the residence time was altered to 3 h (86). After completion of the reaction, the reactors were submerged in an ambient temperature water bath for 30 min, and the gas phase was subsequently sampled using a custom-built (Swagelok) gas trap. The hydrotreated biocrude and the alumina catalyst were sieved using a 1 mm mesh-sized metallic filter by tilting the reactor, and the filtrate phase (hydrotreated biocrude and traces of water phase) was collected in a sampling tube. The tube was then centrifuged (4000 rpm for 5 min) to segregate the hydrotreated oil without the intervention of any extraction solvent. The obtained oil phase was weighed and stored for analysis. The reactor and the residual catalyst were rinsed using a limited volume of acetone, and the extract was filtered through a 5-13 µm filter paper. The collected solid phase was dried at 105 °C overnight and denoted as '*coke*'. The spent catalyst was dried under the same conditions, and the weight difference (compared to the input catalyst weight) was considered in mass balance calculations. The filtrate (acetone and hydrotreated biocrude) was transferred to the vacuum evaporator operating at 65 °C and 50 KPa. The recovered oil was weighed and accounted as a share of obtained hydrotreated oil after the reaction.

2.7. Hydrotreating in Pilot-scale Continuous Hydrotreating Unit

Although optimization of the hydrotreating process was out of the scope of this thesis, it was of high importance to perform mild deoxygenation to stabilize the oxygenated biocrude for further usage. In doing so, a continuous bench-scale hydrotreating system with a fixed-bed technology reactor was utilized. A constant flow rate of 50 mL/h input preheated biocrude (60 °C) to the reactor was supplied through a high-pressure dual-cylinder Teledyne ISCO syringe pump system. An 86 cm long 316 stainless-steel tube with outer and inner diameters of 14.8 and 19.1 mm was employed as the reaction zone of the setup. The hydrogen was pre-mixed with the heated biocrude before entering the top of the reactor with a H_2/oil mixing ratio of approximately 1000 NL/L. The temperature profile of the reactor was monitored using 10 K-type thermocouples (Omega Engineering, U.K.) evenly distributed throughout the reaction tube. The reaction temperature was maintained using a Carbolite Gero TVS12/900 furnace. The obtained products were segregated into two vessels after depressurization. The volumetric flow rate of the off-gases was screened through a Shinagawa (Japan) wet gas meter, while a gas sample was collected using a gas trap (Swagelok) to be analyzed in a GC-BID. The targeted deoxygenation in this study was carried out within the temperature range of 320-330 °C under the pressure of 100 bar with the WHSV (weight hourly space velocity) of 0.5 h^{-1}.

2.8. Distillation of HTL-driven Fuels

Fractional distillation of the biocrude and hydrotreated biocrude was carried out in the setup shown in **Figure 12**. A 15 theoretical plate distillation column with an inner diameter of 25 mm was mounted to the system (No. 5). The column was packed using

Pro-Pak filling, which enables the distillation process to stop and start without a lengthy delay. It also precludes the interlocking and eases the filling and emptying of the column during operation. A controllable heat jacket was implemented around the column to prevent heat loss and maintain adiabatic conditions. A 2 L pot flask placed in an electric mantle (No. 6) was used in the setup to provide a sufficient sample to the system. An Edwards 8 RV rotary vane vacuum pump (No. 9) was employed to aid vacuum distillation by a stepwise vacuum ramp to 100, 20, and 1 torr. During vacuum distillation, the non-condensable gases were collected using a condenser system consisting of a condensing flask and dry ice/acetone mixture pot (No. 8). The system also consisted of a reflux condenser (No.1), reflux valve (No. 2), column head (No. 3), vapor temperature thermocouple (No. 4), a pressure transducer (No. 7), and collecting flasks (No. 10). To avoid any unexpected shootings and unsteady boiling behavior caused by the presence of water in the distillation feedstock, a dehydration process complying with ASTM 2892 was performed prior to the main operation (up to 130 °C). The vapor temperature in the column head and the correlated TBP curves are reported in AET (atmospheric equivalent temperature) following D 5236. Hoffman et al. elaborated on the correlations used to convert the column heat temperature to AET (66). Although based on the ASTM standard, the dehydration step is recommended at atmospheric pressures, herein, vacuum dehydration at 100 torr was preferred in this study. The reason was to prevent the cracking of oxygenates. After dehydration, distinct phase separation was observed in the collector vessel, indicating the presence of water and light organics. The organics were then reintroduced to the distillation pot, and the water was weighed and stored.

In each distillation run, a total amount of 1.2 to 1.4 L of the sample was initially dehydrated. The even boiling of the sample was ensured by performing a vigorous magnetic stirring of the sample in the distillation pot. The IBP (initial boiling point) was correlated to the very first reflux droplet. Hereafter, the distillation ran at total reflux until the heating temperature reached approximately 5 °C below AET of vapor temperature. Thereafter, the reflux valve was slightly opened (1:5 ratio of collecting: refluxing) to collect the distillation fractions. The collecting was continued as long as the vapor temperature increased. When the vapor temperature profile equalized, the system was shut and cooled down. Based on the ASTM 2892 guideline, the pot skin and vapor temperatures should be respectively kept below 310 and 210 °C to avoid the risk of cracking. The second distillation step was initiated with the adjustments of the vacuum pump pressure for pressures below 20 torr, a reflux ratio of 1:2 was applied when collecting the products. The first three cuts were collected in 50 °C intervals and named F1 (IBP to 100 °C), F2 (100-150 °C), and F3 (150-200 °C). Thereafter, the fractions were collected every 25 °C, rendering seven (F4-F10) cuts to a maximum AET of 375 °C. The recovered distillation fractions were stored and kept in cold conditions for further analyses.

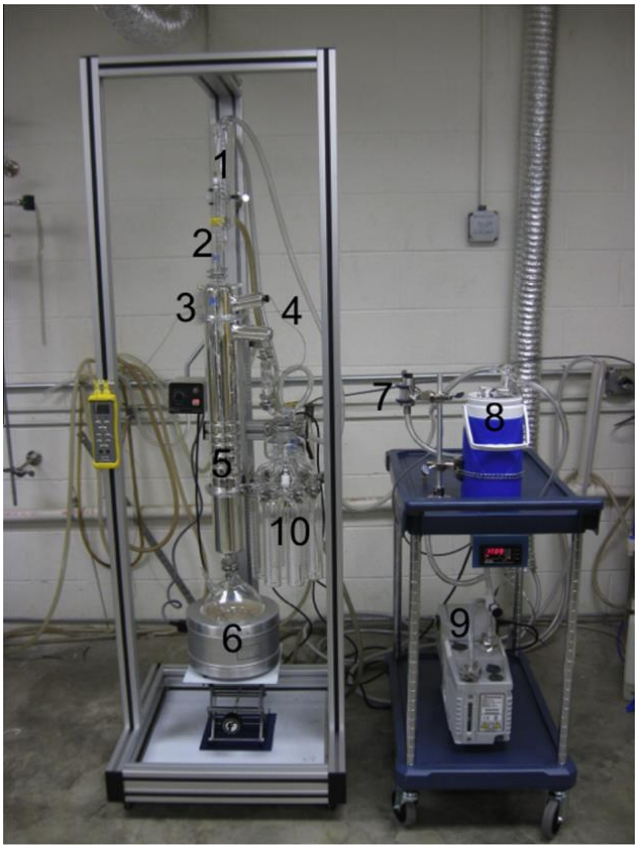

Figure 12. A picture of the distillation setup illustrating different components (39).

2.9. Optimization of Bioblend Mixing

A multi-objective optimization model was designed to optimize the blending of different fractional cuts together and with a standard reference diesel (Coryton Diesel, UK) complying with the EN590 road diesel fuel specification. The model was developed via the *fgoalattain* function in Matlab®. Two different approaches were employed to formulate the objective functions as follows:

1) The blend prediction was carried out by reducing the difference between the blend properties and the maximum values in the specification to zero (**Eq. 2**).

$$\left|z_{blend}(x_i) - z_{max,spec}\right| = 0 \quad (2)$$

2) The blend prediction was pushed to set the objectives equal to or less than the maximum values in the specification (**Eq. 3**).

$$z_{blend}(x_i) \leq z_{max,spec} \quad (3)$$

During optimization, the mass fractions of bio-blendstock were altered following the constraint formulated in **Eq. 4**.

$$1 - \sum_{i=1}^{n} x_{,i} = 0 \quad (4)$$

This study only considered a limited number of elemental and physicochemical properties such as sulfur content (S), density (ρ), kinematic viscosity (v), microcarbon residue (MC), water content (WC), and cloud point (CP) as the optimization objectives, whereas the developed method can be further updated with other important properties, namely oxidation stability, FAME content, and polycyclic aromatics content to acquire more accurate predictions. Note that nitrogen content (N) and higher heating value (HHV) are not strictly regulated parameters; however, this study aimed to keep the HHV as high and N content as low as possible due to their potential impact on the performance and emission profile of the fuel in compression engines. Cloud point and kinematic viscosity of the blends were respectively calculated based on **Eq. 5** and **6**, where "i" represents the individual property of the biobased blend or reference diesel, x_i shows the mass fractions of each blendstock and v_i denotes the blendstock's volumetric fractions. The blend property of the other fuel characteristics was estimated through weighted averages.

$$CP_{blend}(℃) = \left(\sum_{i=1}^{n} v_i \, CP_i(K)^{\frac{1}{0.05}}\right)^{0.05} - 273.15 \quad (5)$$

$$v_{blend}(mm^2/s) = \exp\left(\sum_{i=1}^{n} x_i \ln v_i \, (mm^2/s)\right) \quad (6)$$

2.10. Description of the Engine Setup

An optically accessible compression ignited chamber (OACIC) was used to carry out the engine testing experiments. The setup was a 4-stroke engine that consisted of a re-designed optical accessible engine head. The chamber was equipped with a Bosch solenoid 2nd-generation common rail injector. As in the original engine, the intake and exhaust valves were connected to the engine head, in which the temperature and pressure were monitored through a K-type thermocouple and pressure sensor (Kistler 6011), respectively. A cross-section view of OACIC can be seen in **Figure 13**. The engine details are presented in **Table 2**

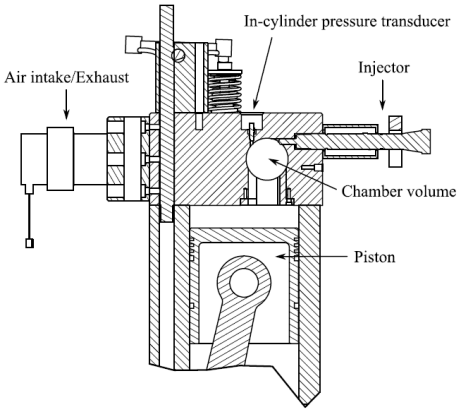

Figure 13. Cross-section view of the optical engine (49).

Table 3. OACIC engine specifications.

Engine Type	Four-stroke, single cylinder, indirect DI engine
Bore\stroke	130 mm\140 mm
Displaced volume	1.85 L
Compression ratio (CR)	16.36
Injector	Bosch CR second generation
Injector nozzle	Single hole, DSLA124P1659, 62 deg wrt central axis
Hole diameter	0.12 mm
Injection pressure	1000 bar
Injection duration	4 ms
Injection timing	3 CAD before top dead center (BTDC)

The cylindrical combustion chamber (diameter of 50 mm and a height of 40 mm) was sealed with 2 fused-silica windows (diameter and thickness of 63 and 25 mm, respectively) and copper gaskets. The windows were held by 2 threaded rings and provided a line-of-sight view of the chamber. The alternating current motor operating at 500 rpm was used to drive the piston and crank. A magnetic shaft encoder was employed to locate the crankshaft position, having 37.5 μs time resolution for 500 rpm. The combustion pressures were recorded by a dynamic pressure sensor (Kistler 6052C), which was synchronized to the shaft encoder. The injection pressure was regulated by an air-driven pump, and the injection condition and timing were controlled by LabVIEW software. The injector nozzle tip temperature was continuously monitored using a thermocouple placed in the center axis. During the experiments, the temperature of the engine cylinder was kept at 60 °C by means of an external heater, while the engine head was not externally heated or cooled.

As optimization of the thermodynamic conditions of the engine was not among the research objectives of this study, a single thermodynamic condition was chosen to conduct the tests. The in-cylinder pressure was adjusted to 1.25 bar, while the in-cylinder temperature (55.3 °C) was calculated through cylinder pressure charts and the thermodynamic models in LOGEresearch software.

The exhaust emissions were analyzed through a Horiba MEXA-ONE RS instrument capable of measuring NO/NOx, total hydrocarbon (THC), O_2, and CO/CO_2 concentrations. The concentration of NO\NOx was screened through a Chemiluminescent detector within the range of 0 to 10,000 ppm. A flame ionization detector working in the range of 0-60,000 ppm (carbon-based) quantitatively detected the concentration of THC. The volumetric concentration of CO and CO_2 was analyzed via a Non-dispersive infrared method. Moreover, an online Combustion DMS 500 analyzer was equipped to the setup to detect the PM size distribution and the total number of particles in the exhaust stream.

2.11. Characterization of HTL Products

The elemental composition of the biocrude, hydrotreated biocrude, and distillation cuts was determined through a PerkinElmer 2400 Series II CHNS/O instrument operating in CHN mode, complying with ASTM D5291. The sulfur content of the liquid HTL products was characterized using a SLFA-60-Horiba analyzer complying with the ISO-20846 guideline, while the oxygen content was calculated by difference. In limited cases, the sulfur content of biocrude was analyzed through an Inductively Coupled Plasma Atomic Emission Spectroscopy (ICP-AES) utilizing a Thermo Scientific iCap 6300 Duo view. The boiling point distribution of biocrude, hydrotreated biocrude, and distillation fractions was measured with a simulated-distillation (SimDis) apparatus equipped with a ZB-1XT column x (Phenomenex) and a Shimadzu gas chromatography–flame ionization detector (GC-FID) (Shimadzu, Kyoto, Japan) following ASTM D7169. The proximate analysis of the oil products was carried out by a DSC/TGA system (SDT 650, Discovery, New York, NY, USA). The system was programmed to heat the samples to 775 °C with a heating rate of 10 K/min and subsequently maintain the temperature for 30 under N_2 atmosphere. For ash measurements, the isothermal condition was performed under O_2 atmosphere. The chemical composition of oil and aqueous phases were inspected through a Thermo Scientific Varian gas chromatography (Trace 1300)-mass spectrometry (ISQ-ID) (GC–MS) employing capillary columns (CP-9036) and (CP-3800). The compounds identification was carried out using the NIST (NIST08) database. The organic functional groups of the biocrude, hydrotreated biocrude, and some of the corresponding fractions were analyzed using a Fourier-transform infrared (FT-IR) (Bruker TENSOR II spectrometer) instrument operating at ambient conditions in the range of 4000 to 400 cm^{-1}. Calibration and normalization were initially performed before each run. The chemical composition of the oil samples was also inspected through a Bruker Advance III 600 spectrometer functioning at 150.9 MHz. The proton-decoupled ^{13}C-NMR spectra of biocrude, and hydrotreated samples could potentially assist in investigating the complex matrix of the biocrude and its derivatives. The corresponding calculations, such as peak integration, baseline corrections, and monitoring of the spectra, were carried out using MestReNova software. The HHV of the oil products was identified using two methods depending on the available sample quantity. When only a limited quantity was available, the HHV was estimated through the Channiwala and Parikh correlation shown in **Eq. 7**(88).

$$HHV_{daf}\ (MJ/kg) = (0.335)\ C + (1.423)\ H - (0.154)\ O - (0.145)\ N \quad (7)$$

In cases where product quantity was not limited, a bomb calorimeter instrument (IKA 2000, Germany) in accordance with ASTM D482 was used to estimate the heating value of the samples. The energy recovery of the biocrude and hydrotreated biocrude samples was calculated as **Eq. 8**, where HHV_P and HHV_F, respectively show the higher heating value of the product and the feedstock. W_P indicates the recovered mass of the product after the process, and W_F is the input weight of the feedstock.

$$ER\ (\%) = HHV_P/HHV_F * W_P/W_F * 100 \quad (8)$$

The cetane index (CI) of the fuels was estimated by using ISO 4264 standard method, while the distillation recovery temperatures were acquired from SimDis results.

Moreover, the density used in the calculations was determined with an Anton Paar density meter at 15 °C according to ISO-17034 standard. Note that in the cases of samples with the cloud point higher than 15 °C, the density was estimated through their linear density-temperature curve. Hence, the density (ρ) of the sample in higher temperatures was measured (at least 3 points), the regression curve was determined, and the density at 15 °C was extrapolated. The cloud and pour points of the distillates and their corresponding feedstocks were concurrently identified through a PAC/OptiCPP (ISL) could/pour point analyzer complying with ISO-3015 and ISO-3016 standard guidelines. Moreover, the flash point of the samples was monitored using a PAC/OptiFlash flash point apparatus following the ISO-2592 standard. Based on the standards (i.e. ISO 3104), the kinematic viscosity has to be determined in manual glass or glass capillary viscometers. In this study, due to the lack of the required equipment, the dynamic viscosity (η) was measured using an AR-G2 magnetic bearing rheometer at 40 °C and atmospheric pressure and following **Eq. 9** converted to kinematic viscosity.

$$\nu\ (mm^2/s) = \eta/\rho \quad (9)$$

A micro carbon residue analyzer (Alcor MCRT-160) was used to measure the micro carbon residue of the oil samples (MC) following ISO-10370 standard method. A Karl-Fischer titration instrument (Titroline 7500 KF) was utilized to measure the water content of biocrude, hydrotreated biocrude, distillation cuts, and aqueous phase complying with the ISO-12937 standard method.

The total organic carbon (TOC), total nitrogen (TN), and total ammonia in the aqueous phase samples were determined through LCK386, LCK138, LCK328, and LCK304 Hach kits, respectively. Thereafter, a spectrophotometer (Hach and Lange, DE3900) was used to analyze the prepared kits. The pH of the aqueous samples was estimated by employing a WTW 3210 pH meter equipped with a SenTix® 41 pH Sensor.

The composition of the gaseous phase from liquefaction and hydrotreating processes was characterized by means of a GC-2010 (Shimadzu Inc.) gas chromatograph equipped with a barrier ionization discharge detector (GC-BID) and a Supelco 1006 PLOT column. Note that the detected concentration of H_2 was utilized to conduct the calculations of H_2 consumption during the hydrotreating process using the ideal gas law. The organic and inorganic elemental content of the solid residue (solid product of the HTL process) was determined using the same CHNS/O, and ICP-AES instruments mentioned above, respectively. Due to insufficient coke quantities extracted from batch hydrotreating experiments, the recovered coke was assumed to be pure carbon, and the carbon balances were conducted upon this assumption. The Ash content of the solid residue samples was measured using an electric muffle furnace mentioned before employing the sampling procedure.

Chapter 3. HTL of Biopulp

This chapter initially focuses on the characterization of biopulp to explore its suitability for being used as a feedstock in the HTL process. Thereafter, the influence of different HTL process conditions, including temperature and the presence of different homogeneous catalysts, are thoroughly investigated. One step further, this section delves into the processing of biopulp on a continuous bench-scale unit. The challenges involved in the continuous operation are thoroughly discussed, and the solutions are provided.

Overall, this chapter aims to fulfill objectives 1 and 2 of the study. Moreover, it plays an essential role in achieving goals No. 2 (Zero hunger), No. 7 (Affordable and clean energy), No. 11 (Sustainable cities and communities), No. 13 (Climate action), and No. 15 (Life on land) of sustainable development goals. The main body of this chapter is based on papers (A) and (B).

3.1. Experimental Results

3.1.1. Biopulp Characteristics

The as-received biomass visualized in **Figure 14a** intuitively seemed to be a favorable feedstock for HTL operation. The Ecogi® process represents an incredible potential in removing non-biodegradable materials. **Figure 14b** indicates a manual pumpability test using a syringe with an outlet orifice diameter of 6 mm. The ideal slurry will continuously pass through the narrow end of the syringe without any sign of clogging. Moreover, the dry matter content of the slurry before and after pumping remains constant. however, the biopulp's manual pumpability test failed with the occasional extra power needed to push the slurry out (the test ceased due to a major clogging). Measuring the dry matter content revealed that the pumped slurry had 89.6 wt. % of water 6.5 wt. % higher than that of the original slurry. The presence of large organic and non-organic particles such as plastic pieces can possibly explain the observed phenomenon.

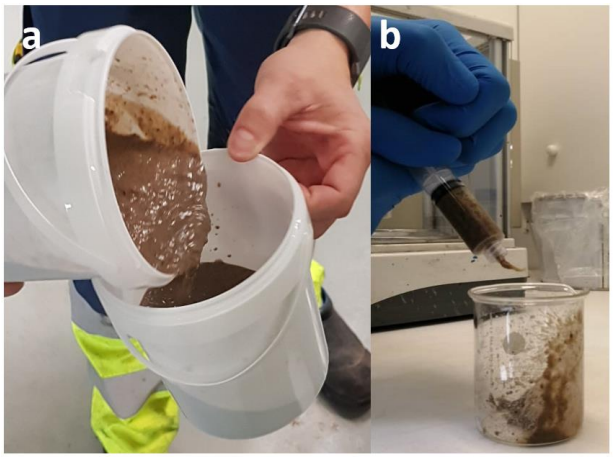

Figure 14. a) Wet organic fraction "Biopulp" and b) Syringe test

Therefore, the plastic impurities of a 900 ml batch of biopulp in terms of covered surface, volume, and weight were exclusively analyzed. The results are indicated in **Table 4.**

Table 4. The results of physical and plastic impurities.

Analysis parameter	Result	Unit
Total volume	900	ml
Area	300	cm^2
Area covered by plastic	1.37	%
Area covered by plastic	0.22	cm^2 per % TS*
Plastic in dry matter	0.0135	g
Plastic in dry matter	0.007	% in TS
Physical impurities in dry matter	0.2112	g
Physical impurities in dry matter	0.113	% in TS

** TS: total solid*

Figure 15 exhibits the dried biopulp fibers along with the segregated impurities. Note that the content of impurities might also vary from batch to batch. The detected non-organic materials were all below 6 mm in maximum diameter and passed through the 6mm-mesh size of Ecogi®'s sieve.

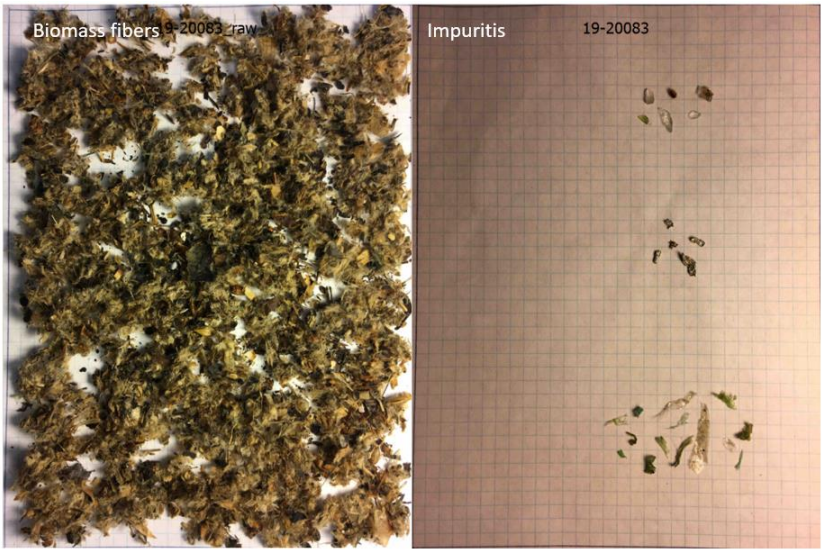

Figure 15. Dried biomass fibers and impurities.

MSW is still heavily landfilled in many countries, ignoring its problematic impurities and their hazardous effects (89). The inefficient household organic waste sorting leads to a conspicuous share of non-biodegradable contaminants such as macro and microplastics in the organic fraction of MSW. Exploring the macro and microplastic pollutants of disposal wastes is highly important as they might end up with adverse impacts on the ecosystem. The thread might end up in serious health issues for humans. This study aimed to detect the type, mass, and particle distribution of different macro and microplastics in biopulp. **Table 5** summarizes the results.

Table 5. Type, mass, and particle distribution of maco and micropolymers in biopulp (Paper A) (90).

Polymer types	Particle concentration	Polymer particle distribution	Mass concentration	Polymer distribution by mass
Unit	[g^{-1}]	[%]	[µg/g]	[%]
Micropolymers				
Polyethylene	53.33	8.89	3.12	11.38
Polypropylene	153.33	25.56	10.35	37.77
Polyester	106.67	17.78	6.4	23.51
Polyamide	33.33	5.56	0.44	1.61
Polystyrene	186.67	31.11	5.36	19.54
Cellulose acetate	66.67	11.11	1.70	6.19
Total	666.67	-	27.40	-
Macropolymers				
Polyethylene	0.25	76.92	206.16	78.24
Polyurethane	0.025	7.69	48.27	18.32
Polyester	0.025	7.69	8.80	3.34
Polystyrene	0.025	7.69	0.25	0.10
Total	0.33	-	263.60	-

Ninety different microplastic (size < 500 µm) particles detected in a 250 g sample were categorized into six main polymer groups, as shown in **Table 5**. The overall mass and particle number concentrations were approximately 27 µg/g dry biopulp and 666 g^{-1}, respectively, disclosing considerable contamination of the organic fraction with micropollutants. On the other hand, only 13 macoplastic (size > 500 µm) polymers were found in the same sample belonging to four polymer groups. The total mass concentration was 263.60 µg/g of dry biopulp, and the total plastic particle concentration was 0.33 g^{-1}. The detected polymers originate from the daily household use of ubiquitous plastic products such as textiles (polyamide), food packaging and personal care (polypropylene and polyethylene), and synthetic cloths (polyester). Some previous studies have evaluated the performance of the HTL process in disintegrating synthetic polymers (91). It has been asserted that polyolefines and polystyrene are resilient toward hydrolysis in subcritical HTL conditions resulting from the lack of hydrolysis active sites in their molecular structure. In contrast, polymers possessing heteroatomic functional groups in their structure, such as polyester, undergo significant degradation (92). Paper E has investigated the destruction of microplastics conjugated with wastewater treatment sewage sludge. The sewage sludge with around 15 to 20 wt. % of dry matter content was hydrothermally treated in a continuous pilot-scale HTL plant with a slurry flow rate of 30 kg/h at 390–420 °C. The polymer particle mass and numbers were respectively reduced by 97 % and 76 %, representing the great potential of supercritical HTL in mitigating microplastics. Polypropylene, polyethylene, and polyurethane were

identified as the most resilient polymers, whereas the remaining microplastics were almost entirely degraded (93). The degradation effect of the HTL process on the existing plastics in biopulp is not within the scope of the thesis; however, a remarkable degradation can be extrapolated by the results in the literature.

As previously mentioned, the elemental, biochemical, and physical properties of the biopulp are significantly dependent on the season and the end user process the feedstock is prepared for. For instance, dry anaerobic digestion (AD) utilizes the feed with 20-40 wt. % dry matter, while wet AD requires the feed to be less concentrated in dry matter content (10-20 wt. %) that is in the range of ideal values for HTL. Therefore, the biopulp plant could potentially deliver the same feed to the HTL plant owner with minor adjustments. A summary of the physical, elemental, and biochemical properties of a batch of biopulp obtained on July 2019 is shown in **Table 6**.

Table 6. Elemental, physical, and biochemical properties of the biomass (Paper B) (94).

Analysis	Value
Elemental analysis (wt. %)	
C [a]	52.3 ± 0.5
H [a]	7.1 ± 0.2
N [a]	3.5 ± 0.1
O [a]	27.4 ± 0.7
HHV (MJ/kg) [a]	23.2 ± 0.02
Physical properties (wt. %)	
Ash [a]	9.7 ± 0.4
Volatile matter	71.9
Fixed carbon	18.4
Moisture	83.1 ± 0.8
Biochemical properties	
Crude fat [b]	19.2
Crude protein [b]	21.8
Carbohydrate [b]	49.3

[a] Dry basis [b] DAF basis

The results reported by Phyllis 2 database for domestic organic waste, the ultimate analysis, and feed calorific value revealed a remarkable resemblance. However, the ash content indicated a considerable difference in various municipalities' disposal and recycling habits (95).

Paper B highlights the ICP analysis results (94). The total detected inorganic elements accounted for approximately 22.3 wt. % of the ash found in biomass. The significant

difference between the ash value (measured through ASTM D1102) and total inorganics (ICP) is likely due to the missing carbon and oxygen bonded to the inorganic elements in the structure of anions like carbonates, sulfates, phosphates, and oxides (96,97). Calcium, sodium, and potassium were the most abundant alkali and alkaline earth metals in the biomass accounting for 722, 494, and 286 ppm, respectively. The following element was phosphorous with 245 ppm of concentration, possibly in the form of orthophosphate and orthophosphate diesters (98). It is also possible that some of the phosphorous found are trapped in the mineral crystal lattices in the solid state (99). Phosphorous is a crucial element of modern agriculture as it aids plants in growing and maintaining their cells and tissues and generating the building blocks of RNA and DNA. The phosphorous used in fertilizers, animal feed, and additives mainly originate from phosphorite, a finite rock formed over millions of years. It has been estimated that by 2033-2034, phosphorous production will peak and subsequently fall as the worldwide resources start to deplete and ultimately threaten food security (100). Thus, closing the phosphorous loop is inevitably an urgent action that has to be taken into consideration. HTL process is capable of distributing embedded elements in biomass, including phosphorous, into various products in different phases. The following sections will extensively elaborate on the inorganic distribution in HTL products.

3.1.2. Lab-scale Experiments

3.1.2.1. Effect of Process Parameters on Products' Mass Distribution

The effect of temperature on the process was screened in this study (**Figure 16**). Biopulp was isothermally liquefied for 15 min without the presence of any catalyst at temperatures 250 to 400 with 50 °C intervals. The lowest biocrude yield was achieved at 250 °C, while the highest yield was obtained at 350 °C, approximately 30 wt. % followed by 400 (supercritical condition). Lower temperatures fail to provide sufficient activation energy for the hydrolysis of biomass macromolecules. On the other hand, with the extra energy given by supercritical conditions, the HTL intermediates might undergo gasification reactions such as steam reforming, water gas shift (WGS), and methanation, producing more unwanted byproducts.

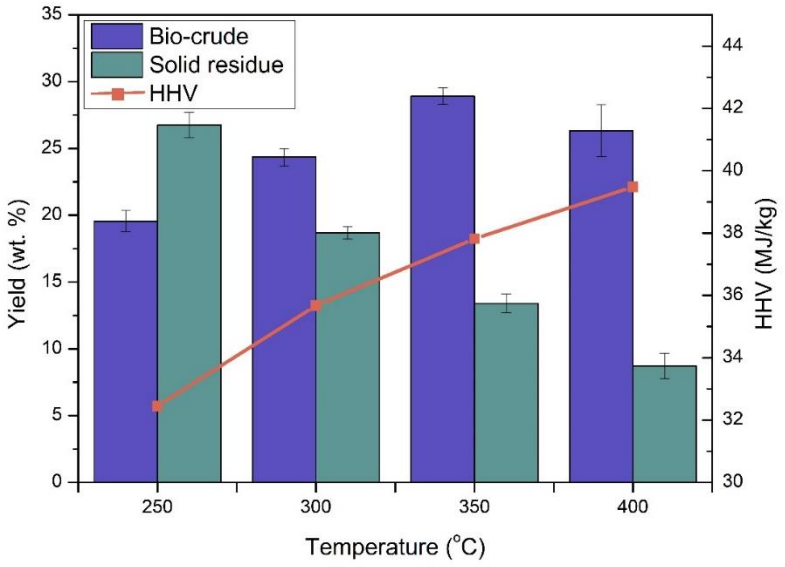

Figure 16. Effect of temperature on biocrude, solid residue yields, and biocrude's calorific value.

The results reported by Brown et al. echoed the same trend producing the maximum biocrude (43 wt. %) at 350 °C. The significantly higher biocrude yield in that study is attributed to the lipid-rich microalgae used in the process (101). The solid residue yield was uninterruptedly decreased as a result of increasing reaction severity. The solid residue (char) formation is principally a function of 1) lower defragmentation of biomass macromolecules and 2) higher repolymerization of HTL intermediates. While defragmentation is directly related to the heat of the reaction provided by the reaction temperature set point, the repolymerization is correlated to various processing conditions, including process residence time. Higher thermal energy eases the hydrolysis of biomass molecules to their corresponding monomers and produces other non-solid products. For instance, lipid hydrolysis takes place at >250 °C, and the subsequent reactions, such as decarboxylation and amidation, occur at around 300-400 °C producing biocrude range straight-chain hydrocarbons and amides, respectively (28). Therefore, lower untreated glycerides and higher biocrude will be resulted when the process temperature elevates to a certain temperature. On the other hand, the supercritical condition varies the governing mechanism and facilitates the secondary HTL intermediates reactions, such as decarbonylation and decarboxylation, that are associated with carbon transfer to other HTL phases. Herein, 350 °C was considered the optimized HTL operation temperature (control test), and the performance of different catalysts was screened at this temperature.

The incorporation of homogeneous alkali salts into the HTL slurry was associated with a considerable increase in the biocrude yield in the case of alkali carbonates. Alkali hydroxides indicated a mild improvement in the biocrude mass (KOH) or a slight reduction (NaOH). The catalyst performance in terms of biocrude production

can be ranked with the following sequence: K_2CO_3>Na_2CO_3>KOH>NaOH. The carbonate gets converted to the formate as follows:

$$K_2CO_3 + H_2O \rightleftharpoons KHCO_3 + KOH \quad (10)$$

$$KOH + CO \rightleftharpoons HCOOK \quad (11)$$

$$HCOOK + H_2O \rightleftharpoons KHCO_3 + H_2 \quad (12)$$

$$2KHCO_3 \rightleftharpoons H_2O + K_2CO_3 + CO_2 \quad (13)$$

The formed formate acts as a reducing agent and transfers hydrogen to the unsaturated and oxygen-containing compounds. Thereafter the carbonate gets regenerated in the medium. Moreover, the in-situ generated formate can play a role in promoting the WGS reaction (28).

$$CO + H_2O \rightleftharpoons CO_2 + H_2 \quad (14)$$

The WGS promotion will deplete the produced carbon monoxide in the medium and promotes the conversion of cellulose. As shown, the decomposition of biomass macromolecules such as cellulose decreases the pH of the medium by producing light organic acids. Acids are well-known for their charring effect; thus, if they remain untreated, the solid residue yield will increase with the expense of less biocrude. Thereby, the presence of alkali salts counteracts the pH reduction during the process.

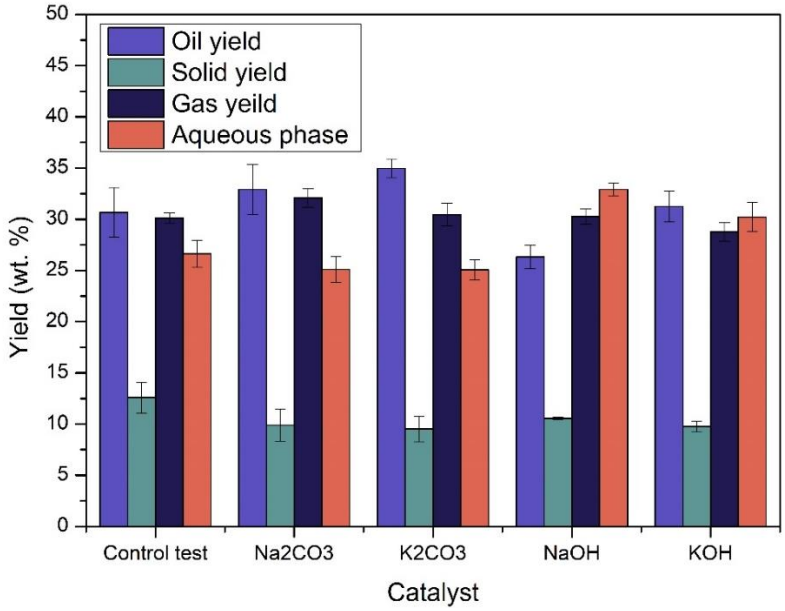

Figure 17. Effect of catalysts on mass distribution of HTL products (Paper B) (94).

With the presence of alkali carbonates, the produced CO_2 in the reaction undergoes a series of reactions releasing CO_3^{2-} (carbonate), HCO_3^-(bicarbonate), and OH^- (hydroxide) to the medium. In this way, the formed acids in the liquefaction medium will get neutralized by reacting to the presented anions and releasing H_2O and CO_2.

The gas composition results (**Figure 18**) confirm the mentioned mechanism where the concentration of CO_2 in the HTL off-gas significantly increased compared to the control test.

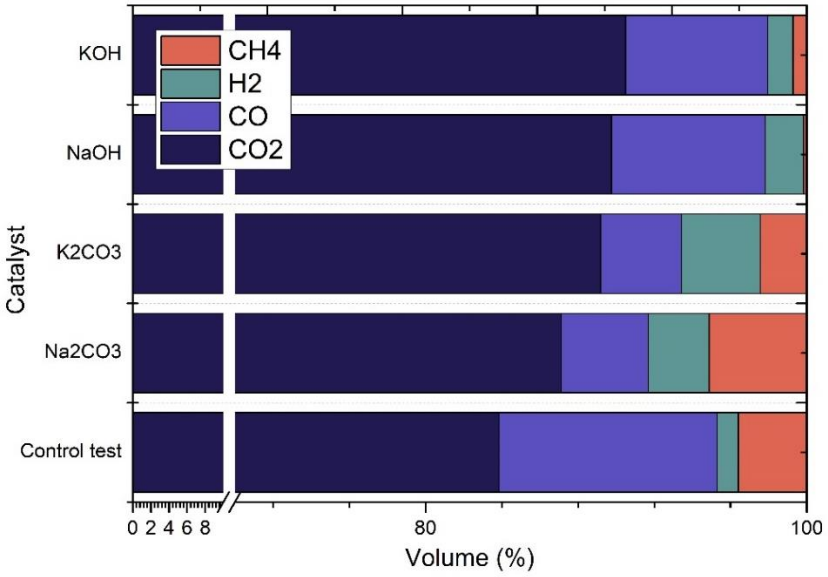

Figure 18. Results of gas composition affected by the presence of different alkali catalysts (Paper A) (102).

3.1.2.2. Effect of Process Parameters on Biocrude's Quality

The elemental analysis of the non-catalytic experiments carried out at 350 and 400 °C was obtained to compare the effect of reaction severity on the heteroatom distribution (shown in **Table 7**).

Table 7. The results of biocrude elemental analysis obtained in different HTL conditions (90).

Sample	Elemental analysis (wt.%)				O/C**	H/C**	HHV*** (MJ/kg)
	C	H	N	O*			
350-Oil	76.16 ± 0.54	9.87 ± 0.08	3.22 ± 0.20	10.72 ± 0.82	0.10	1.55	37.4
350-K_2CO_3-Oil	77.40 ± 0.72	10.58 ± 0.15	3.13 ± 0.07	8.87 ± 0.94	0.086	1.64	38.2
400-Oil	80.07 ± 0.25	10.58 ± 0.21	3.24 ± 0.13	6.09 ± 0.59	0.057	1.58	40.5
400-K_2CO_3-Oil	81.30 ± 0.34	10.95 ± 0.14	3.18 ± 0.14	4.54 ± 0.62	0.041	1.61	40.7

Calculated by difference ** Atomic ratio * Calculated by **Equation 2** **** DAF basis*

Higher process temperature significantly decreased the oxygen content of the resultant biocrude from 10.7 wt. % at 350 °C to 6.1 wt.% at 400 °C. The O/C ratio was also reduced to 0.06, representing relatively higher thermal stability of the biocrude. The lower oxygen content in the oil phase is likely caused by a higher rate of decarbonylation and decarboxylation reactions taking place at higher temperatures. The gas composition results (**Paper A, Figure 3**) conjugated with the gas mass distribution visualizes a higher share of CO_2 at higher processing temperature. On the other hand, the nitrogen content remained relatively unchanged. Two parallel pathways occurring in the higher reaction temperature can explain the observed phenomenon. The severity of the reaction increases 1) the protein hydrolysis rate resulting in the distribution of higher N-containing compounds in the medium, and 2) the side reactions, such as deamination, leading to lower nitrogenates in the biocrude. The aforementioned pathways offset each other and end up with relatively constant N content in the biocrude. The higher heating value of the product of interest experienced an apparent enhancement due to the oxygen removal and higher saturation at 400 °C; however, 350 °C demonstrated a higher energy recovery, explained by a greater biocrude yield.

As shown in **Table 7**, the presence of homogeneous catalysts significantly increased the H/C ratio resulting from the acceleration of the hydrogenation reaction. Moreover, deoxygenation reactions, e.g. decarboxylation, also result in higher H/C and lower O/C ratios. The hydroxyl groups in biomass and biocrude intermediates react with the secondary catalysts generated by the presence of alkali catalysts and release CO and CO_2 (103). In contrast, the nitrogen content of the biocrude produced in the alkali medium was considerably increased. As reported elsewhere, the acidic HTL conditions caused by the degradation and decomposition of cellulose can enhance the hydrolysis of amino acids to ammonia (water-soluble) and decrease the N content of the biocrude. However, the addition of the alkali catalyst increased the medium pH and hampered the formation of ammonia from amino acids (104). The N/C ratio in all biocrudes obtained from different alkali conditions increased (the highest obtained from K_2CO_3 (0.65)). The calorific value of the biocrudes negligibly increased, dominated by the positive impact of oxygen removal. As a consequence, energy recovery was slightly increased. The highest energy recovery was obtained when K_2CO_3 was used as the primary catalyst.

The TGA results presented in **Figure 19** reveal significant volatility of biopulp-driven biocrudes up to 400 °C, which indeed offers promising potential for fuel drop-in/blendsctock production. The presence of alkali catalysts benefited the biocrude by generating more volatiles. All the catalysts had a positive impact and reduced the share of heavy compounds at 775 °C (lower vacuum residue would be expected). In the K_2CO_3 case, for instance, the lower boiling point fraction (below 400 °C) was increased by over 8 % in comparison to the control test biocrude.

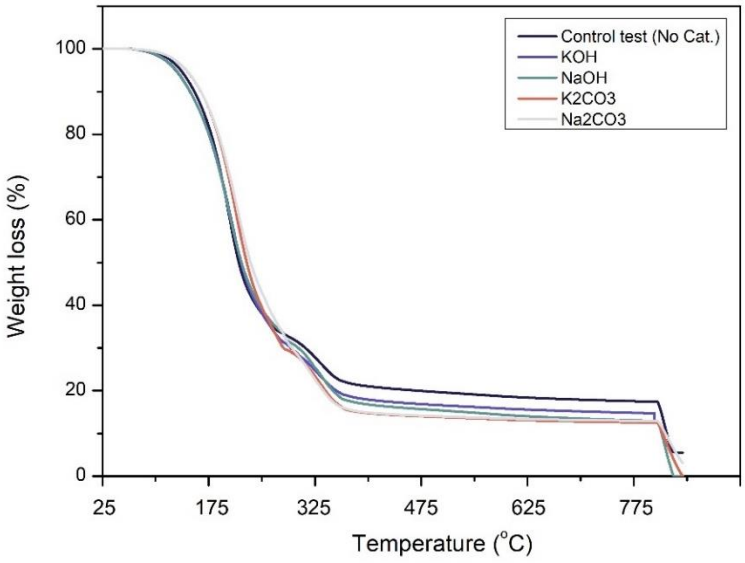

Figure 19. Results of biocrude thermogravimetric analysis obtained from catalytic HTL conditions (94).

GC-MS is capable of analyzing the chemical composition of the relatively volatile fraction of biocrude (up to 320 °C). For simplification purposes, the GC-MS chromatograms (visualized in **Figure 5, Paper B**) were categorized into four different categories, namely: Hydrocarbons (aromatics, cyclic and straight chan aliphatics), Oxygenates (alcohol, ketone, aldehyde, ether, ester, O-heterocyclics), Nitrogenates (N-heterocyclics, amides, amines, O,N-containing compounds), and carboxylic acids. The biocrude obtained at 350 °C revealed a considerable share of carboxylic acids. Although organic acids can also be driven from the hydrolysis of cellulose and protein molecules, for biopulp biocrude the main share originated from the hydrolysis of lipids (triacylglycerides (TAGs)), producing long-chain fatty acids such as hexa and octadecanoic acids and glycerol (the mechanism is provided in **Figure 20**). The presence of glycerol in the recovered aqueous phase has approved the occurrence of the aforementioned reaction. In agreement with the N distribution results, the share of N-compounds did not change significantly by increasing the process temperature, while oxygen was slightly reduced.

The presence of alkali catalysts and the associated secondary catalysts in the medium accelerated the decarboxylation and decarbonylation reactions, releasing CO and CO_2 in the gas phase and hydrocarbons in the biocrude. The most abundant long-chain carboxylic acid in the control test was n-hexadecanoic acid ($C_{15}CO_2H$). In contrast, the corresponding n-pentadecane was detected in the catalyst-assisted HTL test revealing a carbon atom loss in the gaseous products. The carbonate catalysts represented a high carbon loss (**Figure 3, Paper B**), confirming the aforementioned pathway.

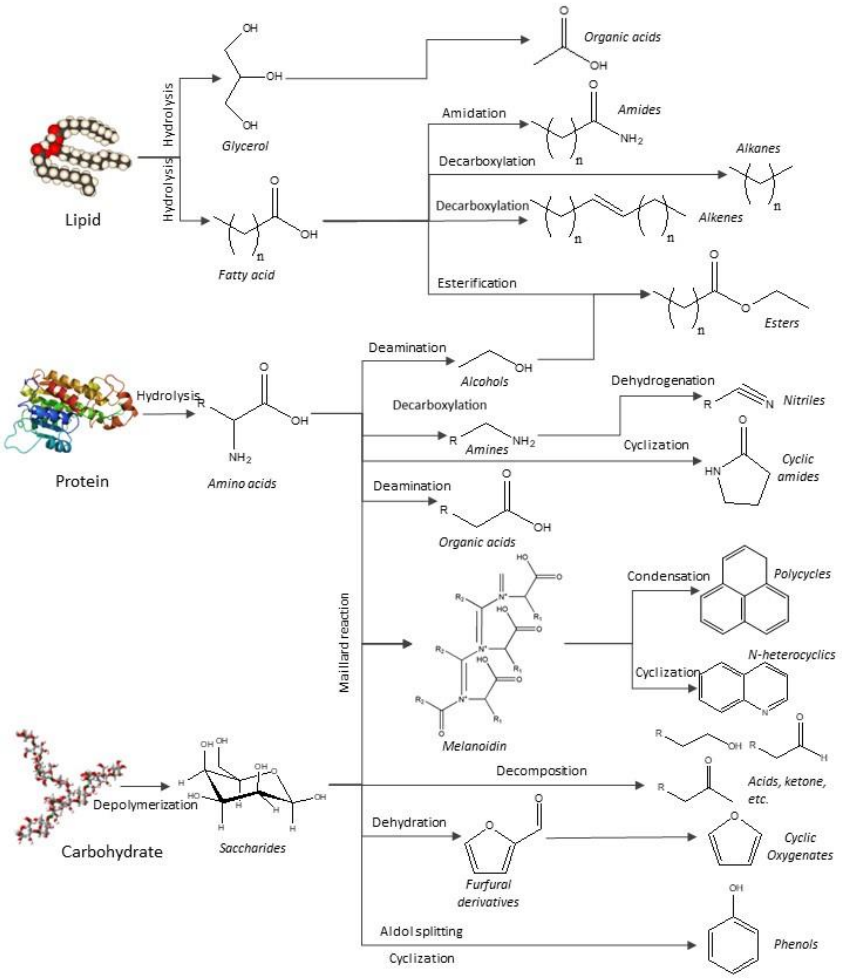

Figure 20. Summary of HTL reactions in protein-rich biomass.

3.1.2.3. Effect of Catalyst on inorganic distribution

The distribution of inorganics among different HTL products is shown in **Figure S6, paper B**. Herein, the deviation made by K_2CO_3 from the test control run is compared in **Figure 20**. The concentration of inorganics in each phase was investigated through ICP and successively multiplied by the mass fraction of the corresponding product. The resultant outcome was normalized to 100.

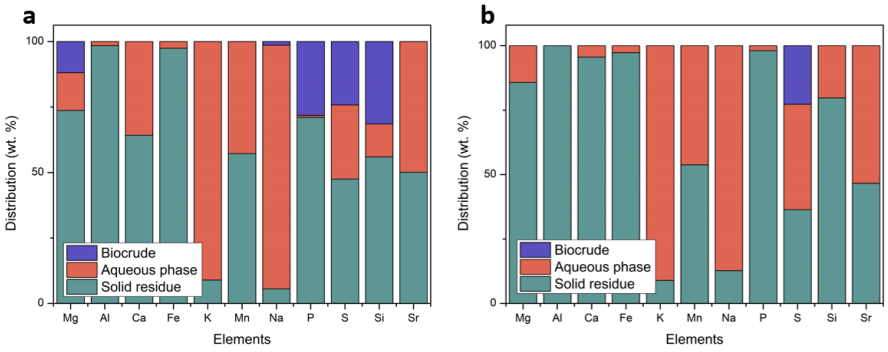

Figure 21. Inorganic distribution in a) control run and b) K_2CO_3 catalyzed experiment (94).

Most of the inorganic elements were predominantly found in the solid residue phase. The aqueous phase contained the second-largest proportion of inorganics mainly attributed to Na, K, and S. Phosphorous was mainly precipitated in the solid phase and biocrude in the control test (**Figure 21a**), whereas the distribution was dramatically switched to the solid phase in the presence of alkali salts (**Figure 21b**). As reported, the addition of the alkali catalysts to the HTL slurry aids in transferring the multivalent cations, such as Ca^{2+}, Fe^{2+}, Fe^{3+}, Al^{3+}, etc., to the solid phase and subsequently increases the insoluble phosphate formation. Among various metal cations, Ca^{2+} is a critical factor that can drastically influence the P liquid-solid distribution due to its affinity in capturing P in insoluble salts. Previous studies have shown that increasing the severity of the hydrothermal reaction by increasing temperature or adding catalysts can disintegrate the labile organic substances coordinated to Ca and make them available for forming Ca-P compounds (99). The ICP analysis shows that the P and Ca are correlated with a Ca/P molar ratio of 1.3 to 2.4 in most cases, possibly revealing the existence of hydroxyapatite's in the solid residue. The formation of $(Ca_5(PO_4)_3(OH))$ is greatly attributed to the pH of the medium, as in acidic pH conditions, traces of Ca were found in the aqueous phase, while in alkaline conditions calcium was mainly concentrated in the solid residue phase. A comparison in the presented figure can also show that the addition of the catalyst shifted Ca and P to the solid phase simultaneously.

The monovalent cations such as K^+ and Na^+ mainly distribute in the aqueous phase and form their hydroxide salt in alkaline conditions. This can open up the possibilities of the catalyst cations recovery to the HTL medium, where with a reaction with carbon monoxide, the formate ion can form and catalyze the hydrolysis of biomass molecules. Therefore, recovery of the homogeneous catalyst and organic matter might help the economy of the process, as the catalyst in the residual bioproduct will be substituted by the make-up catalyst.

3.1.3. Bench-scale Experiments

The optimal temperature found in the lab-scale experiments (350 °C) was applied to the bench-scale continuous reactor (CBS1) operating at 250 bar, a flow rate of 30 kg slurry/h, and without/with the presence of 1.5 wt. % K_2CO_3 homogeneous catalyst

(named screening I and II, respectively). Initially, the aim was to determine the influence of K_2CO_3 as a process promotor on the process operation and the possible challenges. Thereafter, the favorable condition could be applied to the unit to produce biocrude in larger quantities and assess the process stability over longer terms.

3.1.3.1. Effect of K_2CO_3 on the HTL Process Operation

Within approximately 8 hours of operation for the screening campaign, stable conditions were obtained when K_2CO_3 was used. When K_2CO_3 was absent, pressure differences were building up across the second heater and in the reactor. **Figure 22** demonstrates the pressure differences across core process units.

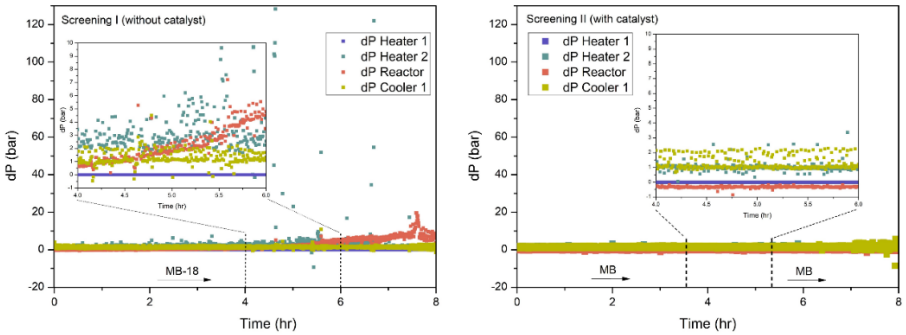

Figure 22. Process pressure differences across process heaters, reactor, and cooling during screenings I and II

During the screening I, three controlled 'blast outs' by which the feed was switched to water were performed due to the reactor and heater 2 pressure drops. After the run, the heaters and the reactor were thoroughly inspected. A tar-like material was collected from heater 2 (shown in **Figure 23**), possibly causing the resultant differential pressures (dP) and succeeding fouling. In contrast, screening II was performed under smooth processing conditions, with minor dPs across the core reaction units.

On the other hand, operating in alkaline conditions did not result in forming such compounds in the heater. Alkalis such as K_2CO_3 and NaOH have been used by many studies (mainly in batch) due to their char reduction and biocrude promotion impacts (105)(106). Alkaline condition enhances the reactions such as retro-aldol and prevents repolymerization from happening (107). This normally leads to a higher biocrude yield and lower solid content, improving the operability of continuous operations (108).

Figure 23. The material found in heater 2 after screening I.

3.1.3.2. Duration Test

Based on the obtained data, the catalytic run was selected for a duration test at subcritical conditions. The plant was run successfully for 47 hours. For the first 30 hours, a smooth operation with minor differential pressure was carried out, while in the last 17 hours campaign was not entirely steady, and several pressure differences in the reaction core units, especially the reactor, were observed. The unsteady operation was addressed using controlled blast outs; however, the system was shut down due to severe operational challenges. Afterward, the reactor was opened and inspected thoroughly. The reactor was found full of sand-like material, containing around 75 wt. % ash content (inorganics) on a dry basis, while no traces of tar was inspected in the pre-heater. The accumulated sand is likely due to the high ash content of biopulp, introduced to the feed either in the sorting and/or pretreatment stages.

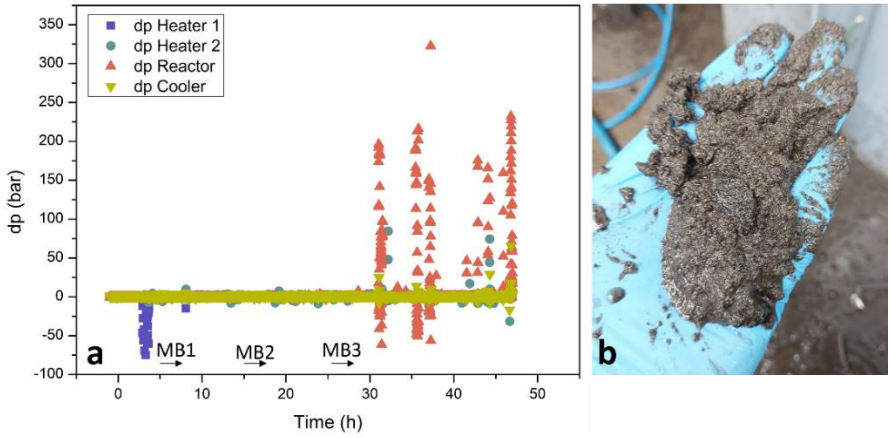

Figure 24. a) Process pressure differences across process heaters, reactor, and cooling during and b) collected material from the reactor at the end of the operation.

Apart from the gaseous products, the remaining HTL effluent appeared in a single phase product denoted as 'Emulsion'. Jensen previously reported the formation of oil-in-water emulsion in the hydrofaction system caused by a phase inversion after the gravimetric separation (27). As previously discussed, the biocrude obtained from HTL of biopulp has a major contribution of carboxylic acids resulting from the hydrolysis of triglycerides. The co-existence of carboxylates and high ash content likely results in saponification that, in turn, stabilizes the emulsion as indicated in **Figure 25**.

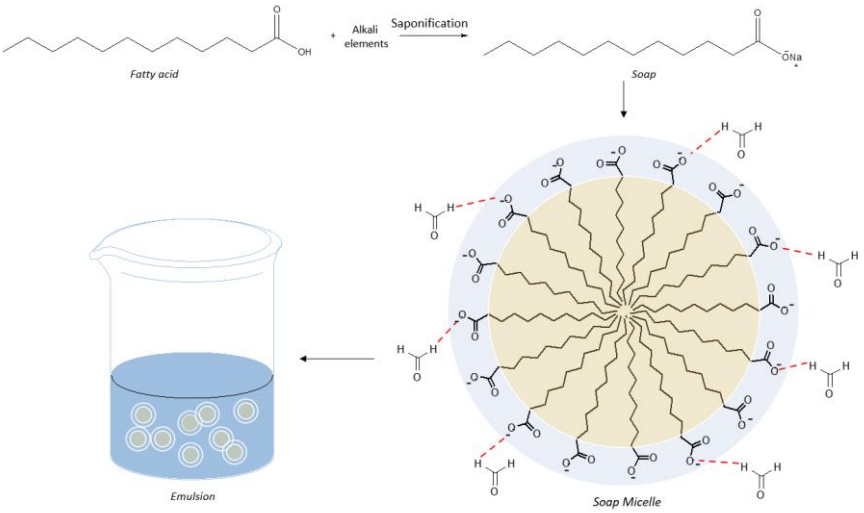

Figure 25. Schematic mechanism of emulsion formation in the presence of high lipid and ash content biomass.

Stoke's law includes the parameters affecting the speed of water-in-oil sedimentation speed. A greater density difference between the continuous and the dispersed phase and the higher radius of the droplets can potentially facilitate the breakage of the emulsion. Moreover, higher gravimetric forces (g) can aid the sedimentation speed (109).

Previous studies have reviewed the different potential solutions, such as flash/extraction, electrocoalescence, filtering, etc. Among them, diluent-assisted acid demineralization has been mentioned as a practical pathway (27). The method initially incorporates an organic solvent that lowers the density of the oil phase along with reducing its viscosity. The operation allows for the removal of cations with the aid of an acid from the structure of the formed surfactants that ultimately break the emulsion. The following section presents the experimental results concerning screening parameters associated with acid-washing demineralization.

3.1.3.3. Demineralization of the Emulsion

The primary goal of the acid-washing demineralization was to segregate different HTL products and acquire the process's mass, energy, and carbon balances. The products' reproducibility and consistency were ensured by obtaining three mass

balances (MB1-3 shown in **Figure 24**) from the campaign's stable operation zone (before 30 h).

The addition of acetic acid (AA) partially broke the emulsion by splitting it into two phases: 1) the 'Oilsand' phase, consisting of the biocrude, the residual solid, and traces of water, and 2) the effluent water phase. Due to its polar nature, the acetic acid likely breaks the alkali surfactant and transfers the cation to the aqueous phase resulting in a lower concentration of surfactants in the emerged Oilsand phase. During the experiments, the release of a gaseous phase was observed with the addition of acetic acid. The phenomenon is due to the formation of potassium acetate and the release of CO_2 according to the reaction below.

$$2\ CH_3COOH + K_2CO_3 \rightarrow H_2O + CO_2 + 2\ CH_3COOK \quad (15)$$

In the second separation stage, different acid concentrations and Oilsand:MEK:CA (MEK: methyl ethyl ketone, CA: citric acid) ratios were introduced to the separation medium to separate the solids from oilsand, as shown in **Table 8**.

Table 8. Optimization of the second separation stage.

Acid Concentration (M)	**1**	**1**	**1**	**0.3**	**0.3**	**0.3**
Ratio (wt. %)	**(1:1:1)**	**(1:0.5:0.5)**	**(1:0.25:0.25)**	**(1:1:1)**	**(1:0.5:0.5)**	**(1:0.25:0.25)**
Oil sand (g)	50.1	50.5	51.4	14.8	15.1	15.1
MEK (g)	50	26	13.2	15	7.6	3.9
CA (g)	50.1	26.2	13.6	15	7.8	3.9
Extracted solid (wt. %)*	21.2	19.8	26.5	25.7	28.5	34.4
Extracted Oil (wt. %)*	ND	ND	ND	53.7	55.71	52.2
pH	ND	ND	ND	3.5 ± 0.5	4.5 ± 0.5	5.5 ± 0.5
Comment	Poor liquid phase separation	Poor liquid phase separation	Poor liquid phase separation	Good phase separation- visibility under intense backlight	Great phase separation- visibility without backlight	Great phase separation- visibility without backlight

**Calculated based on Oilsand -ND: Not detected*

As shown, the excessive concentration of acetic acid might cause strong hydrogen bonds to water molecules that can reversibly emulsify the oilsand and cause difficulties separating biocrude. No clear phase detection was observed when 1M acid was used, confirming the mentioned theory. However, when the acid concentration was reduced to 0.3 M, all the ratios resulted in more-or-less phase separation, and a grey solid phase was precipitated in the bottom of the centrifugation vessel (shown in **Figure 26**). Due to higher biocrude separation and based on the visual inspection,

1:0.5:0.5 was chosen as the optimal condition and applied to the mass balances recovered from the duration test.

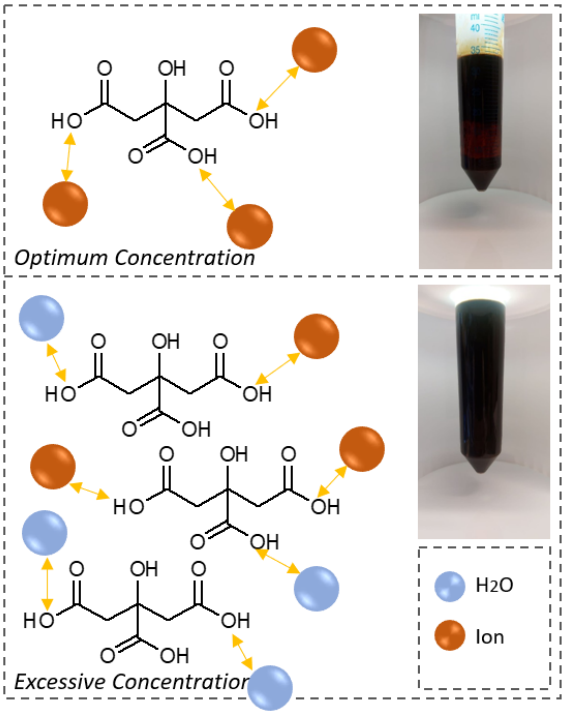

Figure 26. The impact of excessive citric acid presence on phase separation in oilsand.

The ultimate results of phase separation using acid-washing demineralization are shown in **Table 9**. Note that the negligible mass loss is due to 1) the formation of CO_2 after the addition of acetic acid and 2) the adhered products to lab equipments such as beakers and spatulas. The recovered biocrude and solid residue also reveal the consistency of the campaign in terms of HTL products. The following section will elaborate more on the duration test's carbon, mass, and energy distribution among different HTL products.

Table 9. Results of first and second separation stages.

	Test		
	MB1	MB2	MB3
Emulsion (g)	1501.8	1518.4	1536.8
Acetic acid (g)	30.6	30.4	30.8
Process water (wt. %)	89.8	90.9	90.4
Oilsand (wt.%)	9.8	8.7	9.2
Loss (wt. %)	0.4	0.4	0.5
Separated biocrude (wt. %) *	5.8	5.3	5.3
Separated Solid (wt. %) *	2.8	2.6	2.8
Separated Process water (wt. %) *	91.3	92.2	92.1

** wet basis*

3.1.3.4. Mass, Carbon, and Energy Balances

Overall mass, energy, and carbon balances of the duration HTL test are exhibited in **Figure 27**. It should be noted that the reported biocrude yield is a '*theoretical yield*' calculated based on the total DAF organics of the oil emulsion (after 1st stage separation) divided by the total DAF organics of the biomass. The reason for using the theoretical yield was to minimize the separation procedure experimental errors and have an estimation of the separation loss.

Approximately 39.2 wt.% of organics were concentrated in biocrude (theoretical). 2nd stage separation recovered 3.1 wt.% in the form of solids and water phase, ending with a promising yield of 36.1 wt.%. When comparing the biocrude yield with the batch experiments, a higher yield was obtained in the continuous unit, which is possibly due to: water diffusion to the biomass fibers while pre-mixing that significantly facilitates the hydrolysis of the biomass fragments and lower heat and mass transfer limitations. Over 20 wt. % of the loss was detected in the mass balance. A significant share of the loss could be due to malfunction of the gas mass flow controller (MFC); therefore, the gas results were not trustworthy.

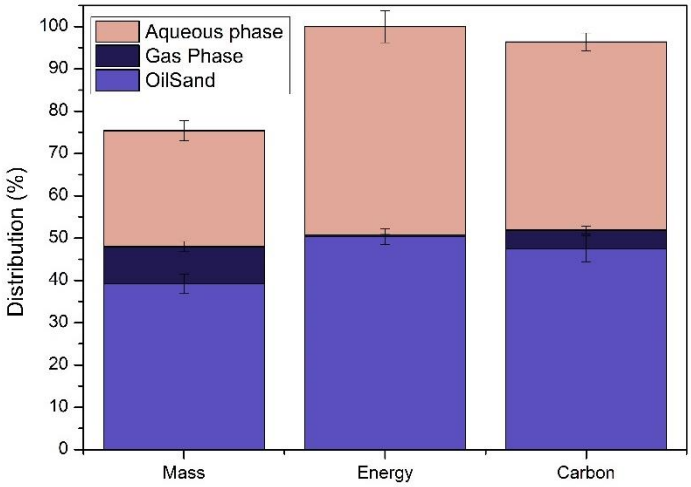

Figure 27. Mass, Energy, and Carbon balances of the duration test.

The energy balance was closed by lost energy in the water effluent, assuming a negligible energy content in the gas (0.4 %) and solid residue phases. As carbon recovery, over 50 % of the energy return was calculated in the biocrude phase. The biocrude ER can potentially increase by preventing further cracking and gasification reactions, which requires comprehensive optimization of various operating parameters such as biomass flow rate, catalyst concentration, utilization of catalyst promoters (e.g. NaOH), etc. The thesis leaves the subject for future investigations. Another proposed pathway can be utilizing the effluent water in succeeding cycles to take advantage of the embedded polar constituents of the residual water. **Chapter 4** thoroughly addresses the opportunities and challenges correlated to this method.

3.2. Conclusion

- The physical properties of biomass herald a promising feedstock for HTL conversion with an as-received optimal dry matter content. Therefore, the Ecogi® process can directly link to HTL plants without further adjustments.
- A considerable number and mass of microplastics were found in the biopulp matrix. Albeit this study did not investigate the destruction effect of HTL on these pollutants, the literature (including paper E) has relied on the technology as an efficient pathway for micropollutants mitigation.
- Subcritical vs. supercritical HTL of biopulp was a trade-off between the quantity and quality of the biocrude. However, higher energy recovery in subcritical condition was the main goal leading to select it as the primary HTL condition for further investigations.
- Alkali catalyst-assisted HTL can aid phosphorous recovery in the solid residue. More research on the bioavailability of the precipitated phosphorous is needed.

Moreover, it improves the biocrude quantity and quality. More importantly, alkalis such as K_2CO_3 facilitate smooth continuous HTL operation.

- Adding K_2CO_3 to the slurry prepared for the continuous HTL run could resolve the tar formation in the pre-heater and ease the steady operation of the unit.
- The HTL products of biopulp containing a considerable amount of crude fat and inorganics appeared as a single phase. The acid-washing process successfully addressed the products' separation.

Chapter 4. Aqueous Phase Recirculation: Challenges and Opportunities

This chapter elucidates the application of aqueous phase recirculation as a potential pathway by which not only the quantity and energy recovery of the biocrude might experience a drastic improvement but also the need for energy-intensive HTL residual water treatment can be diminished. Mass, carbon, and nitrogen distribution among different HTL products are discussed to enlighten the wastewater recycling aspects. Thereafter, the system is coupled with a batch hydrotreating system to monitor the ultimate hydrotreated biocrude with a holistic viewpoint. The opportunities and challenges that emerged by aqueous phase recirculation are comprehensively discussed, and potential solutions are provided.

Overall, the chapter aims to fulfill objective 3 of the Ph.D. thesis. Furthermore, it contributes to achieving goals No. 6 (Clean water and sanity), No. 13 (Climate action), and No. 14 (Life below water) of the sustainable development goals. The Main body of the chapter is built upon papers (A), (B), and (C). A schematic summary of the chapter is viewed in **Figure 28**.

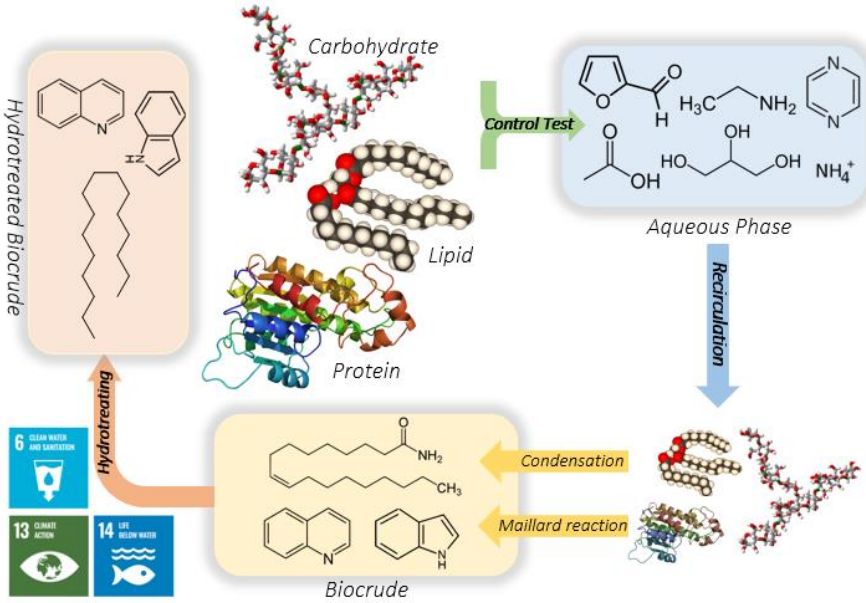

Figure 28. Schematic summary of Chapter 4.

4.1. Experimental Results

4.1.1. Aqueous Phase Concentration

The typical aqueous phase recirculation (APR) process in literature is associated with the recovery of the residual fresh water to the next cycle (substitution with the input freshwater) while using dried biomass. Recirculating fresh aqueous phase while treating moist biomass varies the dry matter content of the slurry ultimately decreasing the biocrude yield by accelerating the gasification reactions and/or increasing the TOC of the residual aqueous phase. Removing the intrinsic moisture in wet feedstock contributes to a cost-intensive process. Therefore, a common practice could be the treatment of the aqueous phase before circulating it to the next cycle. Vacuum evaporation involves reducing the interior pressure of the evaporation flask below the ambient pressure by which the liquids evaporate at a lower temperature than their boiling point. It also ensures the prevention of heat-sensitive substances' decomposition. In this study, the surplus water (distillate) was evaporated (P:60 mbar, T: 60 °C) using a vacuum evaporation system, and the remnant (concentrate) containing the valuable organics (and inorganics) was recovered to the next cycle.

As witnessed by **Figure 3b paper C** and **Figure 4a paper A,** evaporation of the distillate phase concentrated water-soluble organics in the concentrate (Higher TOC and TN). Based on the Maxwell-Bonnel equation, the evaporation AET was around 140 °C, meaning that the low boiling point organics could evaporate and reside in the distillate phase (110). **Table 1, paper C**, demonstrates the presence of light carboxylic acids in the fresh aqueous phase such as acetic acid. The evaporation process likely evaporates such compounds and accumulates the intrinsic alkalis (in the ash or catalyst) in the concentrate phase resulting in an elevated pH. Higher pH favors the presence of gaseous NH_3 over soluble NH_4^+ (**Eq. 16**), leading to a substantial decrease in NH_4^+-N in the concentrate (111).

$$NH_4^+ + OH^- \leftrightarrow NH_3.H_2O \leftrightarrow NH_3 + H_2O \quad (16)$$

Figure 29 shows the evolution of TOC, TN, and NH_4^+-N after and before evaporation, where C0 represents the control test (no APR) and C1 to C3 show the consecutive HTL cycles. As depicted, over 80 wt. % of the total organic carbon is preserved in the concentrate phase, while 60-70 wt. % of total nitrogen is kept in the same phase. The high recovery of N-compounds in the distillate is mainly due to the evaporation of ammonia (45-60 wt. % of NH_4^+-N in distillate). Therefore, the evaporation of surplus water is concluded to benefit the process in two ways: 1) Recovery of a high percentage of carbonaceous compounds (higher biocrude quantity) and 2) Removal of a considerable N-compounds (higher biocrude quality). Moreover, it can also benefit the process by recovering the homogeneous catalyst and mitigating the costs incorporated into the make-up catalyst.

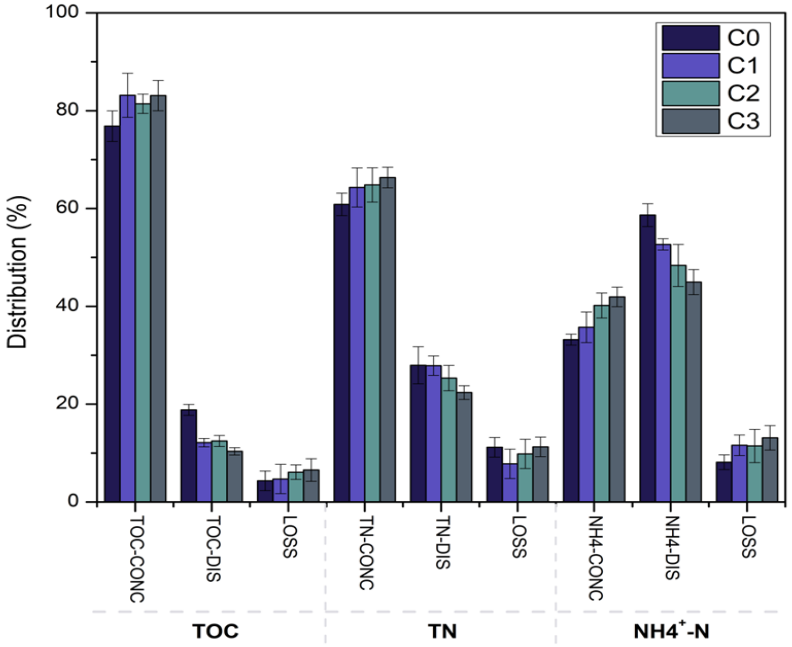

Figure 29. TOC, TN, HH_4^+-N distribution and variation during the APR (112).

4.1.2. Aqueous Phase recirculation

4.1.2.1. Mass Distribution

As concluded in **Chapter 3**, the baseline HTL temperature was selected to be 350 °C. The K_2CO_3 catalyst was found to enhance the biocrude yield; however, in this section, the non-catalytic test was carried out as the control run. The following sections will discuss the impact of the catalyst while performing aqueous phase recirculation (APR).

As depicted in **Figure 30**, the biocrude yield is significantly increased from 34.5 wt. % (control test) to 43.8 wt. % (cycle 3). The enhancement in the biocrude yield is possibly due to the occurrence of condensation reactions between HTL intermediates and incorporated aqueous phase constituents. For instance, highly reactive hydrophilic amine (decarboxylation product of amino acids) recovered to the HTL medium can react with fatty acids to produce amides (amidation reaction) (113). Hydrolysis of carbohydrate constituents forms reducing sugars, which in reaction with amino acids, might form N-heterocyclic molecules (114). The reaction mechanism will be explored in the following sections. However, the increment stopped at a certain point, and the biocrude yield reached a plateau. The reason is likely the asymptotic behavior of the organics in the aqueous phase, which reached a saturation level in the subsequent cycles. **Figure 3a Paper D** visualized the TOC and TN trend in the fresh aqueous phase obtained from different cycles. An analogous trend was observed for the aqueous phase mass distribution.

The solid content remained consistent during the course of APR experiments. Various studies have reported the positive impact of recirculated light organic acids in decomposing biomass macromolecules such as monosaccharides. For instance, the furfural intermediates can undergo condensation reactions and generate aromatic cores of hydrochar that ultimately result in higher solid residue. Another promotion effect of organic acids is generating a hydrophilic shell around the lipophilic core through a polymerization reaction (114). However, in this study, such an increasing trend was not identified, which is likely due to the removal of a considerable share of organics prior to recirculation and a significant pH enhancement.

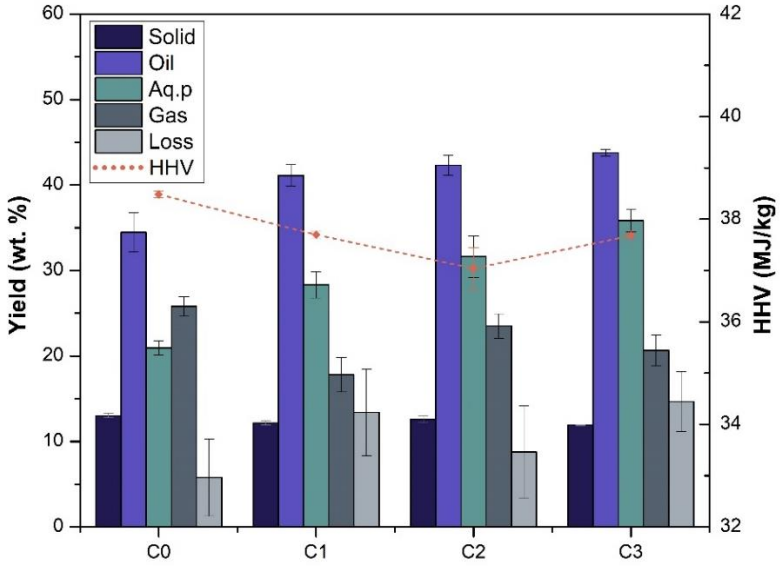

Figure 30. Mass distribution of the HTL products along with biocrude HHV during sequential aqueous phase recirculation.

4.1.2.2. Carbon and Nitrogen Balances

Figure 31a visualizes the carbon distribution among HTL products in the control and subsequent runs. Carbon was primarily concentrated in the biocrude phase, followed by the aqueous and gas phases. The consecutive APR led to a gradual decrease in the carbon content of the biocrude, possibly due to the higher content of heteroatoms (O and N) in their structure. However, the carbon distribution was dominated by the higher biocrude yield, and the trend was ascending. With a similar trend to the mass fraction, the carbon distribution in the aqueous phase initially increased and subsequently reached a steady level. Unfavorably, the nitrogen distribution demonstrated a similar trend, with around 37 % in C0 (control test) and 42 % in C3. Higher nitrogen content in the biocrude is deemed to be highly challenging for the biocrude post-treatment processes. Taking hydrotreating as an instance, many N-containing compounds are among the refractory substances and/or require a significant activation energy and H_2 quantity (113,115). Moreover, depending on the

molecular size and structure, many nitrogenous compounds can significantly decrease catalyst activity by accelerating coke propensity and/or catalyst poisoning (116). However, in-depth knowledge of the mechanism and the type of nitrogenous compounds emerging in APR is needed to be able to draw a solid conclusion.

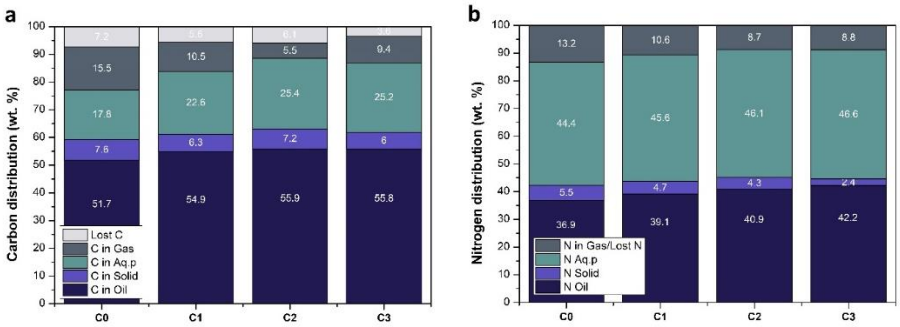

Figure 31. a) Carbon and b) Nitrogen distribution of HTL products during APR set of experiments.

A primary source of reactive amines is the amino acids formed in the present cycle. As can be seen in **Table 1, paper C**, light carboxylic acids were among the most abundant compound in the fresh aqueous phase recovered from any HTL run. Although evaporation might have removed the light acids (e.g. acetic acids), the heavier compounds were recirculated to the next cycle acidifying the medium (descending pH trend in **Figure 3a, paper C**). As reported, lower pH can improve the hydrolysis of the protein to its amino acid intermediates (117). The Amino acids can either decarboxylate to amines or undergo intermolecular condensation to produce N-heterocyclics such as pyrazine (**Figure 32**). The other possible pathway is the reaction with monosaccharides through the Maillard reaction (**Figure 34**).

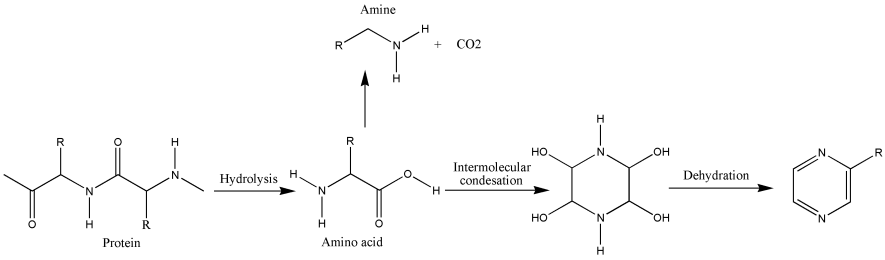

Figure 32. The reaction pathway of protein hydrolysis and the possible obtained molecules (102).

Amines are among the most reactive intermediate components in the HTL medium. Therefore they normally tend to undergo various reactions immediately depending on the process conditions. Three main pathways are elaborated herein based on the experimental observations that are visualized in **Figure 33.** The first and foremost is the condensation reaction (also known as amidation in this case). Condensation

reaction involves the ammonia, primary, and/or secondary amines (from the decarboxylation of amino acids), and fatty acids (obtained from the hydrolysis of glycerides such as 1,2,3-tristearoyl glycerol and 1,2,3-tripalmitoyl glycerol) to form fatty amides (113). The GC-MS analysis results published in **Figure 9, paper C** confirms the occurrence of such a mechanism. After APR, the relative peak area of the fatty acids (primarily hexa and octadecanoic acids) significantly diminished, and instead, the GC chromatographs heralded a significant contribution of fatty acid amides in the biocrude. Hexadecamaide and N-dimethyl-octadecenamide were the most abundant amides detected through GC-MS analysis.

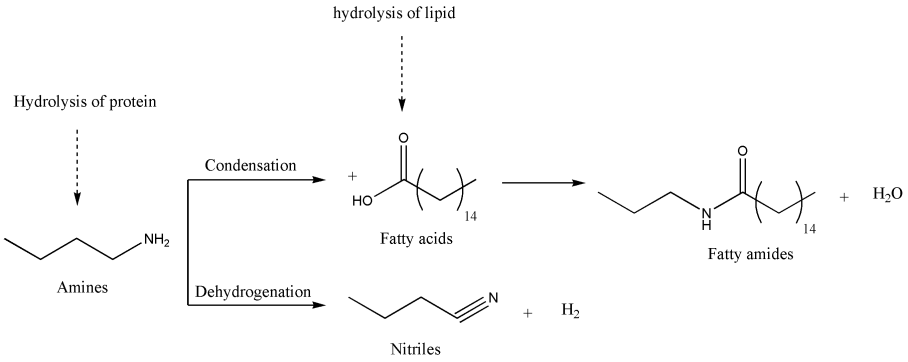

Figure 33. Main amine reaction pathways.

Dehydrogenation can also take place by converting amines to their nitrile counterpart. Traces of nitrile compounds were distinguished in the control run, confirming the occurrence of such a reaction. However, no distinct change was governed by the recirculation of the aqueous phase. Lastly, the amine can undergo a deamination reaction to produce hydrocarbons and ammonia in the reaction medium (118).

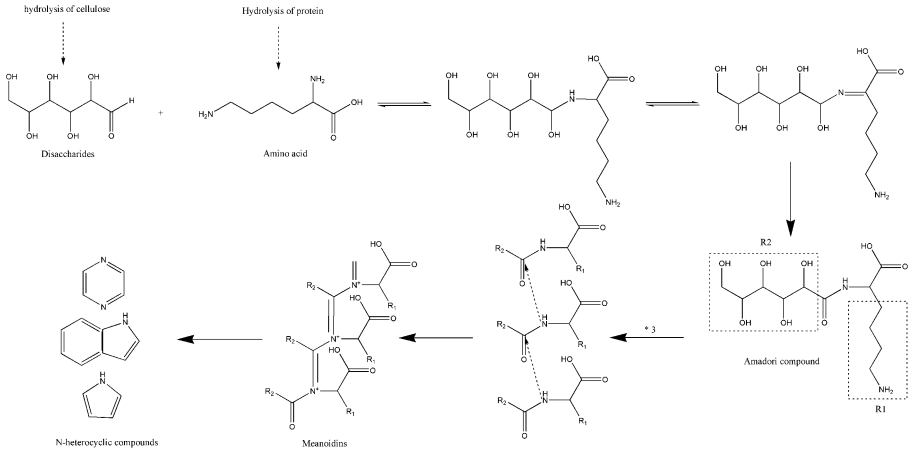

Figure 34. The reaction of monosaccharides and Amino acids (Maillard reaction) and the possible products (119).

The presence of higher amino acid intermediates as a result of APR can also facilitate the Maillard reaction, in which reducing sugars (from hydrolysis of carboxylic acids) react with the amino acid to produce mono or polycyclic N-containing compounds. **Figure 34** suggests the possible pathway in which these compounds are formed. The GC-MS data (**Figure 9, paper C**) highlights N-heterocyclic derivatives as the second abundant group of nitrogenous compounds in the biocrude. The relative peak area of this group was clearly increased in C3 as compared to C0. Indole, quinoline, and pyrazine derivatives were the dominant N-heterocyclics in the C3 biocrude triggered by condensation and Millard reactions. As indicated in the plot, the type of the derivative is directly related to the side R1 and R2 groups conjugated to the main fragments of the heterocycle.

4.1.2.3. Effect of Reactor Type on the Composition of N-compounds

The formation of N-compounds depends on various factors such as reaction temperature, residence time, and pH. Although the effects of the process condition are not directly assessed in this study, the employed batch reactors with considerably different heating and cooling rates could draw an insightful overview of the produced biocrude's quality. Identical operation conditions were set in two different reactors systems with a 15 min residence time counting immediately after reaching the temperature set point. However, as indicated in **Figure 35,** the lengthy heating and cooling rates (~5 $K.min^{-1}$) exposed the autoclave constituents to a milder regime before and after the isothermal condition (residence time). The slow heating rate potentially favors the unfavorable side reaction leading to significant variation in the chemical composition of the biocrude (120).

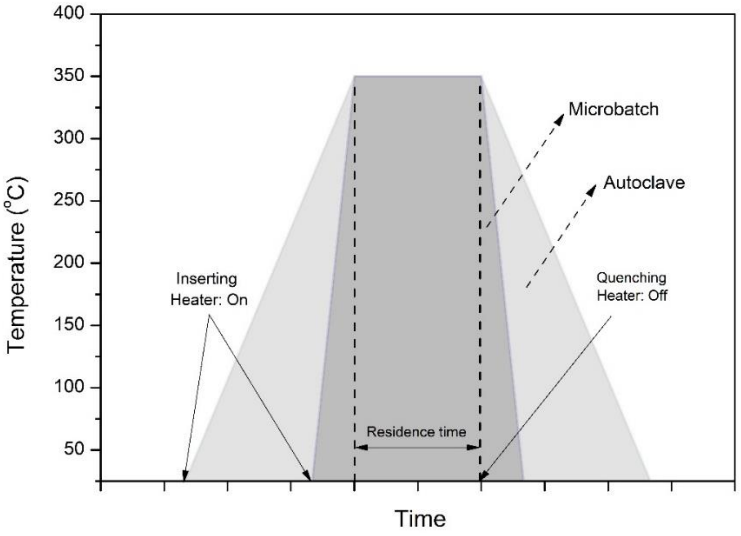

Figure 35. A schematic view of the temperature profile in microbatch and autoclave reactors.

The elemental analysis results gathered in **Table 2, paper C,** and **Table 3, paper B** indicate a higher nitrogen content for the two first cycles of the autoclave experiments 4.1 and 5.1 % in comparison to 3.4 and 4.3 % (microbatch) in C0 and C1, respectively). The reaction mechanism in subcritical HTL mainly consists of two competing reaction pathways, namely: 1) pyrolytic and hydrolytic decomposition and 2) recombination and polymerization. Two main scenarios concerning the elevated N content can be considered as follows:

As reported, the carbohydrate constituents are among the resilient macromolecules in being decomposed at low temperatures; however, the slow heating rate contributes to a prolonged residence time (during the temperature ramping), providing sufficient time for the hydrolytic defragmentation of hemicellulose and cellulose (121). The higher availability of monosaccharides might highlight the occurrence of Millard reaction in low temperatures (240-300 °C) and increase the N-heterocyclic compounds. The effect of prolonged residence time in HTL processing of N-rich biomass was studied by Motavaf et al. They concluded that the dimerization of amino acids and their reaction with carbohydrate intermediates could form N-heterocyclic components in the medium (122).

According to **Figure 33**, the condensation of amines and fatty acids is another possible pathway that might transfer higher nitrogen to the biocrude phase in the form of fatty amides. Decarboxylation of amino acids might compete with the Millard reaction at lower temperatures producing amines that can further react with fatty acids. To clarify the dominant mechanism, some prominent amides and N-heterocyclics as class representatives in the biocrude were quantitatively analyzed.

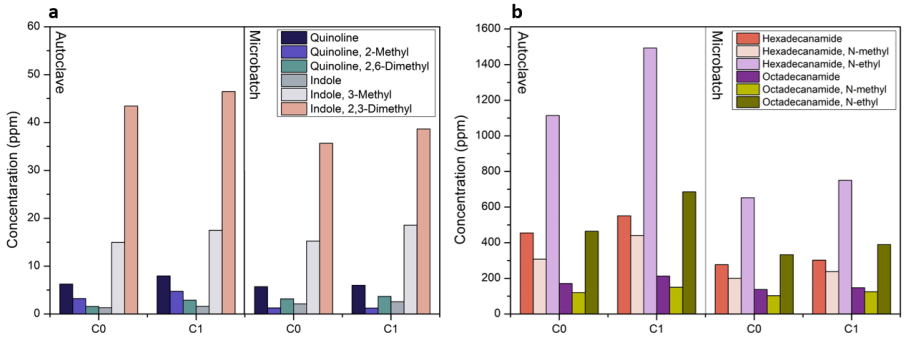

Figure 36. Quantitative analysis of a)N-heterocyclics and b)Fatty amides class representatives in two different batch reactors.

As depicted in **Figure 36**, the autoclave-driven biocrude consisted of slightly higher N-heterocyclics than that in the microbatch. However, the APR consistently increased the N-heterocyclics level regardless of the reactor type. 2,3-Dimethyl Indole was the most prominent N-heterocyclic, with 43.4 and 46.5 ppm in C0 and C1 of the autoclave-obtained biocrude. On the other hand, a significantly higher quantity of fatty amides was identified in the autoclave biocrude. Furthermore, recycling the aqueous phase in the autoclave contributed more to the elevation of fatty amides level. Therefore, it can be concluded that the type of reactor (interconnected to heating and cooling rates) can mutually enhance both mentioned mechanisms with considerable dominance for the second pathway.

4.1.3. Hydrotreating of APR-driven Biocrude

To understand the impact of APR on the final thermochemically upgraded HTL product, the biocrudes from the control experiment (C0) and the consecutive cycle (C3) were hydrotreated in mild and severe conditions. Two primary objectives of this integration were to determine the influence of APR: 1) on the quantity and 2) heteroatom content of the upgraded fuel.

4.1.3.1. Mass Distribution

As Shown in **Figure 5a, paper C**, the severity (temperature) of the reaction significantly affected the distribution of the hydrotreated products. Increasing the reaction temperature enhanced the coking propensity where C0-350 and C3-350 had considerably lower coke distribution than that in C0-350 and C0-400, respectively. Various mechanisms have been proposed in the literature, denoting polycondensation and polymerization reactions as the primary coke drivers (123). Aromatics, alkenes, and heterocyclics are the dominant compounds contributing to coke formation. In a hydrotreating medium, thermal cracking and catalytic hydrogenation compete, producing active radicals and saturated compounds, respectively. Higher activation energy induced by elevated temperature favors thermal cracking leading to the formation of free radicals. When active sites on the catalyst are not sufficiently available to hydrogenate the reactive radicals, condensation reactions take place,

producing heavy compounds that contribute to coke formation (123). **Figure 37** shows anthracene as an example to illustrate the free radical coke formation mechanism. Additionally, many investigations have reported the polymerization of unstable oxygenates (e.g. phenols, furfurals, etc.) as another primary pathway for coke formation, especially in severe hydrotreating conditions (124).

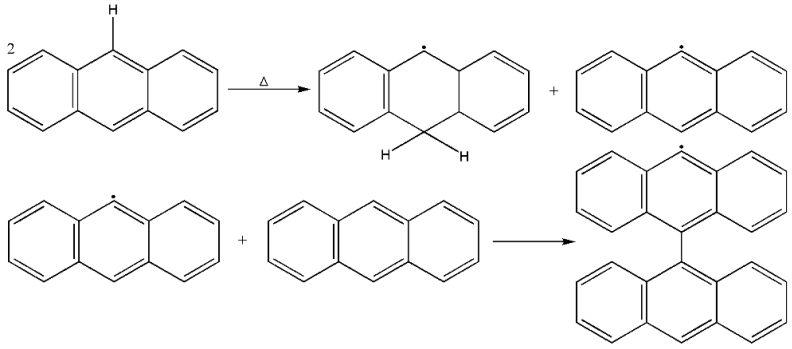

Figure 37. Free radical coke formation mechanism from anthracene (123).

Aqueous phase recirculation meaningfully increased the distribution of coke in the hydrotreated products. As an instance, C0-350 yielded 6.7 wt. % of coke, whereas the coke yield was 7.1 wt. % in C0-400. The contribution of N-heterocyclic compounds in a higher coke propensity is discussed in the literature (125). Many studies claimed that the presence of N-heteroaromatics aid in forming organometallic compounds in the form of heme or porphyrins, which can result in irreversible catalyst pore fouling and cause severe plugging (126,127). Basic N-heterocyclics such as quinoline can also participate in coke disposition on the catalyst. These compounds can be strongly adsorbed (reversibly or irreversibly with regard to the reaction conditions) on the catalyst's acidic sites. When two neighboring adsorbed molecules get partially hydrogenated (from non-heteroring), the hetero-rings might condense with an aromatic ring, forming heavy coke-ranged molecules (123). Another possible pathway is the higher concentration of reactive oxygenates in C3 as a consequence of APR. As shown in **Table 2, paper C**, C0 contained 8.73 wt. % of oxygen, which is 0.6 wt. % lower than that of C3. As mentioned, the reactive oxygenates are susceptible to cracking, condensation, and polymerization reactions, resulting in heavy compounds that highly contribute to coke formation.

A significant difference between the quantity and quality of the hydrotreated biocrude was observed as a function of the hydrotreating temperature. With regard to the control run biocrude (C0), hydrotreating at 350 °C led to a higher hydrotreated biocrude yield (76.9 wt. % vs. 68.2 wt. %) and lower deoxygenation (de-O) (96.17 % vs. 99.45 %) and denitrogenation (de-N) (48.30 % vs. 66.09 %). A closer look at the chemical composition of the raw and hydrotreated biocrude might render an insightful understanding of the impact of temperature before and after APR. The main biocrude constituents can be categorized into carboxylic acids, amides, N-heterocyclics, alcohols, and phenols.

The carboxylic acid can be deoxygenated in two different pathways depending on the reaction conditions. In mild conditions, hydrodeoxygenation leads the oxygen removal, while in severe conditions, hydrodeoxygenation and decarboxylation compete. The reaction network shown in **Figure 38** visualizes the phenomenon.

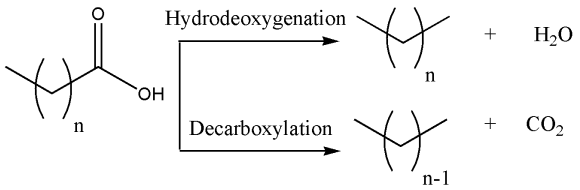

Figure 38. The main reaction network for the complete deoxygenation of carboxylic acids (87).

In severe hydrotreating conditions, decarboxylation aids the removal of oxygen at the expense of generating a CO_2 molecule and subtracting a C atom from the paraffinic structure, which might ultimately contribute to lower hydrotreated biocrude yield. A higher level of carbon dioxide was found in the gas phases (**Figure S3, paper C**) of C0-400 and C3-400, which verifies the mentioned mechanism pathway. Moreover, the GC-MS chromatographs shown below confirm the presence of C_{15}, C_{16}, C_{17}, and C_{18} paraffines in the hydrotreated oil at 400 °C, while the raw biocrude only contained C_{16}OOH and C_{18}OOH.

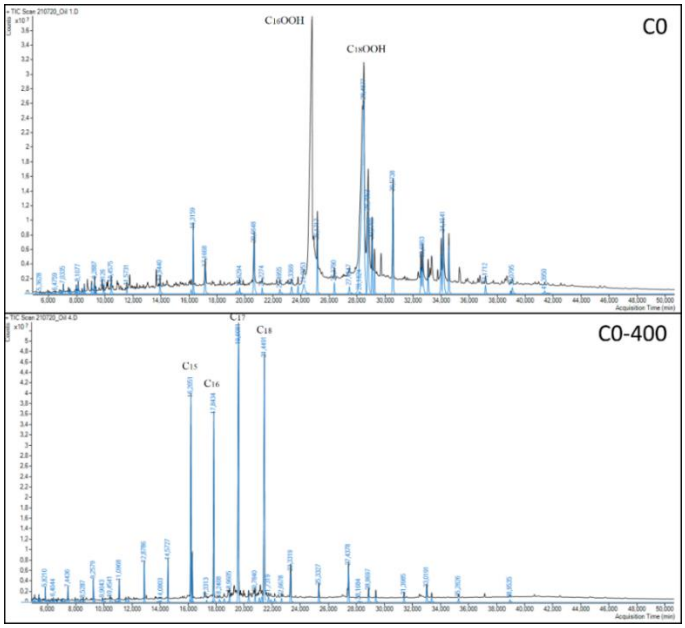

Figure 39. GC-MS chromatograms of raw and hydrotreated biocrude (at 400 °C).

Phenol derivatives can potentially be hydrogenated to produce benzene and cyclohexanol. Hydrogenation in elevated temperatures can further saturate and deoxygenate the intermediate products to cyclohexane, which is the product of interest. The GC-MS results also confirm the mechanism, where hydrotreated biocrudes at 350 °C revealed a higher share of aromatics. The higher unsaturation level at mild hydrotreated biocrudes can also be perceived by comparing the elemental analysis results, where harsh reaction conditions resulted in a higher H/C level.

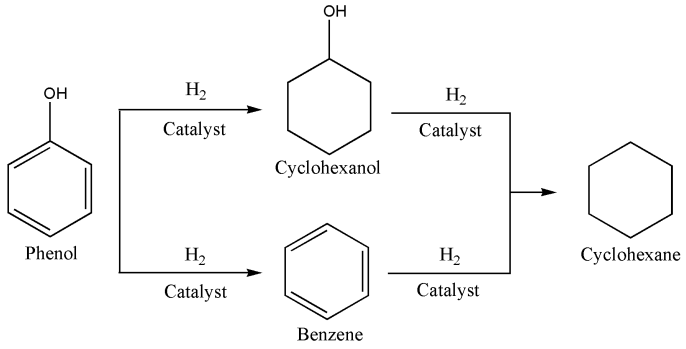

Figure 40. Suggested reaction mechanism for phenol hydrotreating (128).

Amides (primary, secondary, and tertiary) were the most abundant N-containing compounds found in the raw biocrude. However, only a trace of such compounds was detected in the hydrotreated biocrude, with a relatively higher concentration in mild conditions. Based on the semi-quantitative GC-MS results, N-methyl Octadecanamide was detected in high concentrations in C0 (120 ppm) and C3 (150 ppm). Hydrotreating at 350 °C dropped the concentration to 12 ppm and 28 ppm, whereas at 400 °C, merely 2 ppm and 3 ppm of the same compound ppm were monitored, respectively.

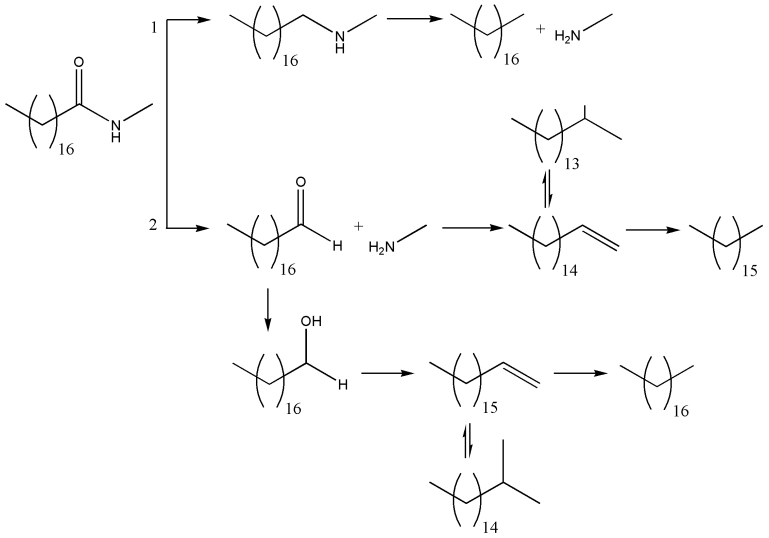

Figure 41. The HDN-HDO reaction network of N-methyl Octadecanamide (129).

Figure 41 summarizes the possible reaction network for heteroatom removal of N-methyl Octadecanamide. The primary pathway at the lower hydrotreating severities is the hydrogenation of the carbonyl functional groups. Elevation of temperature can slide the equilibrium to the co-existence of both pathways, which might result in the production of iso-paraffines and loss of a C atom through decarbonylation. APR considerably increased the amide formation in the C3 biocrude. However, hydrotreating (especially at 400 °C) significantly removed such compounds, regardless of the cycle.

The next abundant nitrogenous group was N-heterocyclics. As indicated in **Figure 36** and **Figure 10, paper C**, APR had an essential role in enhancing N-heterocyclic concentration in the subsequent cycles. Removal of such compounds using the hydrotreating process has been reported to be challenging, as many of them are refractory compounds (130). Quinoline and its derivatives were among the main nitrogenous compounds found in the raw biocrude. Herein, the main hydrotreating pathways of 2-methyl quinoline are visualized in **Figure 42**.

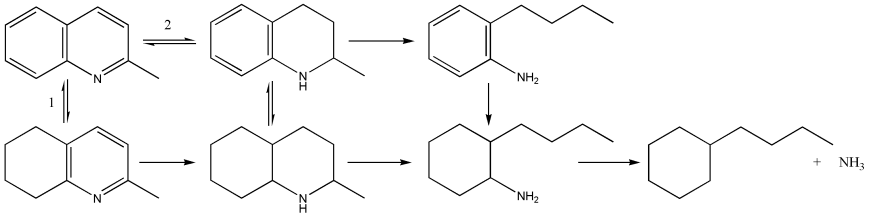

Figure 42. The hydrotreating reaction network of N-methyl quinoline (130).

The bond energy associated with the C-N bond in the heteroring is close to that of the double bond (around 615 kJ/mole). To achieve a suitable C-N bond breakage, the

heteroring requires to be hydrogenated initially, so the bond energy decreases to 305 kJ/mole for the single bond. Therefore, the hydrogenation equilibrium can strongly affect the denitrogenation rate. Due to the exothermic nature of hydrogenation, an elevated process temperature can decrease the equilibrium constants (131). However, a high hydrogen partial pressure can shift the network toward pathway 1 (thermodynamically favorable). On the other hand, pathway 2 provides a rapid hydrogenation to 2-methyl 1,2,3,4- tetrahydroquinoline due to the high Pi electron density of the heteroring. However, the C-N bond scission to o-propylaniline is kinematically restricted; therefore, the denitrogenation proceeds through 2- methyl decahydroquinoline produced via the hydrogenation of 2- methyl 5,6,7,8-tetrahydroquinoline (high hydrogen consumption) (130). All in all, the C-N bond cleavage in many N-heterocyclics takes place as a secondary step and is significantly dependent on the saturation of the aromatic rings; therefore requires specific hydrotreating conditions and high H_2 partial pressure to proceed. The mild hydrotreating conditions in this study (see **Figure 10, paper C**) did not show any significance in N-heterocyclic removal, while severe conditions slightly improved the denitrogenation of such compounds. The effect of APR on the N-heterocyclics of raw biocrudes was still present in the hydrotreated oils, charging C3-350 and C3-400 with higher nitrogen than their C0 counterparts.

4.1.3.2. Carbon and nitrogen distribution

The integrated carbon balance of HTL and HT highlights the overall carbon recovery in the final product with and without APR. Moreover, tracking nitrogen distribution as a challenging element in the final product can also evidence opportunities and challenges associated with APR. **Figure 43** presents the carbon distribution from biomass to hydrotreated fuel. In the C0 case (HTL control run), 51.7 % of carbon was associated with the biocrude phase, while the rest contributed to HTL by-products. The remaining carbon was predominantly found in the aqueous phase that might ultimately take part in expensive wastewater treatment. With this regard, concentrated aqueous phase recirculation was applied to the process. As mentioned before and can be seen here, the evaporation of surplus water only accounted for 4.1 % of carbon lost during the process and distillate phase (13.7 % was preserved in the concentrate). However, the distillate volume was around 9 to 10 times larger than the concentrate phase, translating to a very diluted carbon-containing aqueous phase that likely complies with the regulations of WWT plants. However, a detailed investigation of the different properties of the discharge distillate phase is yet to be carried out.

Recirculation of the concentrate phase increased the carbon concentration in the biocrude by 4.2 %, which can also be appreciated by the increment in the biocrude yield. The aqueous phase, however, contained a higher carbon share due to the saturation of organics. Expectedly, the hydrotreated biocrude (350 and 400 °C) had fewer carbon constituents due to coke and gas formation through reactions including condensation, polymerization, decarboxylation, decarbonylation, etc. As explained, the severity of the reaction can significantly affect the reaction pathways that ultimately change the C distribution. Apart from that, the recirculation of the aqueous phase can also influence the hydrotreating products. For instance, the coking propensity conspicuously increased in C3-350 and C3-400 compared to their C0

counterparts as a consequence of APR. Higher aromatic compounds (lower H/C), N-heterocyclics, and reactive oxygenates could be the potential causes of the change. In a nutshell, the APR can significantly decrease the need for WWT of the residual water and considerably increase the carbon in biocrude, while hydrotreating diminishes the highly distributed C to fewer quantities in the finished fuel.

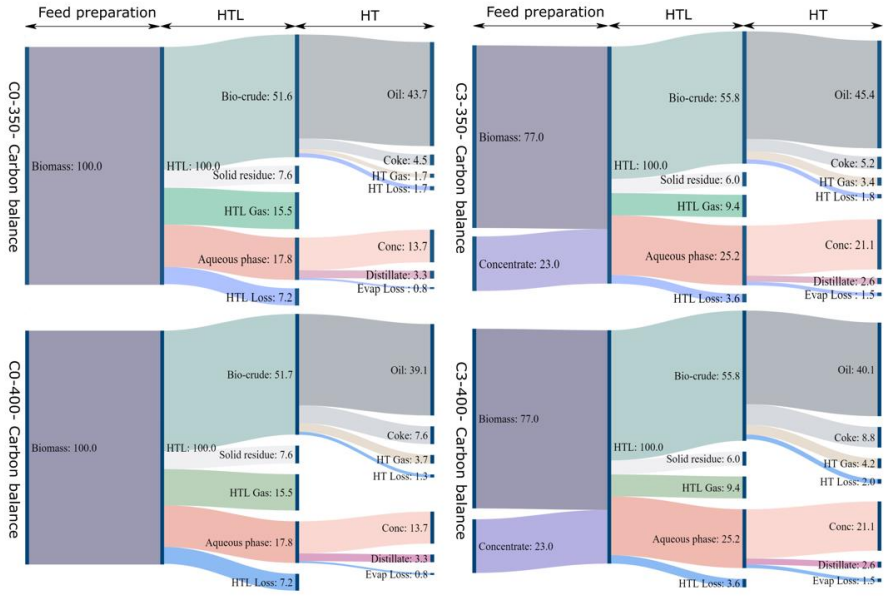

Figure 43. Carbon distribution of C0 and C3 cycles hydrotreated at 350 and 400 °C (132).

Figure 44 indicates the nitrogen distribution throughout the subjected processes. APR significantly increased the nitrogen load in the biocrude, mainly in the form of amides and N-heterocyclics. Hydrotreating at 350 °C remarkably alleviated the amide constituents, whereas it had a minor effect on the refractory N-heterocyclics. Therefore, the N concentration increased by 1.5 % in the final hydrotreated fuel (C3-350). The elevated temperature, on the other hand, could marginally aid the denitrogenation of the resilient compounds resulting in a relatively moderate decrease in the N content of the fuel (C3-400).

Detailed information on the impacts of APR on distillation and chemical properties of the raw and hydrotreated biocrudes can be found in **paper C**.

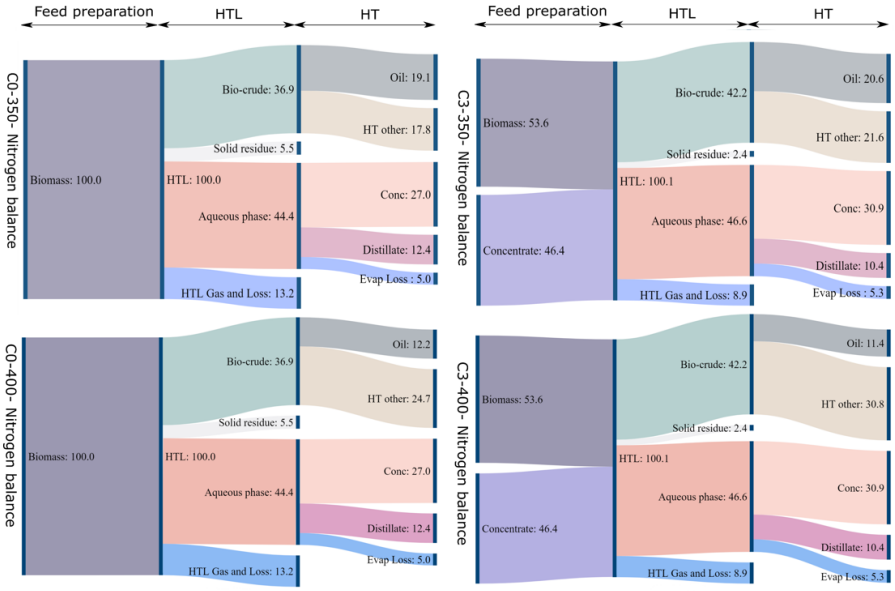

Figure 44. Nitrogen distribution of C0 and C3 cycles hydrotreated at 350 and 400 °C (132).

4.2. Conclusion

- Recirculating the concentrated aqueous phase opens up the possibility of recovering the residual HTL water while treating highly moist biomass.
- Vacuum evaporation of the surplus water demonstrated promising results in preserving the carbonaceous organics and diminishing N-containing compounds of the aqueous phase.
- The prolonged heating and cooling rate of the employed reactor increase the N content of biocrude, mainly in the form of fatty acid amides.
- Aqueous phase recirculation can significantly increase the biocrude yield and energy recovery.
- Aqueous phase recirculation increases the N content of biocrude in the form of fatty acid amides and N-heterocyclics, which deems a challenge in biocrude upgrading processes.
- To achieve high nitrogen removal, the hydrotreating process should perform in harsh conditions (high temperature, H_2 partial pressure, and WHSV) that sacrifices the economy of the process by higher catalyst deactivation, higher H_2 consumption, and lower hydrotreated oil yield and energy recovery.

Chapter 5. Advanced HTL-driven Road Diesel Blendstock Production

The following chapter elaborates on utilizing the biocrude produced in the continuous run (the production is addressed in **Chapter 3**) to produce an advanced HTL-driven road diesel blendstock. Additionally, the possibility of using the raw and partially hydrotreated biocrude (without fractionation) as a road bioblendstock is explored. The blending of the fractionated distillate cuts together and with the reference diesel complying with EN590 is the next objective covered here in this section. The stability of the produced biofuels is studied over the course of time. Lastly, the blend fuels are combusted in a compression engine, and the emission profiles are monitored.

Overall, the chapter serves to address objective 4 of the thesis. The results of the chapter potentially contribute to fulfilling sustainable development goals No.7 (Affordable and clean energy), No.13 (Responsible consumption and production), and No.13 (Climate action).

5.1. Experimental Results

5.1.1. Dehydration and Distillation of Biocrude

The presence of water in hydrocarbon pools such as biocrude induces troubles in regular packed distillation columns. Its high vaporization heat and surface tension typically necessitate unusual heating of the distillation pot that ultimately reduces the separation efficiency. Moreover, the superheated water might lead to 'bumping' in the distillation pot that risks the cracking of the biocrude components. Various techniques such as pre-heating, flash vaporization, adding chemical reagents, and pre-dehydration in distillation have been reviewed previously (133). Among them, water removal by a preliminary distillation step complying with ASTM 2892 offers a versatile and energy-efficient technique. Thereby, the biocrude was dehydrated using the mentioned standard approach.

1.3 wt. % of water was recovered by dehydration up to 130 °C (AET), whereas the Karl-Fischer analyzer detected only 0.88 wt. % of moisture. The difference could have originated from the significant load of oxygenates in the biocrude (shown in **Table 10**) that, in the presence of sufficient heat, might undergo a condensation reaction and release water to the medium. An example of a condensation reaction can be seen below.

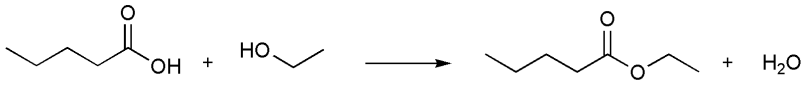

Figure 45. An example of the condensation reaction.

The true boiling point (TBP) curve of the biocrude is shown in **Figure 2a Paper D**. The initial boiling point (IBP) of the biocrude was monitored to be 84 °C. The high

IBP is possibly due to the heteroatomic nature of the light constituents that enhance hydrogen bonding and consequently require higher energy to vaporize. A total mass of 7.1 wt. % was recovered in BCD:F1 to BCD:F5, indicating considerably low gasoline and jet fuel range compounds. The diesel fraction (250-375 °C) recovered in BCD:F6 to BCD:F10 accounted for around 16 wt. %. The higher diesel recovery is due to the presence of long-chain fatty acids such as n-hexadecenoic acid in the structure of biocrude. At high AET (>350 °C), the distillates turned to a wax-like material in the condenser and the collecting vessels. To cope with the issue and prevent piping blockage, the temperature of the condenser was gradually increased to 60 °C. However, after 375 °C AET, the adhered material could not be remelted (melting point above 60 °C), and the operation ceased. Due to the high boiling point, GC-MS could not analyze the material; thus, FT-IR (**Figure 46b**) was utilized to inspect the waxy substances. The distinct peaks at 3300 and 1740 cm^{-1} correspond to O-H stretching and C=O stretching vibration of carboxylic acids, respectively. Moreover, the presence of C-H stretching and C-H bending vibrations at 2840-3000, and 1450 cm^{-1} confirms the dominance of long-chain fatty acids resulting from the hydrolysis of triglycerides.

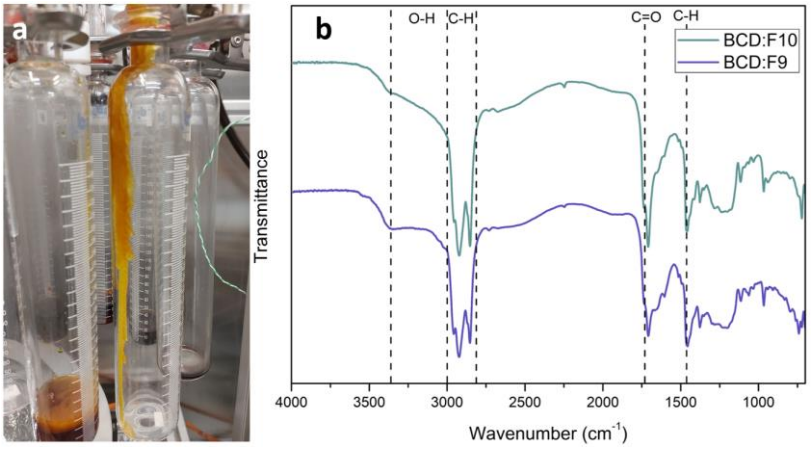

Figure 46. a) the appearance of the waxy material and b) FT-IR of BCD:F9 and BCD:F10.

The total distillation recovery of the biocrude constitutes was 23.1 wt. %, which in comparison to previous studies is conspicuously low (65,66,71). The heteroatomic functional groups containing (shown in **Table 10**) the polymerization and condensation active sites typically lead to the formation of heavy molecules and, consequently, low distillation recovery (134).

Table 10. GC-MS results of biocrude.

Name	Type	Relative abundance
2-methyl, Butane	Alkane	2.22
Hexadecane	Alkane	1.11
8-Heptadecene	Alkene	1.03
o-Cymene	aromatic	2.44
2-methyl, 1-Propanol	Alcohol	1.07
(S)-1,3-Butanediol	Alcohol	1.03
n-Hexadecanoic acid	Carboxylic acid	16.26
Tetradecanoic acid	Carboxylic acid	1.08
ethyl ester, Hexadecanate	Ester	1.57
2-tetradecyl ester, Benzeneacetic acid	Ester	1.13
3,4,6,7-tetramethyl, 2H-Oxocin-2,8(5H)-dione	Ketone	1.15
4-hydroxy-4-methyl, 2-Pentanone	Ketone	1.24
2,3-dimethyl, 2-Cyclopenten-1-one	Ketone	1.42
2,3,4-trimethyl, 2-Cyclopenten-1-one	Ketone	1.24
2-Ethylidenecyclohexanone	Ketone	2.10
2,2,5,5-tetramethyl, 3-Cyclopenten-1-one	Ketone	1.58
4-ethyl-3,4-dimethyl, 2-Cyclohexen-1-one	Ketone	1.40
2-Nonadecanone	Ketone	1.95
2-ethyl, Phenol	Phenol	1.02
4-ethyl, Phenol	Phenol	1.47
1-butyl, 2-Pyrrolidinone	N-heterocyclic	1.41
Cyclohexanespiro-5'-(4'-methyl-2'-phenyl-2'-oxazoline)	N-heterocyclic	1.16

To address the issue, a continuous hydrotreating process under mild conditions (320-330 °C, WHSV: 0.5 h^{-1}, H_2/oil mixing ratio: 1000 NL/L) was carried out. Interestingly, only a minor carbon loss in coke and the gaseous phase was observed. Based on the CHN results represented in **Table 1 Paper D,** almost 96 and 74 % of de-oxygenation and de-sulfurization were achieved, while the nitrogen content did not vary accordingly. The de-sulfurization level can potentially enhance by increasing the severity of the reaction and/or improving the employed catalysts reactivity. In agreement with the existing literature, nitrogen removal was more difficult than oxygen and sulfur removal (115). One possible explanation is the predominant existence of nitrogen in the heterocyclic aromatic compounds (see biocrude composition in **Figure 3 Paper D**). Non-heterocyclics were also present in the volatile part of the biocrude but in much smaller quantities. The thermodynamic limitation of N-heterocyclic's denitrogenation (mostly in basic N-heterocyclic such as quinoline)

requires harsher conditions (higher H_2 partial pressure) for greater nitrogen removal (130).

The chemical composition (GC-MS) of the hydrotreated biocrude (abbreviated as HTBC) was mainly dominated by Hecadecane (C16), Tetradecane (C14), Octadecane (C18), and Heneicosane (C21) along with traces of aromatics, N-heterocyclics, and oxygenates. The dominance of even-numbered alkanes possibly refers to the higher contribution of hydrodeoxygenation (HDO) in oxygen removal than de-carboxylation and de-carbonylation (87).

The HTBC was distilled using the same standard approach. The dehydration and Karl-Fischer analysis results in evidenced similar numbers, being 0.95 and 0.86 wt.%, respectively. The oxygen removal reduced the probability of Columbus bond forces, including hydrogen bonding; therefore, the feedstock had less affinity to hold polar water molecules. The same reason applies to the lower IBP, where the first droplet was observed at 70 °C, 14 °C lower than what was in the biocrude case. Another possible reason can be the higher proportion of lighter molecules originating from the cracking of their heavier precursors in the hydrotreating process. Around 13.4 wt. % of the HTBC was recovered in gasoline and jet fuel fractions, while 42.7 wt.% recovery was acquired for the diesel equivalent range revealing a significant improvement in the total recoverable fuel counterparts.

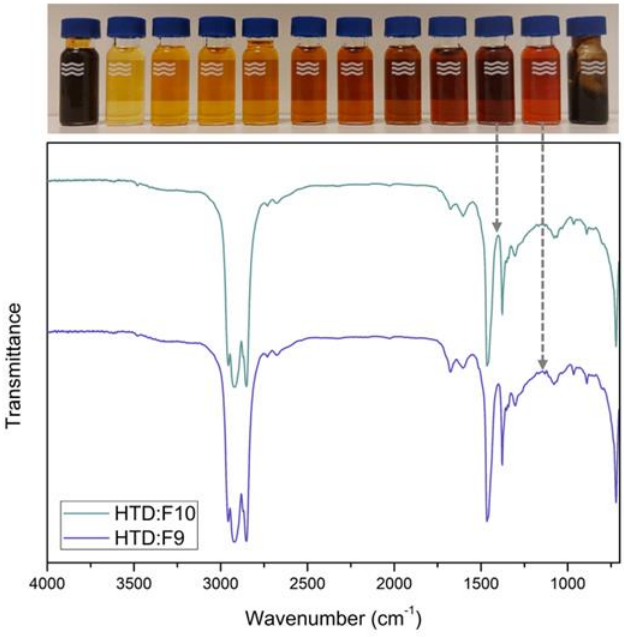

Figure 47. The appearance of the recovered distillates and FT-IR of HTD:F9 and HTD:F10.

5.1.2. Fuel Precursor and Distillate properties

The chemical, thermal, and physical properties of BC and HTBC and their relative distillate fractions are comprehensively elaborated in **Paper D**. Some of the most important physicochemical parameters of the distillation feedstock and distillate fractions are presented in **Table 11**. This section elaborates on the major limiting properties that might affect the physicochemical blending walls while optimizing the blending ratios.

Table 11. Physicochemical properties of BC, HTBC, and the corresponding distillates (Paper D).

Properties	Abbreviation	Ash	HHV	Water content	Cetane index	Density (15 °C)	Kinematic viscosity (40 °C)	Carbon Residue	Flash point	Pour point	Cloud point	Ave. C Number
Unit		(wt.%)	(MJ/kg)	(wt.%)	-	kg/m^3	mm^2/s	(wt.%)	°C	°C	°C	-
Reference diesel	RD	<0.001	43.33	0.006	58.4	823.0	2.53	<0.01	90.5	ND[a]	ND	ND
Biocrude	BC	1.50	38.70	0.88	ND	964.01	337.13	10.40	ND	ND	ND	24.46
below 100	BCD:F1	BDL[b]	37.51	2.98	62.77	904.60	ND	0.01	33	-100.7	-96.5	11.75
100-150	BCD:F2	BDL	38.67	2.12	37.69	904.64	2.65	0.02	60.5	-81.6	-78.56	14.42
150-200	BCD:F3	BDL	38.07	2.43	35.51	922.96	3.0	0.23	59.5	-70	-66.7	12.74
200-225	BCD:F4	BDL	37.99	2.26	35.51	928.78	2.86	0.21	76	-59.8	-54.3	15.12
225-250	BCD:F5	BDL	39.29	1.66	32.91	932.99	4.07	0.01	97	-39.9	-36.8	15.10
250-275	BCD:F6	BDL	38.26	1.0	50.40	933.30	5.27	0.03	105	-27.1	-24.3	16.24
275-300	BCD:F7	BDL	39.84	0.78	80.51	934.46	8.13	0.02	110	-31.6	-28.2	17.56
300-325	BCD:F8	BDL	41.20	0.32	96.10	929.05	10.36	0.01	129.5	-26.5	-22.6	19.58
325-350	BCD:F9	BDL	40.14	0.17	ND	936.07	21.63	0.0	138	-18	-14.3	19.16
350-375	BCD:F10	BDL	40.62	0.15	ND	940.50	29.77	0.0	149	19.5	23.1	20.5
Residue	BCRES	2.40	37.73	ND	ND	971.23	ND	19.61	ND	ND	ND	ND
HT Biocrude	HTBC	0.03	45.98	0.86	70.77	882.69	25.49	2.88	55	15.5	18.1	20.47
below 100	HTD:F1	BDL	40.08	0.57	34.52	779.06	ND	0.02	26	-105	-103	8.34
100-150	HTD:F2	BDL	38.45	0.56	26.16	823.68	0.84	2.64	44	-79.7	-77.5	10.71
150-200	HTD:F3	BDL	40.15	0.54	27.19	836.99	0.79	0.05	57	-63.2	-60.2	11.45
200-225	HTD:F4	BDL	43.71	0.50	26.36	862.11	1.74	0.02	79	-43	-39.9	11.79
225-250	HTD:F5	BDL	44.47	0.16	29.75	870.88	2.36	0.02	97.5	-24.8	-22.3	15.0
250-275	HTD:F6	BDL	45.76	0.13	48.83	845.34	2.51	0.02	116.5	-1.5	-0.4	14.91
275-300	HTD:F7	BDL	48.20	0.10	74.52	813.96	2.57	0.01	135.5	12.3	14.8	16.25
300-325	HTD:F8	BDL	48.92	0.09	82.47	810.86	3.28	0.03	145	15.7	18.2	17.04
325-350	HTD:F9	BDL	48.91	0.10	88.44	805.91	3.52	0.02	147	16.8	20	16.91
350-375	HTD:F10	BDL	49.34	0.11	85.14	821.12	3.90	0.03	158	20	22.4	19.41
Residue	HTRES	0.53	42.80	ND	ND	946.81	ND	3.45	ND	ND	ND	ND

a. ND: Not detected b. BDL: Below detection limit

As discussed before, the biocrude had a considerable sulfur content that was meaningfully reduced after the stabilization step. However, due to the complex matrix, the GC-MS was unable to detect any S-containing substances in BC. Although high S content was monitored in all BC fractions, BCD:F1 and BCD:F2 revealed a considerable share of thiophene and tetrahydrothiophene derivatives that would

address the unpleasant smell of the light fractions. Such compounds were not detected in HTD:F1 and HTD:F2. The non-aromatic structure of tetrahydro thiophenes leads to lower thermodynamic constraints (no need for hydrogenation of an aromatic ring) and therefore makes de-sulfurization relatively feasible at the employed operating condition (130). Despite a high sulfur removal, the stringent EN590 constraint on S content makes it a crucial factor in the blending optimization method.

Water content was the next factor that was evaluated. As mentioned before, the lower oxygen content of the HTBC and its distillates significantly reduced the moisture uptake. A maximum 0.02 wt. % of water is allowed in the marketable diesel, whereas the BC distillates contained 2.98 to 0.15 wt.% of water, led by the light fraction possessing a higher share of polar heteroatomic compounds (see **Figure 3, Paper D**). Therefore, the moisture content was detected as one of the main constraints that could potentially limit the share of bioblend in the final blended fuel.

The kinematic viscosity of BC was significantly reduced from 337.1 to 25.5 mm^2/s after hydrotreating. A similar trend was observed in the distillation cuts. The possible explanation, as schematically shown in **Figure 48**), can be the existence of two different intermolecular forces, namely hydrogen bonding (between polar molecules) and London-London dispersion (between non-polar molecules), resulting in a great resistance of the BC distillates to flow. On the contrary, the removal of oxygenates decreases the affinity of molecules in forming strong hydrogen bonds and consequently makes the fraction more flowable.

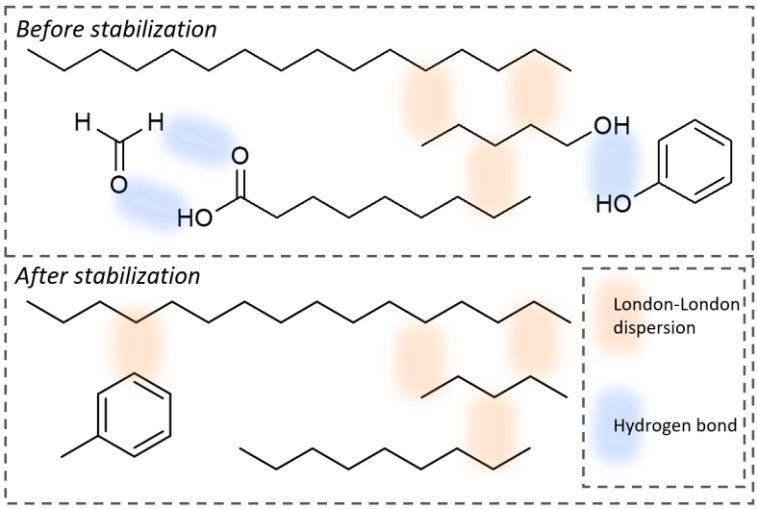

Figure 48. Effect of oxygen removal on intermolecular forces before and after stabilization.

The viscosity of the HTD:F6 to HTD:F10 was in the range required by EN590; thus, no blending constraint would occur by incorporating the viscosity in the blending optimization. Contrarily, the significant deviation of BCDs' viscosity from the acceptable range was detected as a potential challenge limiting the share of bioblend in the fuel.

Density has shown a similar trend with a considerable reduction after hydrotreating. The BC distillate fractions and vacuum residue had relatively comparable density than their precursor, possibly due to negligible recovery of fuel equivalents. On the other hand, the viscosity of HTDs remarkably decreased owing to fewer oxygenates in the fractions. The plateau observed at HTD:F4 to HTD:F6 is likely because of tighter packing of the segregated molecules (130). Similarly, the density of the HTDs is relatively in the desired range, while BCDs showed a considerable difference. Therefore, density was also included among the objective functions of the blending optimization.

The cetane number is typically correlated to the ignition delay (the time interval between injection and combustion) of diesel fuel in compression engines and, therefore, can potentially affect the eject emissions such as unburned hydrocarbons. The cetane number is defined by evaluating the quantity of cetane (n-hexadecane) and 1-methylnaphthalene in the sample, where the former has a cetane number of 100 and the latter a cetane number of 0. However, the low cetane number reference can be replaced by isocetane having higher oxidation stability (cetane number:15) to improve the precision of the measurement. However, the measurement of cetane number through the standardized methods requires a substantial amount of fuel, limiting the technique's feasibility in small-scale investigations. Therefore, the cetane index (CI) -a calculated value that can indicate the fuel's ignition quality without a costly procedure- was substituted in many studies. In this study, ISO 4264:2018 was utilized to evaluate the CI of the fuel distillates. The method utilizes **Eq. 17** to calculate the CI when the density at 15 ℃ and the distillation recovery temperatures were respectively determined via density meter and simulated-distillation instruments.

$$CI = 45.2 + 0.0892T_{10N} + (0.131+0.901B)T_{50N} + (0.0523-0.42B)T_{90N} + 0.00049(T_{10N}^2-T_{90N}^2) + 107B + 60B^2 \quad (17)$$

Where T_{10}, T_{50}, and T_{90} correspond to the temperature at which the sample was recovered 10%, 50%, and 90% of the sample. T_{10N}, T_{50N}, and T_{90N} are correlated to T_{10}-215, T_{50}-260, and T_{90}-310, respectively. D is the density at 15°C, D_N is D-850, and B is equal to $[\exp(-0{,}003\ 5D_N)] - 1$.

Note that the SimDist instrument is calibrated with a calibration mixture consisting of various known n-alkanes, and therefore the presence of O-containing hydrocarbons might interfere with the measurement. Thus, the absolute CI values for the BC and its distillates should not be the basis of any conclusion. **Figure 6b paper D** shows the CI trend in different samples. The data indicate that the CI increases upon increasing the distillate boiling point, which results from the separation of longer and saturated hydrocarbons to the ending cuts.

The thermal properties of the samples, such as flash point, cloud point, and pour point, were also determined, and the results are elaborated on in **paper D**.

5.1.3. Physicochemical blending walls

Based on a comparison with the EN590 values, the most limiting parameters were chosen to be used in the multi-objective optimization when the objective function was set in two different ways. Firstly, the objective function was to maintain the blend

properties equal to the maximum in the standard specification (procedure 1) (eq.18), whereas, in procedure 2, the objective was to retain the values below/equal to the maximum level in EN590 (eq. 19).

$$\left|z_{blend}(x_i) - z_{max,spec}\right| = 0 \quad (18)$$

$$z_{blend}(x_i) \leq z_{max,spec} \quad (19)$$

In the eq. 18 and 19, $z_{blend}(x_i)$ stands for the characteristics of distillate mixtures (bioblendstocks) while x_i represents their composition. $z_{max.spec}$ demonstrates the maximum level specified by EN590. Defining the objective function in a way that suits the purpose of the optimization is of paramount importance since it can determine the quantity and quality of the bioblend in the final mixture. EN590 did not directly specify any limitations for nitrogen content in the fuels. However, in this study, the nitrogen in the fuel was aimed to be kept as low as possible as it can directly affect the emission and the performance of the fuel in the engine.

The effect of the distillate optimization procedure is projected in **Figure 49**. Fraction 1 represents the reference diesel, and fractions 2 to 11 are the distillates obtained from either BC or HTBC. The random solution represents the results of different runs. An average of random solutions was set as the basis of the drawn conclusions. As can be seen, procedure 1 performed a less limiting optimization, introducing more of the biodistillates to the final blend. On the other hand, procedure 2, trying to keep the values well below the maximum range in EN590 was reluctant to use the biodistillates in the final blend. Thereby, procedure 1 was set as the main optimization method for the following studies.

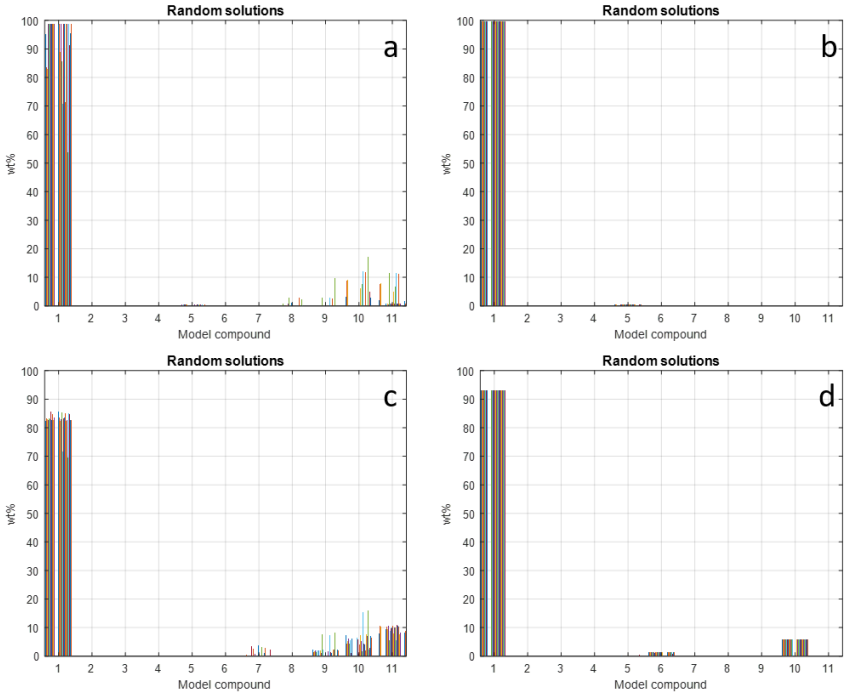

Figure 49. The blending solutions provided by the multi-objective optimization for a) BCDs procedure 1, b)BCDs procedure 2, c)HTDs procedure 1, and d) HTDs procedure 2.

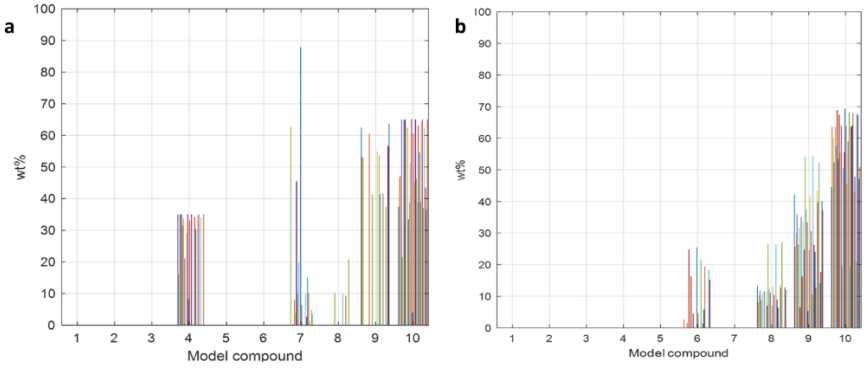

Figure 50. The composition of a) BCDM and b) HTDM biodistillates (paper D).

The optimized composition of the raw and hydrotreated distillate mixtures can be seen in **Figure 50**. Herein, the contribution of the reference diesel to the final blend is substituted for a clear demonstration. **Figure 51** visualizes the results of the mathematically calculated blending of BCDs and HTDs to the reference diesel. As can be seen, in the BCDs case, only a 0.3 wt. % of BCDM can be introduced to the

reference diesel before reaching the first blend wall. The stringent value of 10 ppm sulfur is responsible for the immediate blend limitation. The second blend was observed at approximately 5 wt. % and was related to water content.

The theoretical mixing of HTDM and the reference diesel yielded a significantly higher share of the bioblend in the final mixture, with the first blend wall found at 5.5 wt. %. The cloud point, defined as the lowest temperature at which the fuel gets a cloudy appearance, was found to limit the further share of bioblend in the finished fuel. A high concentration of straight-chain hydrocarbons can increase the cloud point, which might ultimately lead to an adverse performance of the fuel in the engine (and fuel tank), especially in the cold climate (135). The second blend wall was monitored to be the sulfur content emerging at around 9 wt. %. The mild hydrotreating incorporated into the second scenario of biodiesel production partially desulfurized (De-S: 74 %) the distillation feedstock leading to a considerably lower S content in the recovered distillates. The high content of sulfur in the fuel will be projected in the SO_2 and SO_3 emissions from the engine's exhaust.

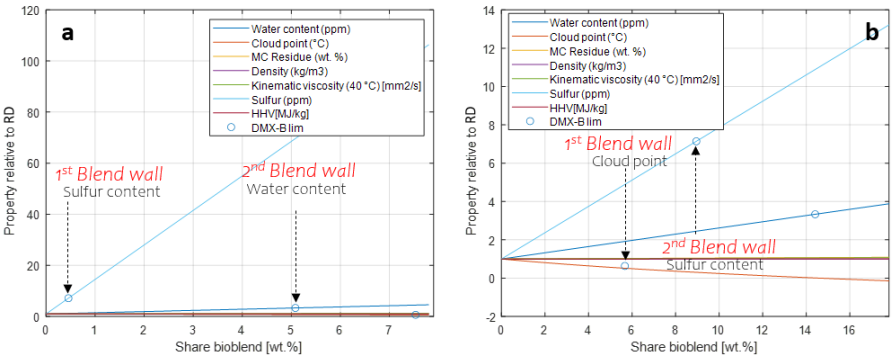

Figure 51. Projected blending elemental and physicochemical walls of a) BCDM and b)HTDM mixing with RD (paper D).

There have been various pathways suggested by previous studies to amend the cloud point and sulfur content of fuels. As an instance, catalytic and thermal cracking has been adopted to shorten the length of kerosene range hydrocarbons in petroleum refineries. However, the presence of nitrogenous compounds in the HTL-based fuel can poison the catalyst of catalytic crackers and add up to the operating cost of the value chain. Tuning hydrotreating of the biocrude based on the desirable share of the bio blend can be applied to the process, by which the operating parameters of the hydrotreater can be adjusted concerning the required bio blend share and the quality. This study serves as an exploratory study in which the potential of the HTL-based fuel being mixed with a reference diesel to produce on-spec diesel is studied, and further developments are yet to be explored in the future.

5.1.4. Physical blending wall

To ensure the mixing capability of the generated blend fuels, a 5, 10, 20, and 50 % mixture of BC, HTBC, BCDM, and HTDM were mixed with the reference diesel and stored for a week at ambient conditions. The samples were labeled as X-Y, where X abbreviates the bioblendstock and Y denotes the mixing ratio. Two samples from the top (T) and bottom (B) of sampling vials were taken and analyzed via FT-IR. A perfectly mixed sample should have the spectral features of both blendstocks and should not represent discrepancies between the top and bottom spectra.

The BC substantially adhered to the sampling tube's inner walls, resulting in a lower actual concentration than what was calculated. The samples were heated up to 45 °C and vigorously shaken to ease the miscibility; however, no significant improvement was observed. The FT-IR spectra did not represent any substantial divergence when comparing the top and bottom phases in all the blends. The spectra mainly resembled the features of the reference diesel, revealing the unsuccessful mixing of the highly polar BC with non-polar diesel. However, BC-50 clearly demonstrated the prominent vibrations of BC, possibly due to switching the solute and solvent. The microscopic image represented in **Figure 52a** verifies the formation of BC agglomerates dispersed in the RD continuous phase. Rizzo et al. identified agglomerates in various sizes when introducing biocrude to marine fuel. They argued that the presence of different polar functional groups attached to hydrocarbons might result in irregular-sized biofuel droplets when mixing them with a non-polar continuous phase. They suggest that the substitution of high-shear techniques with manual mixing can partly resolve the issue (136).

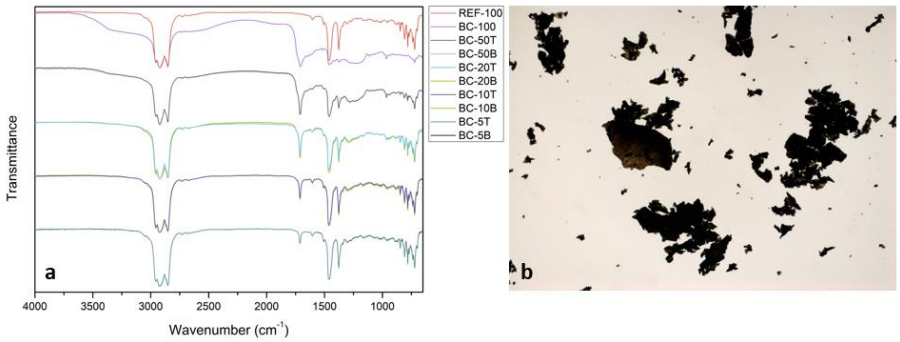

Figure 52. a) FT-IR results of different BC blends upon a week of storage and b) Optical microscopic image of the BC-10 blend (Paper D).

On the contrary, the HTBC represented the spectral characteristics of both blendstocks. However, a significant divergence was identified at 3300 cm^{-1}, especially at higher concentrations. The bottom phase demonstrated a stronger O-H stretching vibration in all cases. The possible explanation is the formation of water-in-oil emulsion in the bottom phase, where the HTBC is dominant due to higher density. The residual heteroatom-containing functionalities interact with water molecules and phase them out in the bottom constituents. The precipitated micelles can explain the

cloudy appearance of the bottom phase after the storage period. The water content of the top and bottom phases of HTBC-20 was measured to confirm the mentioned explanation. The top and bottom phases contained 0.1 and 0.18 wt. % of water, respectively. Moreover, the microscopic images taken from HTBC-10 herald a clear presence of water droplets in the bottom phase.

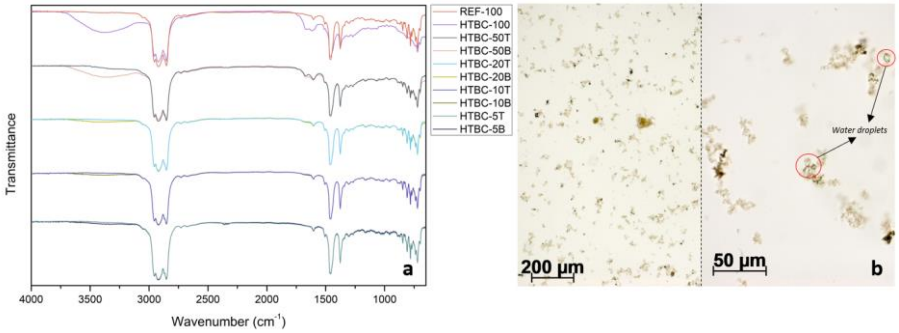

Figure 53. FT-IR results of different HTBC blends upon a week of storage and b) Optical microscopic image of the HTBC-10 blend (Paper D).

The distillate mixtures (BCDM and HTDM) were also mixed with the reference diesel in varying concentrations. After a week of storage, no visual separation was identified in any of the samples. In the case of BCDM, the FT-IR spectra witnessed the spectral features of both blendstocks with almost the same vibration peaks throughout the entire range. The isolation of a substantial quantity of fatty acids in the vacuum residue through distillation mitigates the formation of stable micelles in the blend resulting in a uniform blend composition. Furthermore, the negligible density deference between the blendstocks (RD: 823 kg/m^3 and BCD:831 kg/m^3) aids in forming the stable mixture. The microscopic image (**see Figure 54b**) also verifies the absence of agglomerates and micelles. The results conclude the possibility of physical blending of BCDM to the reference diesel in high concentrations.

Likewise, the HTDM blend samples illustrated the main FT-IR vibrations of both blendstock regardless of the concentration (**Figure 54c**). As discussed, the HTDM had a substantial proportion of non-polar paraffines that resemble the reference diesel. The similarity in the chemical composition led to a stable blend even in HTDM-50, showing the unlimited capacity of physical blending. The fairly similar density could prevent any phase separation from taking place.

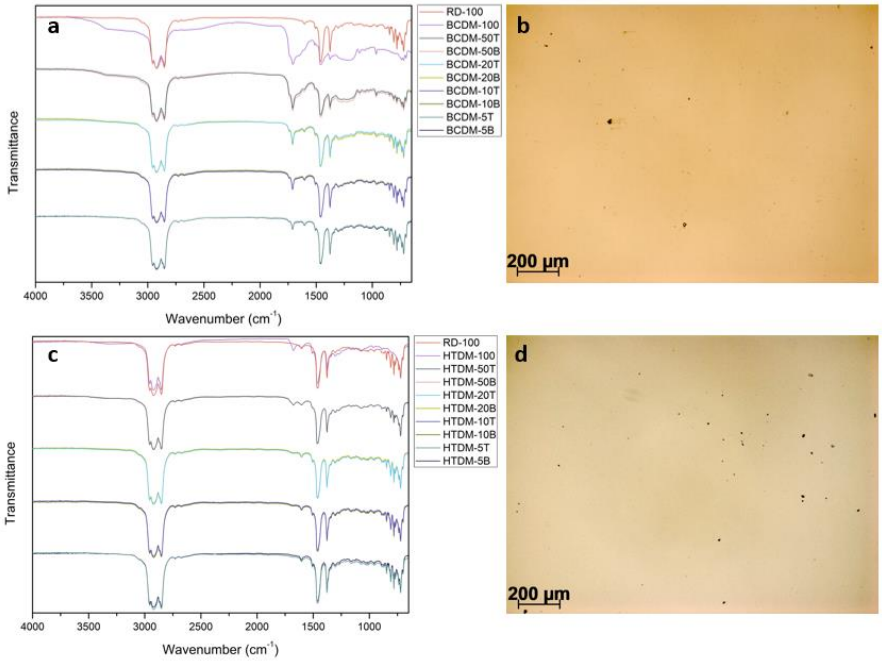

Figure 54. FT-IR results of different a) BCDM and b) HTDM blends upon a week of storage and Optical microscopic image of c) BCDM-10 and d) HTDM-10 blend (Paper D).

5.1.5. Aging and Stability

Figure 55 represents the variation in viscosity and HHV of the tentative blendstocks (HTBC and HTDM) over eight weeks of storage in ambient conditions. The higher heating value directly influencing the engine efficiency and brake-specific fuel consumption was monitored over a course of time. As shown in **Figure 55a**, a minor change was observed in both HTBC and HTDM cases. It has been reported that condensation reactions would increase the aromaticity of the fuel over time, leading to substantial variations in the heteroatom-laden bio-fuels. However, the heteroatom removal and aromatic/olefine saturation induced by partial hydrotreatment, and subsequent fractional distillation suppressed the occurrence likelihood of such a reaction. The minimal change in the HHV of the bio-blendstocks also reflects minor variation in the elemental content (especially oxygen content) of the subjected oils and, subsequently, the untacked energy content of the fuel in the storage period.

The viscosity was the next property that was tracked during storage time. Generally, the change in viscosity has been reported to be in direct relation to the oxygen content of the fuel since oxygenates such as ketones, aldehydes, and acids might induce polymerization and condensation reactions (137). Moreover, nitrogen-containing compounds can accelerate the polymerization reaction and result in higher viscosity during fuel storage (138). The viscosity of HTBC with a minor oxygen content was approximately increased by 20 % from 25.5 to 30.4 mm^2/S. While partial hydrotreating had a major role in removing oxygenates, the nitrogen-containing

compounds were still present in the oil, causing minor thermal instability. The change in thermal stability might be attributed to the change in the chemical composition of the oil containing heavier molecular weight compounds after storage. On the other hand, HTDM represented almost constant viscosity during the storage period resulting from the least oxygenates and N-compounds accommodated in the diesel fractions. The HTDM was found to be rather stable and therefore a candidate to be used as a bioblendstock in future bio-refinery schemes.

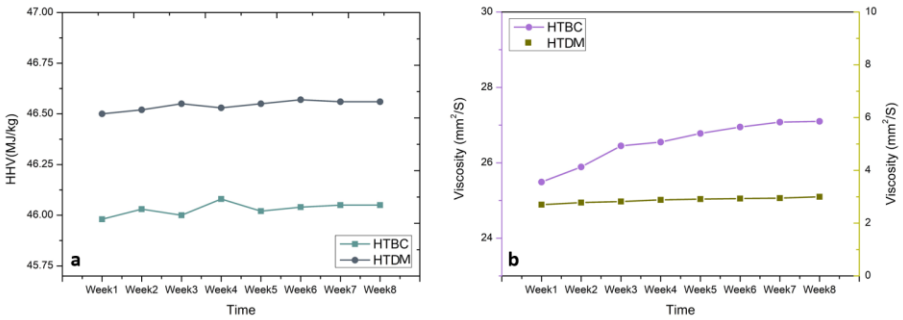

Figure 55. Weekly tracking of a) kinematic viscosity and b) HHV for HTBC and HTDM.

To investigate the stability of the obtained HTD diesel fractions, HTD:F6 to F8 were closely studied during eight weeks of storage time in the ambient condition (21 °C). The change in functionalities of F6 (250-275 °C), F7 (275-300 °C), and F8 (300-325 °C) fractions was monitored to reveal the impact of storage on the aged samples. Aging the studied fractions did not cause any substantial variation in FT-IR spectra, which is accompanied by minor structural deviations during storage. A gradual change was identified at around 3300 $cm^{-1,}$ corresponding to the O-H stretching vibration of carboxylic acid and alcohols. A slight change was also observed at C=O stretching region (around 1700 cm^{-1}). The change in the O-containing functionalities of the distillate fractions likely resulted from the self-oxidation of the hydrocarbons in reaction with O_2 in the air. The occurrence of the oxidation reaction can be verified by **Figure 56b** visualizing the samples in the first (a) and eighth (b) weeks of storage. The presence of in-situ oxygen and nitrogen can accelerate the deposit formation in the fuel, ultimately causing color change (139). As measured, the HTD:F6 had the highest oxygen (1.21 wt. %) and nitrogen (0.04 wt. %) content among the subjected samples. Moreover, the amount and type of contaminants in bio-diesel can determine the intensity of the color (140). **Figure 56b** visualizes the color change of HTD:F6 to HTD:F8 before and after two months of storage. F6 contained higher heteroatoms and indicated an intense color change, while such a change was not observed for F8.

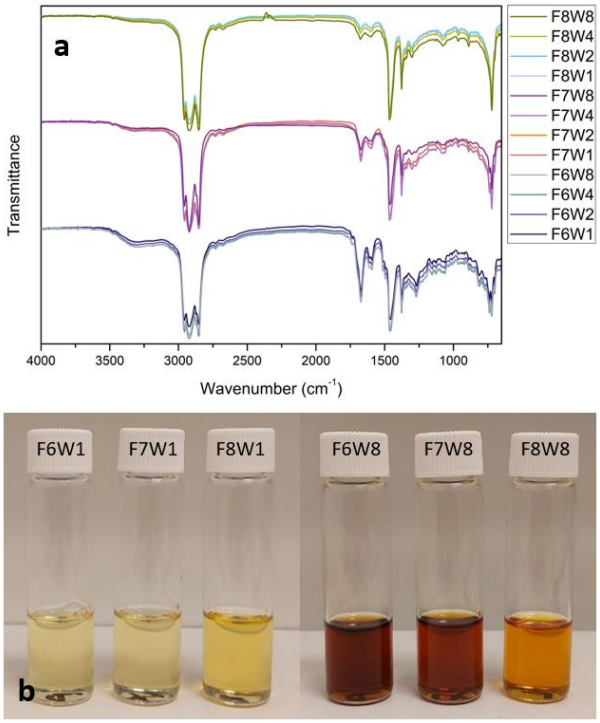

Figure 56. a) FT-IR spectra of HTD: F6 to F8 after eight weeks of storage (F and W respectively abbreviate Fraction and Week) and b) Visualization of HTD:F6-F8 in the First and eighth weeks of storage.

5.1.6. Fuel selection for engine testing

Based on the European Committee for standardization, the quality of European diesel fuels providing by fuel suppliers must be according to EN590 (the standard specification for road diesel). Although no additional specifications are established regarding the proportion of the biomass-derived diesel blendstocks, the properties of the final blend fuel must still fall in the range announced by the guidelines. In this regard, four different scenarios to produce a competent road diesel blendstock, including BC:RD, HTBC:RD, BCDM:RD, and HTDM:RD was investigated. A suitable bioblendstock must firstly be miscible with the reference diesel and secondly generate a mixture that complies with EN590.

As previously described, the raw biocrude was a highly viscous organic bulk with a semi-polar nature. BC's challenging manual blending with the reference diesel may cause additional operating costs. Additionally, it possessed an incredibly high sulfur content (270 times higher than EN590 max). High density, viscosity, water content, etc., were the other properties that could impose limits to the blending with RD. Therefore, the BC case was set aside as a potential pathway for producing road diesel blendstocks.

Hydrotreated biocrude revealed significantly augmented blending properties with easy manual blending at the first point. Nonetheless, the HTBC blends, even at least concentration (5 wt. %), had troublesome stability after only a week of storage by precipitation of micelles in the container. In terms of properties, despite a significant improvement compared to BC, it still contained a high sulfur and nitrogen content. Additionally, other properties were not in the range required by specifications. Thus, this strategy was also rolled out as an option for fuel production.

BCDM, on the other hand, represented no blending and stability issues in the studies' time period. However, the on-spec BCDM:RD had an insignificant contribution of the bioblend to the finished fuel (0.3 %) due to limiting properties such as sulfur and water contents. Likewise, HTDM stood out as a potential blendstock in terms of physical blending, stability, and storability. The on-spec HTDM-5 (5 % HTDM, 95 % RD) had all the properties in the EN590 range and therefore was selected for engine experiments. HTDM-10 complied with most of the properties with the exception of being slightly off in sulfur content and having a high cloud point. Thus, with a slight modification of the pre-stabilization step (hydrotreating), 10 wt. % contribution of the Bioblend in the finished diesel fuel can be envisaged. Hereupon, HTDM-10 was also selected for the testing engine.

The performance of the model in predicting the blend properties was validated by measuring various properties of the fuels. As can be seen in **Table 12,** the model managed to predict the results with high accuracy.

Table 12. Theoretical and Experimental estimated properties of the selected fuels.

Sample name	Water content [ppm]	Cloud point [°C]	MC Residue [wt. %]	Density [kg/m3]	Kinematic viscosity (40 °C) [mm2/s]	Sulfur [ppm]	Nitrogen [ppm]	HHV [MJ/kg]
EN590 (max)	200	-7	0.3	845.0	4.5	10	-	-
RD-100 (E)*	60	-11	<0.01	823.0	2.53	1.4	-	-
HTDM-5 (Th)**	108.58	-6.16	0.01	822.66	2.58	6.20	1272.98	46.30
HTDM-5 (E)	105.5	-	-	823.50	2.54	7.10	-	46.12
HTDM-10 (Th)	157.16	-2.57	0.01	822.31	2.62	11.01	2545.97	46.34
HTDM-10 (E)	165.81	-	-	824.65	2.71	11.41	-	46.30
BCDM-10 (Th)	335.43	-6.82	0.01	834.40	3.12	190.47	3920.60	45.67
BCDM-10 (E)	350.65	-	-	838.65	3.45	195.65	-	45.55

** **E** abbreviates: Experimental ** **Th** abbreviates: Theoretical*

5.1.7. Fuel Emission Profile

The GHG footprint of the obtained HTL-driven fuels is among the major bottlenecks that have rarely been addressed or explored in the existing literature. Here, the impact of the presence of the bioblendstocks in various generated finished diesel fuels is

discussed. The CO_2 emission was 1.38, 1.38, 1.37, and 1.40 % for Ref, HTDM-5, HTDM-10, and HTBC-10, respectively. It is well established that carbon dioxide formation is proportional to the mass of fuel burnt through complete combustion (141). Although substituting the carbon atoms with heteroatoms can potentially vary the CO_2 emission, such a phenomenon did not occur here, likely due to a low share of the bioblendstocks in the blends.

The CO emission is known as a primary indication of incomplete combustion (eq .20) of the air-fuel mixture in the engine (142).

$$C_xH_y + zO_2 \rightarrow aCO_2 + bCO + cH_2O + dH_2 \quad (20)$$

All the blend fuels reduced CO emissions that is due to the higher oxygen content of the blends compared to the reference fuel. However, BCDM-10 having the highest oxygen content, emitted more CO compared to its hydrotreated counterpart. As reported by Agrawal, viscous fuels might experience challenging atomization and vaporization that ultimately results in the promotion of incomplete combustion producing more CO, unburned hydrocarbons, and particulate matter (143). Herein, BCDM-10 was the most viscous fuel (ν = 4.45 mm^2/s). The poor atomization causes large fuel droplets while spraying triggers CO production.

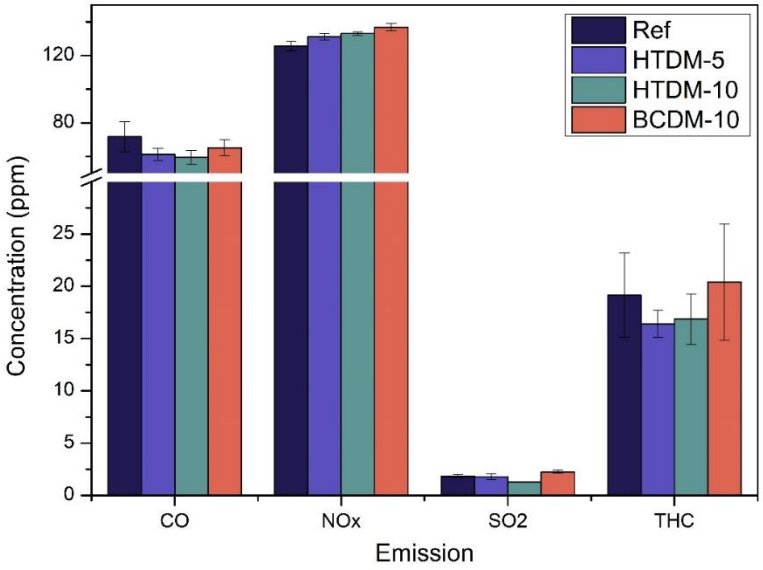

Figure 57. GHG emissions profile of the reference diesel and blend diesel fuels.

Compared to the reference diesel, all blends emitted higher NOx in the exhaust gas. Changes in the fuel chemistry, flame composition, and temperature are the most influential parameters determining the concentration of NOx during combustion. Though all the physical properties of the engine were kept constant for all the experiments, the chemical composition of the fuels was significantly changed by the addition of HTL-driven blendstocks. A possible explanation for higher NOx can be

the higher concentration of oxygen in the blend fuels. As described by the Zeldovich mechanism, during combustion, the oxygen in the fuel becomes chemically reactive and reacts with N_2 in the air producing NO, and N. NO can be further oxidized to produce NO_2 and reactive O, while N can react with OH to generate more NO (79). Not only that but also the nitrogen in the fuel can also trigger NOx production (142). The nitrogen in the fuels follows the BCDM-10> HTDM-10> HTDM-5>Ref sequence as represented in **Table 12**. Interestingly, the same order was observed for NOx production. However, it should be noted that in contrast to the dramatic difference in nitrogen concentration of the fuels (N in HTDM-10: 1273 ppm, N in BCDM-10: 3921 ppm), the NOx emission does not contribute to a significant difference (NOx in HTDM-10: 133 ppm, NOx in BCDM-10: 136 ppm) revealing the governance of the first explanation.

As described by previous studies, the SO_2 and SO_3 emissions are directly related to the sulfur content in the fuel. It is also evident that SO_2 is significantly more dominant than its oxidized form. Therefore, this study only focused on measuring SO_2. As indicated by **Figure 57**, the SO_2 emission did not considerably change when the fuel was switched to the on-spec HTDM-5. Surprisingly it even decreased with going higher in the concentration of the HTDM in the blend (HTDM-10). The on-par SO_2 generation is possibly due to the compliance of HTDM-5 with the standard specification (7.1 ppm of sulfur), while the decreasing trend is possibly due to further oxidation of SO_2 to SO_3 when higher in-situ oxygen is available (144). HTDM-10 having 196 ppm of sulfur, on the other hand, emitted the highest sulfur dioxide (2.3 ppm) in the exhaust. Note that the detected SO_2 in BCDM-10 is merely 22 % higher than the reference diesel, while there is a massive difference in the sulfur content of the fuels. The reason, as described before, is probably the significant amount of oxygen in the blend that facilitates the oxidation reaction.

Figure 57 also visualizes the concentration of total unburned hydrocarbons (THC) in the engine exhaust. The THC emissions of the fuel can be ordered as 16.4, 16.9, 19.2, and 20.5 for HTDM-5, HTDM-10, Ref, and BCDM-10, respectively. The addition of the bioblendstocks to the fuel enhances the cetane number (index) of the fuel, subsequently causing a lower ignition delay, higher combustion quality, and lower THC. Conversely, the high viscosity of the fuel challenges the air-fuel mixing and offsets the improvement resulting from a higher cetane number (141).

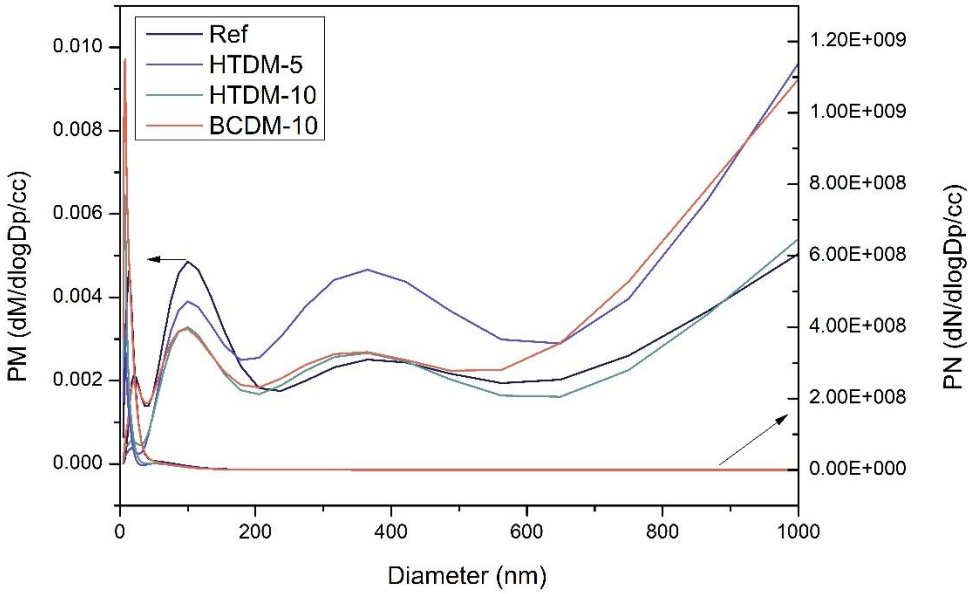

Figure 58. Soot particle and mass distribution.

Figure 58 represents the soot particle and mass distribution with a function of particle size. The average total particulate mass TPM was 5.12E-03, 5.35E-03, 3.81E-03, and 5.35E-03 µg/cc for Ref, HTDM-5, HTDM-10, and HTBC-10, respectively. As reported, the higher the in-situ oxygen content of the fuel, the less the soot emission will be in the exhaust. The reason is likely the oxidation of soot precursors that prevents further PAHs and soot growth. Oxidation of PAH precursors decreases the particle number, whereas oxidation of soot reduces the particle mass (145). Despite having the highest oxygen content, BCDM-10 revealed a significant particle mass. This could be due to the high level of unsaturation (lowest H/C) in the sample, which can potentially facilitate the formation of soot precursors in the pyrolysis section of the flame (146). Moreover, some studies have pointed out that the presence of S-containing compounds might trigger soot formation (141).

5.2. Conclusion

- Raw biocrude, without any upgrading, is not suitable for diesel blendstock production as it is fairly unstable and associated with blending challenges.
- Hydrotreating of biocrude in mild conditions significantly improves its stability, leading to higher distillation recovery and augmented physicochemical properties. However, the deficient storability of the fuel and various divergences from EN590 makes it an unfavorable choice for Bioblend production.

- Distillation of the hydrotreated biocrude encapsulates the remnant heteroatom-containing molecules in low and high boiling point cuts and improves the quality of the diesel range distillate fractions.
- The multiobjective optimization successfully predicted the properties of the distillate mixture and the blend with the reference diesel. Using that, a 5 wt.% introduction of the distillate mixture was monitored to end up with an on-spec fuel, whereas the 10 wt. % had the cloud point off.
- The emission profiles of the on-spec blend fuels revealed a relatively negligible difference from the reference diesel. However, the BCDM-10 emissions, especially NOx and SO_2 were considerably higher than that of the reference fuel, emphasizing the impact of the in-situ heteroatom content of the BCDs.

Chapter 6. Scientific Significance and Recommendations

This chapter highlights the prospects correlated to the activities in the prescribed chapters. The challenges are identified and the corresponding recommendation to improve future research are provided.

Chapter 3 elaborated on the utilization of biopulp as a potential HTL highly moist feedstock by answering the following research questions:

- How does integrating an MSW pretreatment process into HTL benefit the waste valorization value chain?
- What are the impacts of the most influential HTL parameters on the liquefaction of biopulp?

The proximate characteristics of bioplup promise it as ideal biomass for being used in the HTL process, while the existence of micro and macroplastics and the corresponding pumping challenges could potentially risk the continuous operation. The successful degradation of the microplastics through HTL was addressed in a different study when the given biomass was sewage sludge. Hence, investigating the evolution/removal of microplastic constituents in biopulp during the HTL process is of paramount importance which should be addressed in future researches. The parametric screening highlighted the necessity of incorporating an alkali catalyst (e.g. K_2CO_3) into the process as it not only could increase the bio-crude ER but also facilitate the continuous processing by mitigating the risk of HTL intermediates condensation in the preheaters. However, the nature of the plugging material is yet to be explored in future research. The catalytic run also represented promising results in terms of phosphorous recovery, whereas the impact of HTL conditions (e.g. residence time, pH, etc.) on phosphorous distribution needs to be explored through a screening study.

Chapter 4 investigated the feasibility of aqueous phase recirculation as a potential pathway for valorizing residual HTL wastewater to enhance the biocrude characteristics and quantity. The chapter was mainly built upon the following research question:

- How does aqueous phase recirculation benefit and challenge the HTL process and final marketable fuel?

Evaporation of the surplus water of the HTL aqueous phase and circulating the concentrate to the next cycle significantly increased the biocrude yield, carbon, and energy recovery. The mechanism network is also extensively discussed. To highlight the potential drawbacks that aqueous phase recirculation might possess, the obtained fuels were hydrotreated in different operating conditions. The results of this study revealed that circulating the concentrate could potentially increase the nitrogen content of the fuel precursor, and in return reflects in severe hydrotreating conditions needed. Severe hydrotreating conditions might offset the quantity enhancement by sliding the product distribution to unwanted constituents. The author recommends the incorporation of biomass pretreatment methods in which, the source of HTL N-containing compounds could get eliminated. The other possible pathway is the treatment of the aqueous phase before concentration with various extraction or adsorption techniques.

Additionally, advanced analytical techniques such as HSQC or FTICR-MS could be employed to draw a better conclusion on the distribution of oxygen and nitrogen-containing compounds in the raw and hydrotreated compounds before and after aqueous phase recirculation.

Chapter 5 explored the current potential of the biopulp raw and upgraded biocrude in being employed as a road diesel blendstock. The compliance of the obtained bioblendstock to commercial diesel specifications was closely followed. The chapter aims to provide adequate answers to the following research questions:

- What are the impacts of biocrude pre-stabilization on mass recovery, chemical and physicochemical properties of the resultant distillates?
- What is the current maximum blending potential of biopulp biocrude distillates in being used as an on-spec diesel blendstock?
- How does incorporating HTL blendstock influence the emission profiles of a compression engine?

In this study, the impact of employing a pre-stabilization process prior to any further upgrading techniques is investigated in terms of distillate recovery and properties. Moreover, a multiobjective optimization was developed to simulate blending various biodistillates based on the most limiting physicochemical properties. Furthermore, the physical and physicochemical blending walls limiting the contribution of the HTL-based bioblendstock to the final blend were detected. In the next step, the compatibility and storability of the produced fuels to a reference diesel are thoroughly investigated. Lastly, the emission profile of the blend fuels is studied and compared to the reference diesel correlating their characteristics to the exhaust emissions.

Based on the information provided here, this study recommends further complications of the method by feeding the properties such as oxidation stability, FAME content, copper corrosion, and polycyclic aromatic content to the multiobjective blending simulation. By doing so the model would be able to predict the blending ratios more realistically with higher accuracy. Moreover, the optimization of the downstream processing based on the blending walls could be carried out. For instance, the cloud point is the only limiting property in HTDM-10. Hydrocracking and/or harsher hydrotreating conditions can shift the blend wall to further values, allowing a higher quantity of the bioblendstock to the final blend. The performance of the blend fuels in the engine and the spray characteristics are among the research points that are not covered in this thesis but will be presented in a separate study in the future.

6. Reference

1. NASA. GLOBAL CLIMATE CHANGE- Vital Signs of the Planet [Internet]. 2022. Available from: https://climate.nasa.gov/vital-signs/global-temperature/
2. DAVID HERRING. Climate Change: Global Temperature Projections [Internet]. Climate.gov. 2012. Available from: www.climate.gov
3. REBECCA LINDSEY. Climate Change: Atmospheric Carbon Dioxide [Internet]. NOAA. 2022. Available from: www.climate.gov
4. Keeble BR. The Brundtland Report: "Our Common Future." Med War. 1988;4(1):17–25.
5. United States Environmental Protection Agency. GHG Reduction Programs & Strategies. EPA Center for Corporate Climate Leadership. 2022.
6. Iea. OECD total final consumption by source, 1971-2018 [Internet]. IEA, World Energy Balances. 2020. Available from: www.iea.org
7. Final energy consumption in Europe by mode of transport [Internet]. European Environment Agencey. Available from: www.eea.europa.eu
8. Christian Fetie. Statistics on Energy Consumption in Households. Eurostat Energy Community – Energy Stat Work 11-12 Novemb 2014. 2014;(November):170.
9. Translate Energy consumption in households [Internet]. Eurostat Statistics Explained. 2015. Available from: https://ec.europa.eu/
10. Priest T. Hubbert's Peak: The Great Debate over the End of Oil. Hist Stud Nat Sci [Internet]. 2014 Feb 1;44(1):37–79. Available from: https://doi.org/10.1525/hsns.2014.44.1.37
11. Iea. World Energy Outlook 2006. World energy outlook. 2006;
12. Lee RA, Lavoie J-M. From first- to third-generation biofuels: Challenges of producing a commodity from a biomass of increasing complexity. Anim Front [Internet]. 2013 Apr 1;3(2):6–11. Available from: https://doi.org/10.2527/af.2013-0010
13. EU. Directive (EU) 2018/2001 of the European Parliament and of the Council of 11 December 2018 on the promotion of the use of energy from renewable sources (recast). Off J Eur Union. 2018;2018(L 328):82–209.
14. Dhanamurugan A, Subramanian R. Performance and emission characteristics of a diesel engine with various injection pressures using bael biodiesel. Appl Mech Mater. 2014;592–594(1):1714–8.
15. Alternative Fuel Data Canter- Diesel Vehicles Using Biodiesel [Internet]. U.S. Department of Energy. Available from: https://afdc.energy.gov/
16. International Institute for Applied Systems Analysis (IIASA). The land use change impact of biofuels in the EU: Quantification of area and greenhouse gas impacts. Eur Comm [Internet]. 2015;1–261. Available from: https://ec.europa.eu/energy/sites/ener/files/documents/Final

Report_GLOBIOM_publication.pdf

17. Tovstopyat A, Zimmer Y. Russian Oilseed Production on the Rise. 2018;
18. FAO. the Importance of Ukraine and the RussianFederation for Global AgriculturalMarkets and the Risks Associated With theWar in Ukraine. 2022;(June):1–47.
19. Greenhouse gas emissions from waste [Internet]. Eurostate Your key to European statistics. 2020. Available from: https://ec.europa.eu/
20. Eurostat. Municipal Waste by Waste Management Operations - Waste Generated UNIT: Kilograms Per Capita. 2020.
21. EPA. Greenhouse Gas Reporting Program (GHGRP) [Internet]. United States Environmental Protection Agency. 2021. Available from: https://www.epa.gov/ghgreporting/ghgrp-waste
22. Sharma KD, Jain S. Municipal solid waste generation, composition, and management: the global scenario. Soc Responsib J. 2020;16(6):917–48.
23. Wei Y, Li J, Shi D, Liu G, Zhao Y, Shimaoka T. Environmental challenges impeding the composting of biodegradable municipal solid waste: A critical review. Resour Conserv Recycl [Internet]. 2017;122:51–65. Available from: https://www.sciencedirect.com/science/article/pii/S0921344917300332
24. Twan Venner. What is the Organic Fraction of Municipal Solid Waste (OFMSW)? [Internet]. 2018. Available from: https://www.royaldutchkusters.com/blog/what-is-the-organic-fraction-of-municipal-solid-waste-ofmsw
25. Uddin MM, Wright MM. Anaerobic digestion fundamentals, challenges, and technological advances. Phys Sci Rev. 2022;
26. Toor SS, Rosendahl L, Rudolf A. Hydrothermal liquefaction of biomass: A review of subcritical water technologies. Energy [Internet]. 2011;36(5):2328–42. Available from: https://www.sciencedirect.com/science/article/pii/S0360544211001691
27. Version D. Aalborg Universitet PIUS - Hydrofaction (TM) Platform with Integrated Upgrading Step Jensen , Claus Uhrenholt. 2018.
28. Pedersen TH. HydroThermal Liquefaction of Biomass and Model Compounds. 2015. 1–217 p.
29. Machmudah S, Wahyudiono, Kanda H, Goto M. Chapter 3 - Hydrolysis of Biopolymers in Near-Critical and Subcritical Water. In: Dominguez González H, González Muñoz MJBT-WE of BC, editors. Elsevier; 2017. p. 69–107. Available from: https://www.sciencedirect.com/science/article/pii/B9780128093801000036
30. Mahesh D, Ahmad S, Kumar R, Chakravarthy SR, Vinu R. Hydrothermal liquefaction of municipal solid wastes for high quality bio-crude production using glycerol as co-solvent. Bioresour Technol [Internet]. 2021;339:125537. Available from: https://www.sciencedirect.com/science/article/pii/S0960852421008774
31. Snowden-Swan L, Li S, Jiang Y, Thorson M, Schmidt A, Seiple T, et al. Wet Waste Hydrothermal Liquefaction and Biocrude Upgrading to Hydrocarbon

Fuels: 2021 State of Technology. Pacific Northwest Natl Lab [Internet]. 2022;(30982). Available from: https://www.ntis.gov/about%0Ahttps://www.osti.gov/biblio/1617028%0Ahttps://www.osti.gov/servlets/purl/1617028%0Ahttps://www.osti.gov/servlets/purl/1863608/

32. Bayat H, Dehghanizadeh M, Jarvis JM, Brewer CE, Jena U. Hydrothermal Liquefaction of Food Waste: Effect of Process Parameters on Product Yields and Chemistry. Front Sustain Food Syst [Internet]. 2021;5. Available from: https://www.frontiersin.org/articles/10.3389/fsufs.2021.658592
33. Wang L, Chi Y, Shu D, Weiss-Hortala E, Nzihou A, Choi S. Experimental studies of hydrothermal liquefaction of kitchen waste with H+, OH− and Fe3+ additives for bio-oil upgrading. Waste Manag Res [Internet]. 2020 Sep 19;39(1):165–73. Available from: https://doi.org/10.1177/0734242X20957408
34. Elliott DC, Biller P, Ross AB, Schmidt AJ, Jones SB. Hydrothermal liquefaction of biomass: Developments from batch to continuous process. Bioresour Technol [Internet]. 2015;178:147–56. Available from: http://dx.doi.org/10.1016/j.biortech.2014.09.132
35. Katakojwala R, Kopperi H, Kumar S, Venkata Mohan S. Hydrothermal liquefaction of biogenic municipal solid waste under reduced H2 atmosphere in biorefinery format. Bioresour Technol [Internet]. 2020;310:123369. Available from: http://www.sciencedirect.com/science/article/pii/S0960852420306416
36. Anastasakis K, Biller P, Madsen RB, Glasius M, Johannsen I. Continuous Hydrothermal Liquefaction of Biomass in a Novel Pilot Plant with Heat Recovery and Hydraulic Oscillation. Energies. 2018;11(10):1–23.
37. Ghadge R, Nagwani N, Saxena N, Dasgupta S, Sapre A. Design and scale-up challenges in hydrothermal liquefaction process for biocrude production and its upgradation. Energy Convers Manag X [Internet]. 2022;14(September 2021):100223. Available from: https://doi.org/10.1016/j.ecmx.2022.100223
38. Biller P, Ross AB. Potential yields and properties of oil from the hydrothermal liquefaction of microalgae with different biochemical content. Bioresour Technol [Internet]. 2011;102(1):215–25. Available from: http://www.sciencedirect.com/science/article/pii/S0960852410010096
39. Yu G, Zhang Y, Schideman L, Funk T, Wang Z. Distributions of carbon and nitrogen in the products from hydrothermal liquefaction of low-lipid microalgae. Energy Environ Sci [Internet]. 2011;4(11):4587–95. Available from: http://dx.doi.org/10.1039/C1EE01541A
40. Ranganathan P, Savithri S. Techno-economic analysis of microalgae-based liquid fuels production from wastewater via hydrothermal liquefaction and hydroprocessing. Bioresour Technol [Internet]. 2019;284:256–65. Available from: https://www.sciencedirect.com/science/article/pii/S0960852419304468
41. Orfield ND, Fang AJ, Valdez PJ, Nelson MC, Savage PE, Lin XN, et al. Life cycle design of an algal biorefinery featuring hydrothermal liquefaction:

Effect of reaction conditions and an alternative pathway including microbial regrowth. ACS Sustain Chem Eng. 2014;2(4):867–74.

42. Chen PH, Venegas Jimenez JL, Rowland SM, Quinn JC, Laurens LML. Nutrient recycle from algae hydrothermal liquefaction aqueous phase through a novel selective remediation approach. Algal Res [Internet]. 2020;46:101776. Available from: https://www.sciencedirect.com/science/article/pii/S2211926419304746
43. Hajinajaf N, Mehrabadi A, Tavakoli O. Practical strategies to improve harvestable biomass energy yield in microalgal culture: A review. Biomass and Bioenergy [Internet]. 2021;145:105941. Available from: https://www.sciencedirect.com/science/article/pii/S0961953420304736
44. Biller P, Ross A, Skill S, Lea-Langton A, Balasundaram B, Hall C, et al. Nutrient recycling of aqueous phase for microalgae cultivation from the hydrothermal liquefaction process. Algal Res. 2012 May;1:70–76.
45. Tommaso G, Chen WT, Li P, Schideman L, Zhang Y. Chemical characterization and anaerobic biodegradability of hydrothermal liquefaction aqueous products from mixed-culture wastewater algae. Bioresour Technol [Internet]. 2015;178:139–46. Available from: http://dx.doi.org/10.1016/j.biortech.2014.10.011
46. Erkelens M, Ball AS, Lewis DM. The application of activated carbon for the treatment and reuse of the aqueous phase derived from the hydrothermal liquefaction of a halophytic Tetraselmis sp. Bioresour Technol [Internet]. 2015;182:378–82. Available from: http://dx.doi.org/10.1016/j.biortech.2015.01.129
47. Wang M, Schideman L, Lu H, Zhang Y, Li B, Cao W. Zeolite-amended microalgal-bacterial system in a membrane photobioreactor for promoting system stability, biomass production, and wastewater treatment efficiency to realize Environmental-Enhancing Energy paradigm. J Appl Phycol. 2019;31(1):335–44.
48. Si B, Yang L, Zhou X, Watson J, Tommaso G, Chen W-T, et al. Anaerobic conversion of the hydrothermal liquefaction aqueous phase: fate of organics and intensification with granule activated carbon/ozone pretreatment. Green Chem [Internet]. 2019;21(6):1305–18. Available from: http://dx.doi.org/10.1039/C8GC02907E
49. Valsania MC, Fasano F, Richardson SD, Vincenti M. Investigation of the degradation of cresols in the treatments with ozone. Water Res [Internet]. 2012;46(8):2795–804. Available from: https://www.sciencedirect.com/science/article/pii/S0043135412001431
50. Zhang J, Chua QW, Mao F, Zhang L, He Y, Tong YW, et al. Effects of activated carbon on anaerobic digestion – Methanogenic metabolism, mechanisms of antibiotics and antibiotic resistance genes removal. Bioresour Technol Reports [Internet]. 2019;5:113–20. Available from: https://www.sciencedirect.com/science/article/pii/S2589014X19300027
51. Shen R, Jiang Y, Ge Z, Lu J, Zhang Y, Liu Z, et al. Microbial electrolysis treatment of post-hydrothermal liquefaction wastewater with hydrogen

generation. Appl Energy [Internet]. 2018;212:509–15. Available from: https://www.sciencedirect.com/science/article/pii/S0306261917317804

52. Watson J, Wang T, Si B, Chen WT, Aierzhati A, Zhang Y. Valorization of hydrothermal liquefaction aqueous phase: pathways towards commercial viability. Prog Energy Combust Sci. 2020;77.
53. Zhen G, Lu X, Kumar G, Bakonyi P, Xu K, Zhao Y. Microbial electrolysis cell platform for simultaneous waste biorefinery and clean electrofuels generation: Current situation, challenges and future perspectives. Prog Energy Combust Sci [Internet]. 2017;63:119–45. Available from: https://www.sciencedirect.com/science/article/pii/S0360128516301563
54. Silva Thomsen LB, Anastasakis K, Biller P. Wet oxidation of aqueous phase from hydrothermal liquefaction of sewage sludge. Water Res. 2022;209(October 2021).
55. Hansen NH, Pedersen TH, Rosendahl LA. Techno-economic analysis of a novel hydrothermal liquefaction implementation with electrofuels for high carbon efficiency. Biofuels, Bioprod Biorefining. 2019;13(3):660–72.
56. Lee I-G, Ihm S-K. Hydrogen Production by SCWG Treatment of Wastewater from Amino Acid Production Process. Ind Eng Chem Res [Internet]. 2010 Nov 3;49(21):10974–80. Available from: https://doi.org/10.1021/ie100469n
57. Hu Y, Feng S, Yuan Z, Xu C (Charles), Bassi A. Investigation of aqueous phase recycling for improving bio-crude oil yield in hydrothermal liquefaction of algae. Bioresour Technol [Internet]. 2017;239:151–9. Available from: http://dx.doi.org/10.1016/j.biortech.2017.05.033
58. Biller P, Madsen RB, Klemmer M, Becker J, Iversen BB, Glasius M. Effect of hydrothermal liquefaction aqueous phase recycling on bio-crude yields and composition. Bioresour Technol [Internet]. 2016;220:190–9. Available from: http://dx.doi.org/10.1016/j.biortech.2016.08.053
59. Zhu Z, Rosendahl L, Toor SS, Yu D, Chen G. Hydrothermal liquefaction of barley straw to bio-crude oil: Effects of reaction temperature and aqueous phase recirculation. Appl Energy [Internet]. 2015;137:183–92. Available from: http://dx.doi.org/10.1016/j.apenergy.2014.10.005
60. Shah AA, Toor SS, Seehar TH, Nielsen RS, Nielsen AH, Pedersen TH, et al. Bio-crude production through aqueous phase recycling of hydrothermal liquefaction of sewage sludge. Energies. 2020;13(2).
61. Patel PD, Lakdawala A, Chourasia S, Patel RN. Bio fuels for compression ignition engine: A review on engine performance, emission and life cycle analysis. Renew Sustain Energy Rev [Internet]. 2016;65:24–43. Available from: https://www.sciencedirect.com/science/article/pii/S136403211630226X
62. Watson J, Si B, Wang Z, Wang T, Valentine A, Zhang Y. Towards transportation fuel production from food waste: Potential of biocrude oil distillates for gasoline, diesel, and jet fuel. Fuel [Internet]. 2021;301:121028. Available from: https://www.sciencedirect.com/science/article/pii/S0016236121009054

63. Pedersen T, Jensen C, Sandström L, Rosendahl L. Full characterization of compounds obtained from fractional distillation and upgrading of a HTL biocrude. Appl Energy. 2017 Sep;202:408–19.
64. Maros H, Juniar S. 2022 statistical report. 2016;1–23.
65. Taghipour A, Hornung U, Ramirez JA, Brown RJ, Rainey TJ. Fractional distillation of algae based hydrothermal liquefaction biocrude for co-processing: changes in the properties, storage stability, and miscibility with diesel. Energy Convers Manag [Internet]. 2021;236(November 2020):114005. Available from: https://doi.org/10.1016/j.enconman.2021.114005
66. Hoffmann J, Jensen CU, Rosendahl LA. Co-processing potential of HTL bio-crude at petroleum refineries - Part 1: Fractional distillation and characterization. Fuel [Internet]. 2016;165:526–35. Available from: http://dx.doi.org/10.1016/j.fuel.2015.10.094
67. Chen L, Yoshikawa K. Bio-oil upgrading by cracking in two-stage heated reactors. AIMS Energy. 2018;6(1):203–315.
68. Zhang Q, Chang J, Wang TJ, Xu Y. Upgrading bio-oil over different solid catalysts. Energy and Fuels. 2006;20(6):2717–20.
69. Chen WT, Zhang Y, Lee TH, Wu Z, Si B, Lee CFF, et al. Renewable diesel blendstocks produced by hydrothermal liquefaction of wet biowaste. Nat Sustain [Internet]. 2018;1(11):702–10. Available from: http://dx.doi.org/10.1038/s41893-018-0172-3
70. Haider MS, Castello D, Rosendahl LA. The Art of Smooth Continuous Hydroprocessing of Biocrudes Obtained from Hydrothermal Liquefaction: Hydrodemetallization and Propensity for Coke Formation. Energy and Fuels. 2021;35(13):10611–22.
71. Watson J, Si B, Wang Z, Wang T, Valentine A, Zhang Y. Towards transportation fuel production from food waste: Potential of biocrude oil distillates for gasoline, diesel, and jet fuel. Fuel [Internet]. 2021;301(May):121028. Available from: https://doi.org/10.1016/j.fuel.2021.121028
72. Fonquerne F. Sulfur dioxide. Synlett. 2005;(8):1340–1.
73. EPA (USA). Nitrogen oxides (NOx), why and how they are controlled. Epa-456/F-99-006R. 1999;(November):48.
74. Rodríguez E, Arqués JL, Rodríguez R, Nuñez M, Medina M, Talarico TL, et al. We are IntechOpen , the world ' s leading publisher of Open Access books Built by scientists , for scientists TOP 1 %. Intech [Internet]. 1989;32(tourism):137–44. Available from: https://www.intechopen.com/books/advanced-biometric-technologies/liveness-detection-in-biometrics
75. Rahman SMA, Masjuki HH, Kalam MA, Abedin MJ, Sanjid A, Sajjad H. Impact of idling on fuel consumption and exhaust emissions and available idle-reduction technologies for diesel vehicles – A review. Energy Convers Manag [Internet]. 2013;74:171–82. Available from:

https://www.sciencedirect.com/science/article/pii/S0196890413002781

76. Nielsen VG, Chawla N, Mangla D, Gomes SB, Arkebauer MR, Wasko KA, et al. Carbon monoxide-releasing molecule-2 enhances coagulation in rabbit plasma and decreases bleeding time in clopidogrel/aspirin-treated rabbits. Blood Coagul Fibrinolysis. 2011;22(8):756–9.
77. Carbon Dioxide [Internet]. Wisconsin Department of Health Services. 2022. Available from: www.dhs.wisconsin.gov
78. Hossain FM, Nabi MN, Rainey TJ, Bodisco T, Rahman MM, Suara K, et al. Investigation of microalgae HTL fuel effects on diesel engine performance and exhaust emissions using surrogate fuels. Energy Convers Manag [Internet]. 2017;152:186–200. Available from: https://www.sciencedirect.com/science/article/pii/S0196890417308294
79. Obeid F, Van TC, Horchler EJ, Guo Y, Verma P, Miljevic B, et al. Engine performance and emissions from fuels containing nitrogen and sulphur. Energy Convers Manag X [Internet]. 2022;14:100179. Available from: https://doi.org/10.1016/j.ecmx.2022.100179
80. Yang Z, Lee TH, Li Y, Chen W-T, Zhang Y. Spray and combustion characteristics of pure hydrothermal liquefaction biofuel and mixture blends with diesel. Fuel [Internet]. 2021;294:120498. Available from: https://www.sciencedirect.com/science/article/pii/S0016236121003744
81. Conti F, Toor SS, Pedersen TH, Seehar TH, Nielsen AH, Rosendahl LA. Valorization of animal and human wastes through hydrothermal liquefaction for biocrude production and simultaneous recovery of nutrients. Energy Convers Manag [Internet]. 2020;216:112925. Available from: https://www.sciencedirect.com/science/article/pii/S0196890420304635
82. Mariotti F, Tomé D, Mirand PP. Converting nitrogen into protein - Beyond 6.25 and Jones' factors. Crit Rev Food Sci Nutr. 2008;48(2):177–84.
83. Conti F, Toor SS, Pedersen TH, Seehar TH, Nielsen AH. Valorization of animal and human wastes through hydrothermal liquefaction for biocrude production and simultaneous recovery of nutrients. Energy Convers Manag [Internet]. 2020;216(February):112925. Available from: https://doi.org/10.1016/j.enconman.2020.112925
84. Liu F, Olesen KB, Borregaard AR, Vollertsen J. Microplastics in urban and highway stormwater retention ponds. Sci Total Environ [Internet]. 2019;671:992–1000. Available from: https://www.sciencedirect.com/science/article/pii/S0048969719314226
85. Watson J, Lu J, de Souza R, Si B, Zhang Y, Liu Z. Effects of the extraction solvents in hydrothermal liquefaction processes: Biocrude oil quality and energy conversion efficiency. Energy [Internet]. 2019;167:189–97. Available from:
https://www.sciencedirect.com/science/article/pii/S0360544218322072
86. Haider DanieleAU - Michalski, Karol M.AU - Pedersen, Thomas H.AU - Rosendahl, Lasse A.TI - Catalytic Hydrotreatment of Microalgae Biocrude from Continuous Hydrothermal Liquefaction: Heteroatom Removal and Their

Distribution in Distillation Cuts MSAU-C. No Title. Vol. 11, Energies. 2018.

87. Castello D, Haider MS, Rosendahl LA. Catalytic upgrading of hydrothermal liquefaction biocrudes: Different challenges for different feedstocks. Renew Energy [Internet]. 2019;141:420–30. Available from: https://doi.org/10.1016/j.renene.2019.04.003

88. Taghipour A, Hornung U, Ramirez JA, Brown RJ, Rainey TJ. Aqueous phase recycling in catalytic hydrothermal liquefaction for algal biomass and the effect on elemental accumulation and energy efficiency. J Clean Prod [Internet]. 2021;289:125582. Available from: https://www.sciencedirect.com/science/article/pii/S0959652620356286

89. Blumenthal K. Generation and treatment of municipal waste. Eurostat Stat Focus [Internet]. 2011;Environmen(2001):1–12. Available from: http://www.eds-destatis.de/en/downloads/sif/KS-SF-11-031-EN-N.pdf

90. Kohansal K, Toor S, Sharma K, Chand R, Rosendahl L, Pedersen TH. Hydrothermal liquefaction of pre-treated municipal solid waste (biopulp) with recirculation of concentrated aqueous phase. Biomass and Bioenergy [Internet]. 2021;148(September 2020):106032. Available from: https://doi.org/10.1016/j.biombioe.2021.106032

91. Seshasayee MS, Savage PE. Oil from plastic via hydrothermal liquefaction: Production and characterization. Appl Energy [Internet]. 2020;278:115673. Available from: https://www.sciencedirect.com/science/article/pii/S0306261920311703

92. dos Passos JS, Glasius M, Biller P. Screening of common synthetic polymers for depolymerization by subcritical hydrothermal liquefaction. Process Saf Environ Prot [Internet]. 2020;139:371–9. Available from: https://doi.org/10.1016/j.psep.2020.04.040

93. Chand R, Kohansal K, Toor S, Pedersen TH, Vollertsen J. Microplastics degradation through hydrothermal liquefaction of wastewater treatment sludge. J Clean Prod [Internet]. 2022;335(December 2021):130383. Available from: https://doi.org/10.1016/j.jclepro.2022.130383

94. Kohansal K, Sharma K, Toor SS, Sanchez EL, Zimmermann J. Bio-Crude Production Improvement during Hydrothermal Liquefaction of Biopulp by Simultaneous Application of Alkali Catalysts and Aqueous Phase Recirculation. 2021;1–22.

95. TNO innovation for life. Phyllis2 (ECN Phyllis classification) [Internet]. Available from: https://phyllis.nl/Browse/Standard/ECN-Phyllis

96. ASTM International. Standard Test Method for Ash on Wood. D 1102 – 84. 2001;84(June 1984):2.

97. Ali Shah A, Sohail Toor S, Hussain Seehar T, Sadetmahaleh KK, Helmer Pedersen T, Haaning Nielsen A, et al. Bio-crude production through co-hydrothermal processing of swine manure with sewage sludge to enhance pumpability. Fuel [Internet]. 2021;288:119407. Available from: https://www.sciencedirect.com/science/article/pii/S0016236120324030

98. Cade-Menun BJ. Characterizing phosphorus in environmental and

agricultural samples by 31P nuclear magnetic resonance spectroscopy. Talanta [Internet]. 2005;66(2):359–71. Available from: https://www.sciencedirect.com/science/article/pii/S0039914004007362

99. Deng Y, Zhang T, Clark J, Aminabhavi T, Kruse A, Tsang DCW, et al. Mechanisms and modelling of phosphorus solid–liquid transformation during the hydrothermal processing of swine manure. Green Chem [Internet]. 2020;22(17):5628–38. Available from: http://dx.doi.org/10.1039/D0GC01281E
100. Van Kauwenbergh SJ. World Phosphate Rock Reserves and Resources Technical Bulletin IFDC-T-75. Ifdc-T-75. 2010;48.
101. Brown TM, Duan P, Savage PE. Hydrothermal Liquefaction and Gasification of Nannochloropsis sp. Energy & Fuels [Internet]. 2010 Jun 17;24(6):3639–46. Available from: https://doi.org/10.1021/ef100203u
102. Kohansal K, Toor S, Sharma K, Chand R, Rosendahl L, Pedersen TH. Hydrothermal liquefaction of pre-treated municipal solid waste (biopulp) with recirculation of concentrated aqueous phase. Biomass and Bioenergy. 2021 May 1;148.
103. Onwudili JA, Williams PT. Hydrothermal reactions of sodium formate and sodium acetate as model intermediate products of the sodium hydroxide-promoted hydrothermal gasification of biomass. Green Chem [Internet]. 2010;12(12):2214–24. Available from: http://dx.doi.org/10.1039/C0GC00547A
104. Fan Y, Hornung U, Dahmen N, Kruse A. Hydrothermal liquefaction of protein-containing biomass: study of model compounds for Maillard reactions. Biomass Convers Biorefinery. 2018;8(4):909–23.
105. Karagöz S, Bhaskar T, Muto A, Sakata Y, Oshiki T, Kishimoto T. Low-temperature catalytic hydrothermal treatment of wood biomass: Analysis of liquid products. Chem Eng J. 2005;108(1–2):127–37.
106. Yin S, Mehrotra AK, Tan Z. Alkaline hydrothermal conversion of cellulose to bio-oil: Influence of alkalinity on reaction pathway change. Bioresour Technol [Internet]. 2011;102(11):6605–10. Available from: http://dx.doi.org/10.1016/j.biortech.2011.03.069
107. Liu HM, Wang FY, Liu YL. Alkaline pretreatment and hydrothermal liquefaction of cypress for high yield bio-oil production. J Anal Appl Pyrolysis [Internet]. 2014;108:136–42. Available from: http://dx.doi.org/10.1016/j.jaap.2014.05.007
108. Grigoras IF, Stroe RE, Sintamarean IM, Rosendahl LA. Effect of biomass pretreatment on the product distribution and composition resulting from the hydrothermal liquefaction of short rotation coppice willow. Bioresour Technol [Internet]. 2017;231:116–23. Available from: https://www.sciencedirect.com/science/article/pii/S0960852417300937
109. Spasic AM. Chapter 1 - Introduction. In: Spasic AMBT-IS and T, editor. Rheology of Emulsions [Internet]. Elsevier; 2018. p. 1–25. Available from: https://www.sciencedirect.com/science/article/pii/B9780128138366000015

110. Maxwell JB, Bonnell LS. Derivation and Precision of a New Vapor Pressure Correlation for Petroleum Hydrocarbons. Ind Eng Chem. 1957;49(7):1187–96.

111. Rezagama A, Hibbaan M, Arief Budihardjo M. Ammonia-Nitrogen (NH 3-N) and Ammonium-Nitrogen (NH 4 +-N) Equilibrium on The Process of Removing Nitrogen By Using Tubular Plastic Media. J Mater Environ Sci. 2017;8(S):4915–22.

112. Kohansal K, Sharma K, Haider MS, Toor SS, Castello D, Rosendahl LA, et al. Sustainable Energy & Fuels Hydrotreating of bio-crude obtained from hydrothermal liquefaction of biopulp : e ff ects of aqueous phase recirculation on the hydrotreated. 2022;

113. Chiaberge S, Leonardis I, Fiorani T, Bianchi G, Cesti P, Bosetti A, et al. Amides in Bio-oil by Hydrothermal Liquefaction of Organic Wastes: A Mass Spectrometric Study of the Thermochemical Reaction Products of Binary Mixtures of Amino Acids and Fatty Acids. Energy & Fuels [Internet]. 2013 Sep 19;27(9):5287–97. Available from: https://doi.org/10.1021/ef4009983

114. Leng S, Leng L, Chen L, Chen J, Chen J, Zhou W. The effect of aqueous phase recirculation on hydrothermal liquefaction/carbonization of biomass: A review. Bioresour Technol [Internet]. 2020;318:124081. Available from: https://www.sciencedirect.com/science/article/pii/S0960852420313535

115. Castello D, Haider MS, Rosendahl LA. Catalytic upgrading of hydrothermal liquefaction biocrudes: Different challenges for different feedstocks. Renew Energy [Internet]. 2019;141:420–30. Available from: https://www.sciencedirect.com/science/article/pii/S0960148119304768

116. Philippov AA, Martyanov ON. Poisoning effect of N-containing compounds on performance of Raney® nickel in transfer hydrogenation. Catal Commun [Internet]. 2021;161:106361. Available from: https://doi.org/10.1016/j.catcom.2021.106361

117. Jazrawi C, Biller P, He Y, Montoya A, Ross AB, Maschmeyer T, et al. Two-stage hydrothermal liquefaction of a high-protein microalga. Algal Res [Internet]. 2015;8:15–22. Available from: http://dx.doi.org/10.1016/j.algal.2014.12.010

118. Wu B, Berg SM, Remucal CK, Strathmann TJ. Evolution of N-Containing Compounds during Hydrothermal Liquefaction of Sewage Sludge. ACS Sustain Chem Eng [Internet]. 2020 Dec 14;8(49):18303–13. Available from: https://doi.org/10.1021/acssuschemeng.0c07060

119. Yang W, Li X, Li Z, Tong C, Feng L. Understanding low-lipid algae hydrothermal liquefaction characteristics and pathways through hydrothermal liquefaction of algal major components: Crude polysaccharides, crude proteins and their binary mixtures. Bioresour Technol [Internet]. 2015;196:99–108. Available from: https://www.sciencedirect.com/science/article/pii/S0960852415009736

120. Qian L, Wang S, Savage PE. Fast and isothermal hydrothermal liquefaction of sludge at different severities: Reaction products, pathways, and kinetics. Appl Energy [Internet]. 2020;260:114312. Available from:

https://www.sciencedirect.com/science/article/pii/S0306261919319993

121. Brand S, Hardi F, Kim J, Suh D. Effect of heating rate on biomass liquefaction: Differences between subcritical water and supercritical ethanol. Energy. 2014;68:420–427.
122. Motavaf B, Savage PE. Effect of Process Variables on Food Waste Valorization via Hydrothermal Liquefaction. ACS ES&T Eng [Internet]. 2021 Mar 12;1(3):363–74. Available from: https://doi.org/10.1021/acsestengg.0c00115
123. Furimsky E, Massoth FE. Deactivation of hydroprocessing catalysts. Catal Today. 1999;52(4):381–495.
124. Wang H, Male J, Wang Y. Recent Advances in Hydrotreating of Pyrolysis Bio-Oil and Its Oxygen-Containing Model Compounds. ACS Catal [Internet]. 2013 May 3;3(5):1047–70. Available from: https://doi.org/10.1021/cs400069z
125. Zeuthen P, Bartholdy J, Wiwel P, Cooper BH. Formation of Coke on Hydrotreating Catalysts and its Effect on Activity. In: Delmon B, Froment GFBT-S in SS and C, editors. Catalyst Deactivation 1994 [Internet]. Elsevier; 1994. p. 199–206. Available from: https://www.sciencedirect.com/science/article/pii/S016729910862741X
126. Prado GHC, de Klerk A. Metals Removal from Metal-Bridged Molecules by Acid Treatment of Oilsands Bitumen and Subfractions. Energy & Fuels [Internet]. 2016 Jan 21;30(1):20–30. Available from: https://doi.org/10.1021/acs.energyfuels.5b01482
127. Jarvis JM, Sudasinghe NM, Albrecht KO, Schmidt AJ, Hallen RT, Anderson DB, et al. Impact of iron porphyrin complexes when hydroprocessing algal HTL biocrude. Fuel [Internet]. 2016;182:411–8. Available from: https://www.sciencedirect.com/science/article/pii/S0016236116304227
128. Mortensen PM, Grunwaldt J-D, Jensen PA, Jensen AD. Screening of Catalysts for Hydrodeoxygenation of Phenol as a Model Compound for Bio-oil. ACS Catal [Internet]. 2013 Aug 2;3(8):1774–85. Available from: https://doi.org/10.1021/cs400266e
129. Zhu C, Gutiérrez OY, Santosa DM, Flake M, Weindl R, Kutnyakov I, et al. Kinetics of nitrogen-, oxygen- and sulfur-containing compounds hydrotreating during co-processing of bio-crude with petroleum stream. Appl Catal B Environ [Internet]. 2022;307:121197. Available from: https://www.sciencedirect.com/science/article/pii/S0926337322001370
130. Girgis MJ, Gates BC, Girgis MJ. Reactivities, Reaction Networks, and Kinetics in High-Pressure Catalytic Hydroprocessing. Ind Eng Chem Res. 1991;30(9):2021–58.
131. Streitwieser, A and Heathcock C. Introduction to Organic Chemistry. New York London: Macmillan ; Collier Macmillan; 1976.
132. Kohansal K, Sharma K, Haider MS, Toor SS, Castello D, Rosendahl LA, et al. Hydrotreating of bio-crude obtained from hydrothermal liquefaction of biopulp: effects of aqueous phase recirculation on the hydrotreated oil.

Sustain Energy Fuels [Internet]. 2022;6(11):2805–22. Available from: http://dx.doi.org/10.1039/D2SE00399F

133. Gouw TH. Removal of Water in the Distillation of Hydrocarbon Mixtures. Anal Chem. 1977;49(12):1887–8.
134. Taghipour A, Ramirez JA, Brown RJ, Rainey TJ. A review of fractional distillation to improve hydrothermal liquefaction biocrude characteristics; future outlook and prospects. Renew Sustain Energy Rev [Internet]. 2019;115(February):109355. Available from: https://doi.org/10.1016/j.rser.2019.109355
135. Loganathan SBT-I in FE and SRT. Biohydro-fined diesel (BHD) and biodiesel (BOD) production process and property review. In Woodhead Publishing; 2011. p. 97–107. Available from: https://www.sciencedirect.com/science/article/pii/B9780857092137500097
136. Rizzo AM, Chiaramonti D. Blending of Hydrothermal Liquefaction Biocrude with Residual Marine Fuel: An Experimental Assessment. Energies. 2022;15(2).
137. Chen D, Zhou J, Zhang Q, Zhu X. Evaluation methods and research progresses in bio-oil storage stability. Renew Sustain Energy Rev [Internet]. 2014;40:69–79. Available from: https://www.sciencedirect.com/science/article/pii/S136403211400611X
138. Oh S, Choi HS, Kim U-J, Choi I-G, Choi JW. Storage performance of bio-oil after hydrodeoxygenative upgrading with noble metal catalysts. Fuel [Internet]. 2016;182:154–60. Available from: https://www.sciencedirect.com/science/article/pii/S0016236116303593
139. Buckner CA, Lafrenie RM, Dénommée JA, Caswell JM, Want DA, Gan GG, et al. We are IntechOpen , the world ' s leading publisher of Open Access books Built by scientists , for scientists TOP 1 %. Intech [Internet]. 2016;11(tourism):13. Available from: https://www.intechopen.com/books/advanced-biometric-technologies/liveness-detection-in-biometrics
140. Elkelawy M, Esmaeil K, Alm Eldin H, Radwan A. Effect of Transesterification Reaction Process Variables Variation on Biodiesel Color. 2019.
141. Nabi MN, Rahman MM, Islam MA, Hossain FM, Brooks P, Rowlands WN, et al. Fuel characterisation, engine performance, combustion and exhaust emissions with a new renewable Licella biofuel. Energy Convers Manag [Internet]. 2015;96:588–98. Available from: https://www.sciencedirect.com/science/article/pii/S0196890415002083
142. Hossain FM, Nabi MN, Rainey TJ, Bodisco T, Rahman MM, Suara K, et al. Investigation of microalgae HTL fuel effects on diesel engine performance and exhaust emissions using surrogate fuels. Energy Convers Manag. 2017;152(September):186–200.
143. Agarwal AK, Rajamanoharan K. Experimental investigations of performance and emissions of Karanja oil and its blends in a single cylinder agricultural

diesel engine. Appl Energy [Internet]. 2009;86(1):106–12. Available from: https://www.sciencedirect.com/science/article/pii/S0306261908001025

144. Agarwal AK, Chandra Shukla P, Patel C, Gupta JG, Sharma N, Prasad RK, et al. Unregulated emissions and health risk potential from biodiesel (KB5, KB20) and methanol blend (M5) fuelled transportation diesel engines. Renew Energy [Internet]. 2016;98:283–91. Available from: https://www.sciencedirect.com/science/article/pii/S0960148116302427

145. Frenklach M. Reaction mechanism of soot formation in flames. Phys Chem Chem Phys [Internet]. 2002;4(11):2028–37. Available from: http://dx.doi.org/10.1039/B110045A

146. Knothe G, Sharp CA, Ryan TW. Exhaust Emissions of Biodiesel, Petrodiesel, Neat Methyl Esters, and Alkanes in a New Technology Engine. Energy & Fuels [Internet]. 2006 Jan 1;20(1):403–8. Available from: https://doi.org/10.1021/ef0502711

ISSN (online): 2446-1636
ISBN (online): 978-87-7573-757-4

AALBORG UNIVERSITY PRESS